Robert Weitenhüller, BSc

Modulated Dilatometry as Tool for Simultaneous Study of Vacancy Formation and Migration

MASTER'S THESIS

to achieve the university degree of

Diplom-Ingenieur

Master's degree programme: Technical Physics

submitted to

Graz University of Technology

Supervisor

Univ.-Prof. Dipl.-Phys. Dr.rer.nat. Roland Würschum

Institute of Materials Physics

Graz, November 2020

AFFIDAVIT

I declare that I have authored this thesis independently, that I have not used other than the declared sources/resources, and that I have explicitly indicated all material which has been quoted either literally or by content from the sources used. The text document uploaded to TUGRAZonline is identical to the present master's thesis.

Date, Signature

Abstract

This work's focus lies in the development of a new method for the investigation of thermal vacancies by time-linear heating with superimposed temperature modulation. It allows to simultaneously determine the formation and migration enthalpy together with the corresponding prefactors for selected materials, such as $Fe_{62}Al_{38}$, for which several measurements were conducted.
In the course of this method formulas for the corresponding vacancy signal were derived, on the basis of which two approaches were developed to obtain these material parameters with a minimum of two measurements with different modulation frequencies. On the basis of these two approaches dilatometric measurements were performed. In addition, a couple of measurements were conducted in order to investigate systematic variations caused by the measurement setup. The most probable reason for these systematic deviations was identified constituting the basis for further improvements.

Contents

1 Introduction

With the development of a new type of dilatometer, which is capable of temperature-modulated measurements at high temperatures, new methods for the investigation of bulk metallic alloys became available [1]. There are many alloys, which are of great importance to the industry as for example iron-aluminum, which is used as high-temperature structural material because of its excellent physical, chemical and mechanical properties. To get a deeper insight into these materials, it is important to understand the diffusion processes taking place in these materials. Diffusion is the movement of atoms in the material along defects like point defects, dislocations and grain boundaries, the last two of which are high-diffusivity paths. In crystalline solids point defects, such as vacant lattice sites, play an important role for the diffusion mechanisms, which is why the focus of this work lies in the investigation of vacant lattice sites that are thermally induced. [2]

In the course of this work several approaches were developed, which are making use of the time-dependency of the length change due to vacancies by applying a sinusoidal temperature profile (and a constant heating rate) to the specimen in question. This results in a phase-shifted length signal, from which vacancy properties such as the formation enthalpy or the migration enthalpy can be deduced. Time-dependent dilatometry (and hence this method) requires the material to have a high vacancy concentration, while the diffusion of these vacancies should be rather slow. For this reason $Fe_{62}Al_{38}$ was chosen [3].

Since the performed measurements exhibited some systematic variations caused by the measurement setup, some zero measurements were conducted to investigate the reason for these and how to counteract them. For this purpose, this work consists of two parts, from which the first one comprises a description of the measurement setup together with an analysis of the systematic variations by means of zero measurements and the corresponding solution to counteract these systematic variations. The second part is considered as the main part of this work and focuses on the development and application of the aforementioned method and is concluded with some suggestions for future measurements.

2 Measurement Setup and Improvement

In the following chapter the measurement setup will be described. While measurements as described in chapter 4 and 5 were conducted, some systematic variations caused by (fast) temperature changes were observed, which are considered to be not negligible thus requiring a deeper look into the source of these systematic variations. The occurrence and analysis of these systematic variations by means of zero measurements will be presented here together with a solution counteracting these systematic variations.

2.1 Setup

The following description of the measurement setup is taken from [1].
The measurement setup used in this work is capable of performing non-contact high-precision dilatometric measurements for temperatures ranging from ambient temperatures up to 1300 K at superior long-term stability. It allows to conduct isothermal measurements on time scales exceeding 10^6 s as well as non-isothermal measurements, i.e. at constant heating rates ranging from 0.01 K/min to a several 100 K/min, while it is possible to modulate the temperature signal in both cases.

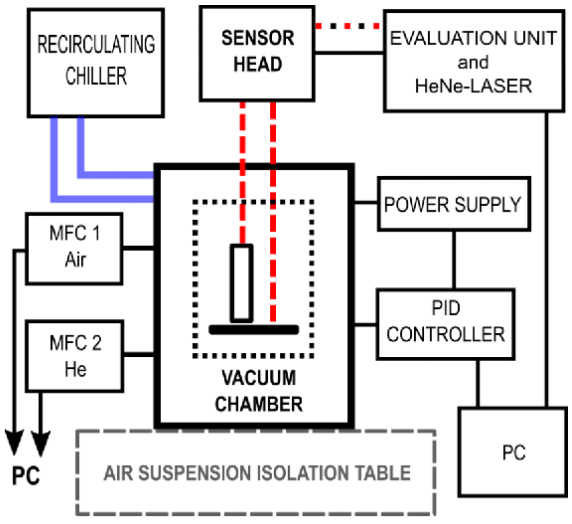

Figure 2.1: Block diagram of the measurement setup in side view (a more detailed view of the furnace is shown in fig. 2.2). Reprinted from [1], with the permission of AIP Publishing.

In fig. 2.1 a block diagram of the measurement setup is shown. Since the high-precision measurements require for various reasons a maximum degree of stability of the ambient conditions, i.e. ambient pressure and in particular ambient temperature, the whole measurement setup is located inside a constant climate chamber guaranteeing a great absolute temperature stability with fluctuations less than 0.1 K. Furthermore, the vacuum chamber and the interferometer sensor head are mounted on a heavy stone table which is isolated from vibrations by a passive air suspension system.

Length measurement:
For the non-contact length change measurement a two-beam Michelson laser interferometer (sensor head, evaluation unit and HeNe-Laser) is placed above the furnace, which is, being located in a vacuum chamber, evacuated to a pressure of 10^{-5} mbar for measuring purposes. The laser beams enter the furnace through a transparent fast-entry door, which is also used for sample loading. The interferometer is based on a SP120 DI manufactured by SIOS Messtechnik Ilmenau, Germany, which measures the direction-dependent length change between the reflection planes of the two beams (differential plane-mirror interferometer) with a resolution down to 20 pm allowing two measuring modes: a sample together with a reference (differential dilatometry) and a sample together with a reference plane (high-stability absolute measurement).

Furnace:
In fig. 2.2 the inside of the furnace (vacuum chamber in fig. 2.1) is shown. The heating is done by three 117 mm R7s tungsten halogen lamps[1] which are placed in one of the two focal points (position T) of the three elliptically shaped reflectors[2]. Each lamp is placed in a fused silica tube to separate it from the vacuum. Because the temperature is measured directly at the sample by thermocouples spot-welded onto it, its temperature can be controlled very precisely by means of a PID-controller, which is adjusting the voltage and therefore the power of the lamps. In order to heat up the specimen very fast a special type of furnace, a so-called “cold-mirror furnace”, was chosen where only the heating elements, the sample and the sample holder are heated in contrast to conventional radiation furnaces, where also the furnace

[1] Halogen lamps are capable of temperature changes up to 2000 K/s.
[2] In the other focal point the specimen holder insert (SI) is placed.

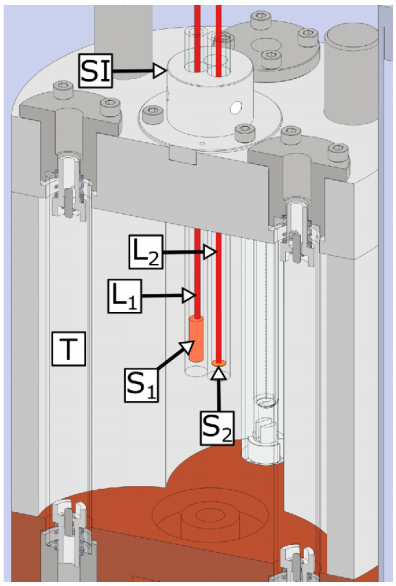

Figure 2.2: Longitudinal cut through the furnace showing the sample holder insert (SI) together with the fused silica tubes in the focal points where the specimen or a reflector can be placed (S_1 and S_2) and the elliptically shaped reflectors with fused silica tubes in the other focal point (T), in which the tungsten halogen lamps are put inside. Reprinted from [1], with the permission of AIP Publishing.

chamber is heated. Heating the furnace chamber would use up quite a lot of energy causing a contribution to the length from the furnace. In order to reduce the heating up of the mirror the whole furnace is cooled by water running through the copper plate at the bottom of the furnace[3] (reddish brown part in fig. 2.2 and fig. 2.3). The water is held at 20 $^\circ\mathrm{C}$ by a recirculating chiller with a temperature stability of $\pm 0.05\,\mathrm{K}$. However, due to the imperfect reflection of aluminum and the insufficient transition of heat from the mirror to the water-cooled bottom plate, the furnace is still heating up to a temperature of 50-70 $^\circ\mathrm{C}$. To guarantee a high temperature stability the whole furnace is placed within a vacuum chamber preventing heat transfer by means of convection.

In order to permit quenching there is a mass flow controller for helium (see fig. 2.1). The pressure can be adjusted in the range of 10^{-5} to 1 mbar by letting argon flow in through a mass flow controller. Furthermore, a mass flow controller for air ensures that the lamps are cooled by a continuous air-flow through the fused silica tubes (T in fig. 2.2) to keep them in the optimum range for halogen lamp operation.

[3] Beneath the copper plate is the actual bottom plate, which is not water-cooled.

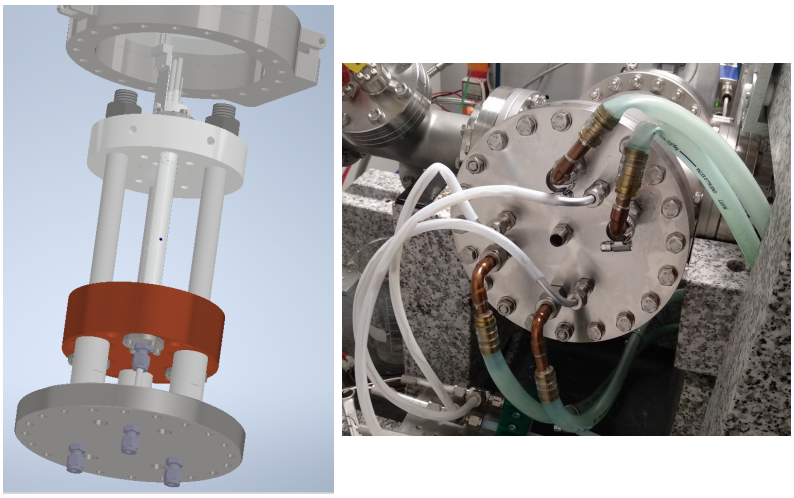

Figure 2.3: **Left:** Side view of the main parts of the system (without the elliptically shaped reflectors) showing from top to bottom the transparent fast-entry door, the plate, which seals the furnace at the top, together with the sample holder insert, the copper plate (reddish brown), above which the elliptically shaped reflectors are placed (see fig. 2.2) and the bottom plate. **Right:** Bottom of the vacuum chamber showing the outlets of the cooling water of the recirculating chiller (bottom plate is not water-cooled, unlike the copper plate) and of the aluminum tubes where the air stream coming from the lamps is going through.

Sample holder insert:

In fig. 2.2 the sample holder insert (SI) inside the furnace (vacuum chamber in fig. 2.1) is shown. It is placed in the other focal points of the elliptical reflectors. At position S1 and/or S2 a specimen (S1) or a reference reflector (S2) can be placed inside a fused silica tube. The laser beams L1 and L2 are reflected either by the specimen itself or by a nickel coated fused silica rod which is placed on top of the sample.

The specimen holder is made of fused silica because it has a low thermal expansion coefficient and the specimen can be radiated through it. In addition, fused silica has a low thermal conductivity preventing the heat from leaking out into the rest of the system through heat conduction.

In order to conduct isothermal high-precision measurements the thermocouple is directly welded to the specimen, for which specimen holders with a small hole on the bottom are available. In this way the specimen temperature can be adjusted precisely with an repeatability of $\pm 2\,\mathrm{K}$. For these measurements the third site remains unused.

In case of zero measurements the third focal point is used for the temperature measurement by spot-welding a thermocouple on a dummy sample, which must be identical to the sample intended to be measured, i.e. the dummy sample's only purpose is to have the same temperature as the actual sample and is not used for length measurements.

2.2 Analysis of systematic Dilatometer Signals caused by fast Temperature Changes

While taking measurements systematic variations upon fast temperature changes occurred regarding the length measurement which could not be explained by any behavior of the specimen itself. In order to see the influence of the measurement setup we decided to conduct some zero measurements, for which the signal should be as small as possible or at least should only have large length changes at the very beginning of the measurement.

To get a first insight into the type of systematic variation we are facing, we conducted some zero measurements where we heated up and cooled down the furnace to give various temperatures at the dummy sample (fig. 2.4 and 2.5) and also conducted some isothermal measurements with different modulation frequencies (fig. 2.6).

By looking at these measurements one can see that the systematic variation lies in the time range of a few thousand seconds and mainly occurs for large temperature differences. As shown in fig. 2.4 and 2.5 the systematic variation lies in the range of a few hundred nm in contrast to fig. 2.6, where the systematic variation is only a few tens of nm.

To figure out the source of these systematic variations, we conducted measurements where we always changed exactly one parameter and compared these measurements with each other. For all of these measurements the water temperature of the recirculating chiller was set to 20 $^{\circ}\mathrm{C}$ and the room temperature was set to 21.9 $^{\circ}\mathrm{C}$.

First of all we checked if the specimen holder could have any influence on the measurement since tiny deviations from the nominal dimensions of the specimen holder

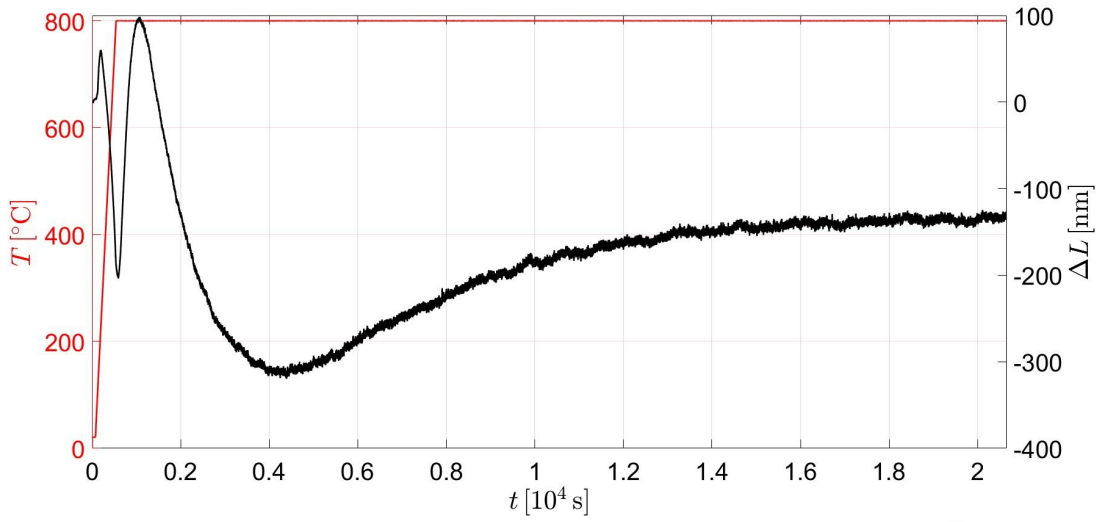

Figure 2.4: Zero measurement. Length change ΔL in dependence of time t upon and after fast heating from temperature T = 21 °C to T = 800 °C with a heating rate of 100 K/min.

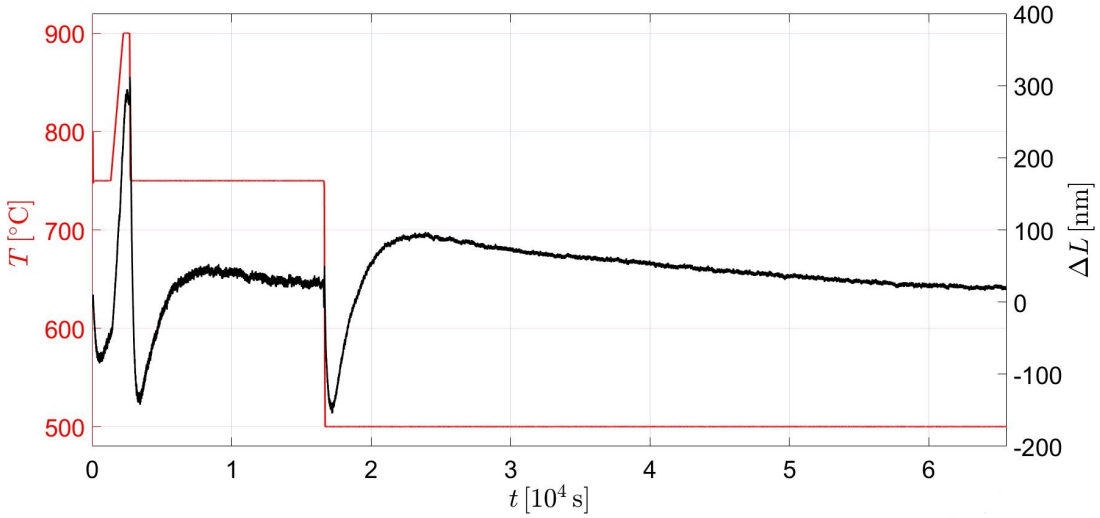

Figure 2.5: Zero measurement. Length change ΔL in dependence of time t upon and after fast temperature changes with a heating rate of 10 K/min and quasi-instantaneous cooling rates. Temperature profile in red.

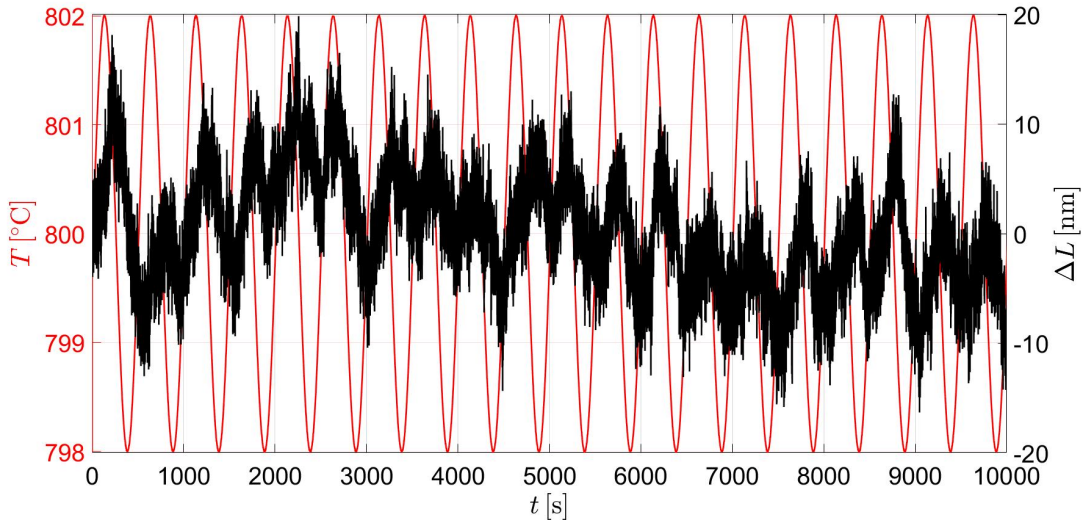

Figure 2.6: Zero measurement. Length change ΔL in dependence of time t in response to a modulated temperature profile at the average temperature T = 800 °C with a modulation frequency f = 2 mHz and an amplitude $\Delta\widehat{T}$ = 2 K.

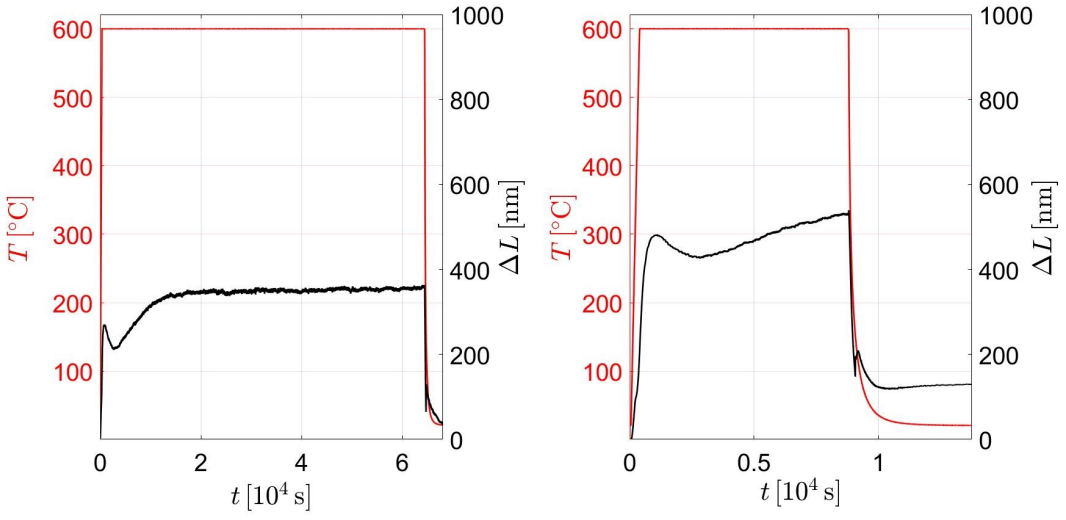

Figure 2.7: Testing any influence of the specimen holder by using two different sample holder inserts (SI in fig. 2.2) with a drill hole diameter for the fused silica tubes of 6.9 mm **(left)** and 7.2 mm **(right)**. Length change ΔL versus time t upon imposing temperature profile T(t).

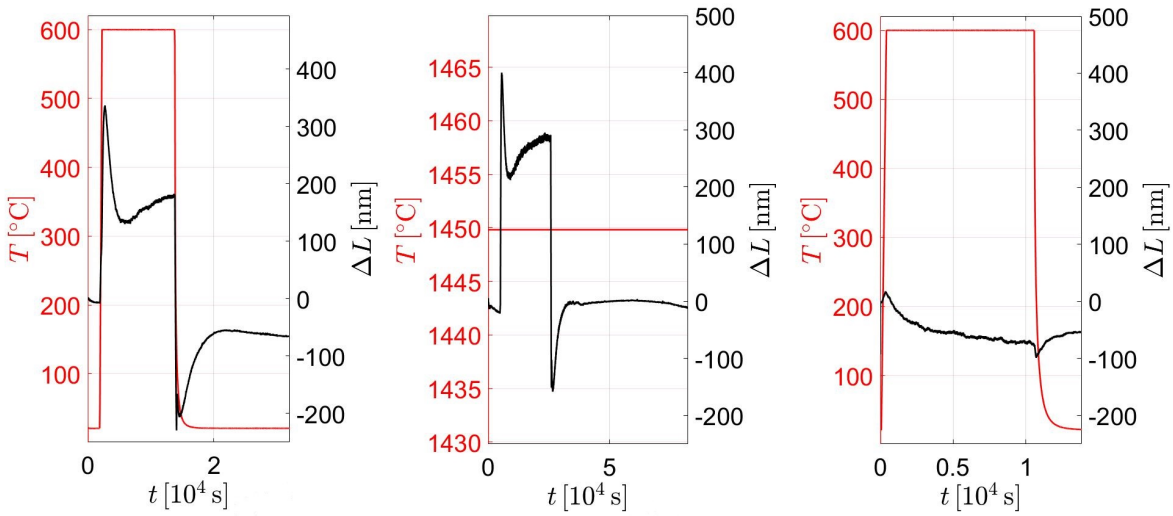

Figure 2.8: Testing any influence of the measuring plane, which corresponds to the surface the laser beams hit. Length change ΔL versus time t upon imposing temperature profile T(t). **Left:** Specimen holder; **Middle:** Drill hole of sample holder insert covered; **Right:** Transparent fast-entry door (see fig. 2.3).

can lead to quite large errors. Therefore, we used two sample holder inserts (SI in fig. 2.2) with a different drill hole diameter for the fused silica tubes, which is where the sample is put in. We concluded that the sample holder with a drill hole diameter of 6.9 mm improved indeed the quality of the measurement significantly as this can be seen in fig. 2.7.

Then we investigated the measuring plane, which corresponds to the surface the laser beams hit. In fig. 2.8[4] one can see that as long as the measuring plane is outside the chamber (chamber lid) the systematic variation stays small, which is why we concluded that the source of the systematic variation has to lie inside the chamber. If there had not been any significant difference between any of these three measurements, the conclusion could have been that, since the interferometer is mounted on a bridge, it could get skew with respect to the chamber when heating up. This would have resulted in a systematic variation regardless of the measuring plane.

[4]The measurement in the middle shows a constant temperature of 1450 °C, which was due to an error of the temperature sensor. The temperature profile is the same as for the first and last measurement.

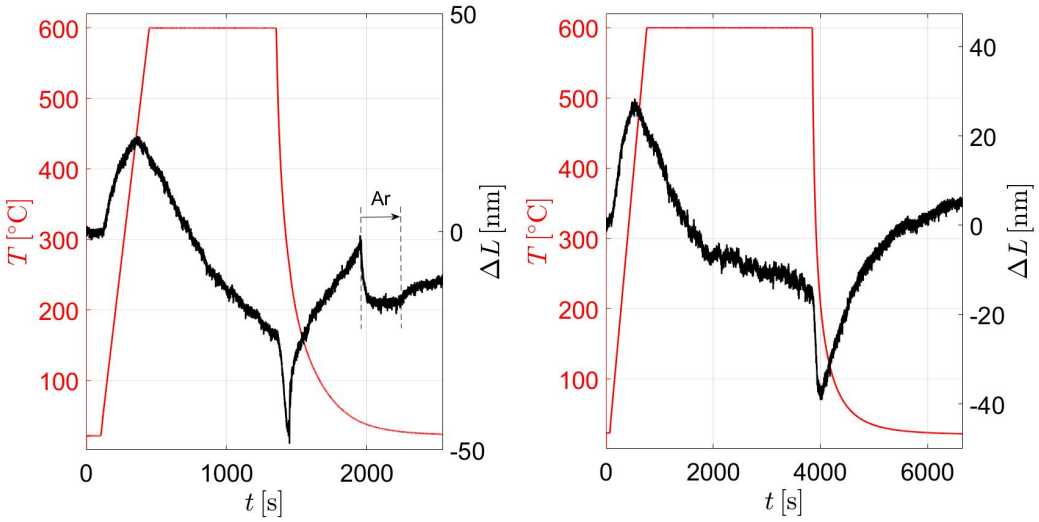

Figure 2.9: Testing any influence of Ar. Length change ΔL versus time t upon imposing temperature profile T(t). **Left:** With Argon (indicated by vertical lines); **Right:** No Argon.

Since the systematic variation mainly occurs for large temperature differences we took a measurement where we let Argon, which has a cooling effect, inside the chamber for a short while (fig. 2.9), where we chose the measurement plane to be the transparent fast-entry door. This turned out to have a great impact on the length measurement since at the time, when the Argon is let in, the length rapidly decreases and stays at a constant value until the Argon is turned off (left plot). In contrast to that one can see that without any Argon the length continuously increases (right plot). This effect might be explained by a cool down of the furnace due to the Argon.

Since up to now the measurements showed strong indication for the influence of the temperature, we further investigated different methods for cooling the system and chose the specimen holder as the measuring plane for all subsequent measurements. At this point it should be mentioned that while performing these measurements we noticed that the bottom of the chamber was quite hot, which should not be the case because the water of the recirculating chiller should keep the system at moderate temperatures. We therefore put a fan in front of the dilatometer to increase the air flow around the measurement setup. In fig. 2.10 three measurements are shown. For the one in the middle the fan was put to different positions while the

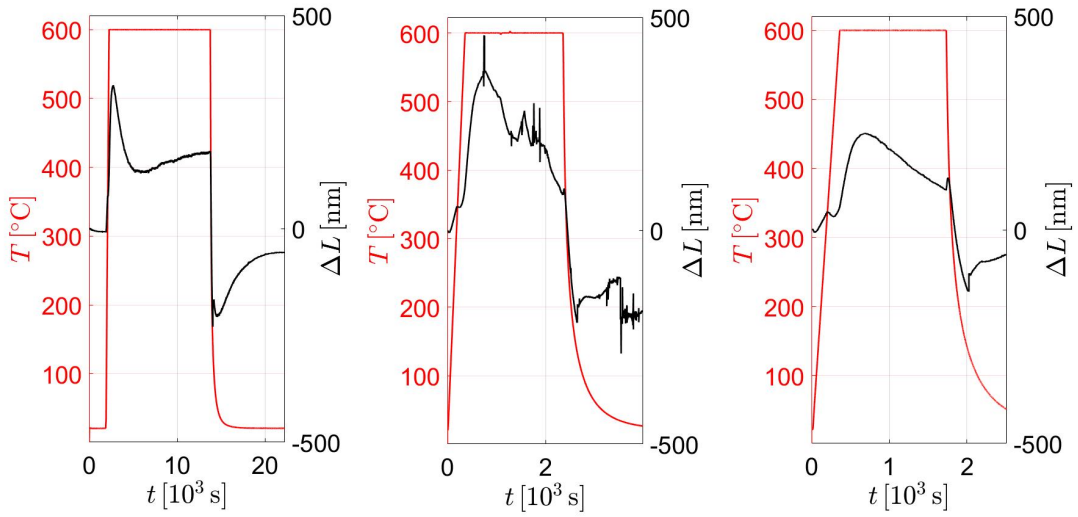

Figure 2.10: Testing any influence of an outside air flow. Length change ΔL versus time t upon imposing temperature profile T(t). **Left:** No air stream; **Middle:** Fan at different positions; **Right:** Air stream coming from the upper left corner.

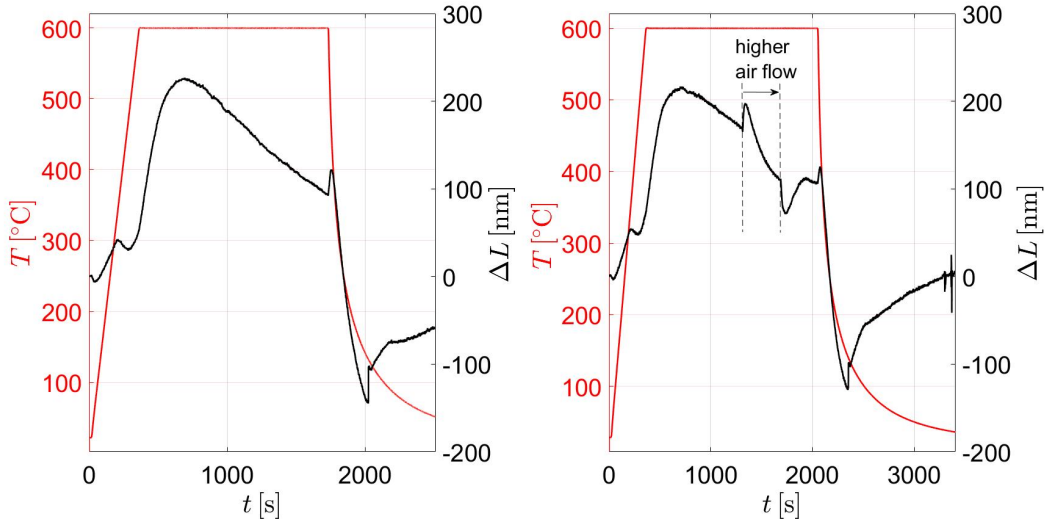

Figure 2.11: Testing any influence of the air flow, which is cooling the lamps. Length change ΔL versus time t upon imposing temperature profile T(t). **Left:** Automatic control; **Right:** Manual control (higher air flow indicated by vertical lines).

measurement was running. After another few measurements the most effective position for the fan was concluded to be in the upper left corner, for which we conducted a measurement with the same temperature profile again. By looking at the right plot in fig. 2.10 the influence of the fan is evident since the peaks of the length upon the fast temperature changes are significantly smaller than in the left plot.

We also had a try on how changing the air flow through the fused silica tubes, which is cooling the lamps, affects the systematic variation. We did this by setting the air flow manually instead of having the automatic control, which sets the air flow to a value that the lamps are within their optimum temperature range. As shown in fig. 2.11 also in this case a significant influence on the length measurement could be observed.

2.3 Conclusion

After all these measurements we came to the conclusion that there are three reasons for the large systematic variations: the **first reason** is the direct influence of the specimen holder as this becomes obvious when looking at fig. 2.7. The origin of the other two reasons becomes evident in fig. 2.12, where we had a look at the other two sensors, from which one is inside the chamber measuring the furnace temperature while the other one is measuring the room temperature. We can see that the furnace temperature, which should stay constant as in the case of the room temperature, is going up and down just in the same time range as the systematic variation occurs. This contributes to the large systematic variation in two ways: Due to the heating up the furnace itself is expanding asymmetrically (**second reason**), which affects the length measurement, and, in addition, the heating up of the bottom plate of the vacuum chamber causes the furnace in the vacuum chamber to tilt with respect to the bottom plate as indicated by the green arrows in fig. 2.13 (**third reason**).

Since we now know that the systematic variation is caused by the heating up of the chamber, we have to find a way to avoid this. Therefore, we need to analyze the whole system in terms of heat sinks and sources (see fig. 2.13). In section 2.1 we saw that the lamps are cooled by a stream of air going through the fused silica tubes (T in fig. 2.2 and yellow part in fig. 2.13) from the top to the bottom. The copper plate in fig. 2.3 is the one where the water of the recirculating chiller is running through.

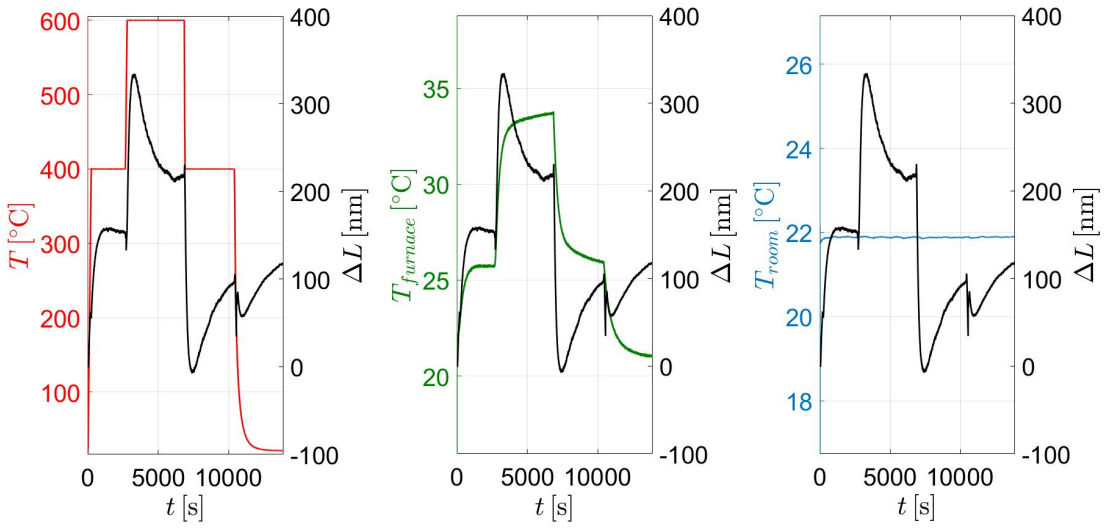

Figure 2.12: Testing any influence of the furnace and environmental temperature. Length change ΔL versus time t upon imposing temperature profile T(t). **Left:** Specimen temperature; **Middle:** Furnace temperature; **Right:** Room temperature.

Beneath this plate there is the bottom plate (see fig. 2.3) which is not water-cooled (this is the plate which was hot during the measurements as mentioned before). The hot air stream going through the copper and the bottom plate usually should be cooled down to low enough temperatures at the copper plate to ensure that the bottom plate is not heating up. However, as seen in fig. 2.12 this holds only for lower temperatures since the heating up of the furnace increases with increasing measuring temperatures, i.e. at a measuring temperature of 400 $^\circ\mathrm{C}$ (left plot) the furnace temperature is 26 $^\circ\mathrm{C}$ (right plot), whereas at 600 $^\circ\mathrm{C}$ the furnace temperature goes up to 34 $^\circ\mathrm{C}$. The reason for this lies in the fused silica tube, which goes over into an aluminum tube when going through the copper plate (horizontal, dashed line in fig. 2.13). This causes the heat to dissipate into the system even faster than it would if we had a fused silica tube at the bottom plate due to the much higher thermal conductivity of aluminum compared to fused silica.

Therefore, our solution to counteract the heating up of the system is to put a fused silica tube inside this aluminum tube, where the hot air is going through. This thermally isolates the bottom plate from the hot air stream. In addition, the bottom plate will be water-cooled too (as this is already the case for the copper plate) allowing us to go to much higher temperatures while keeping the systematic variation small.

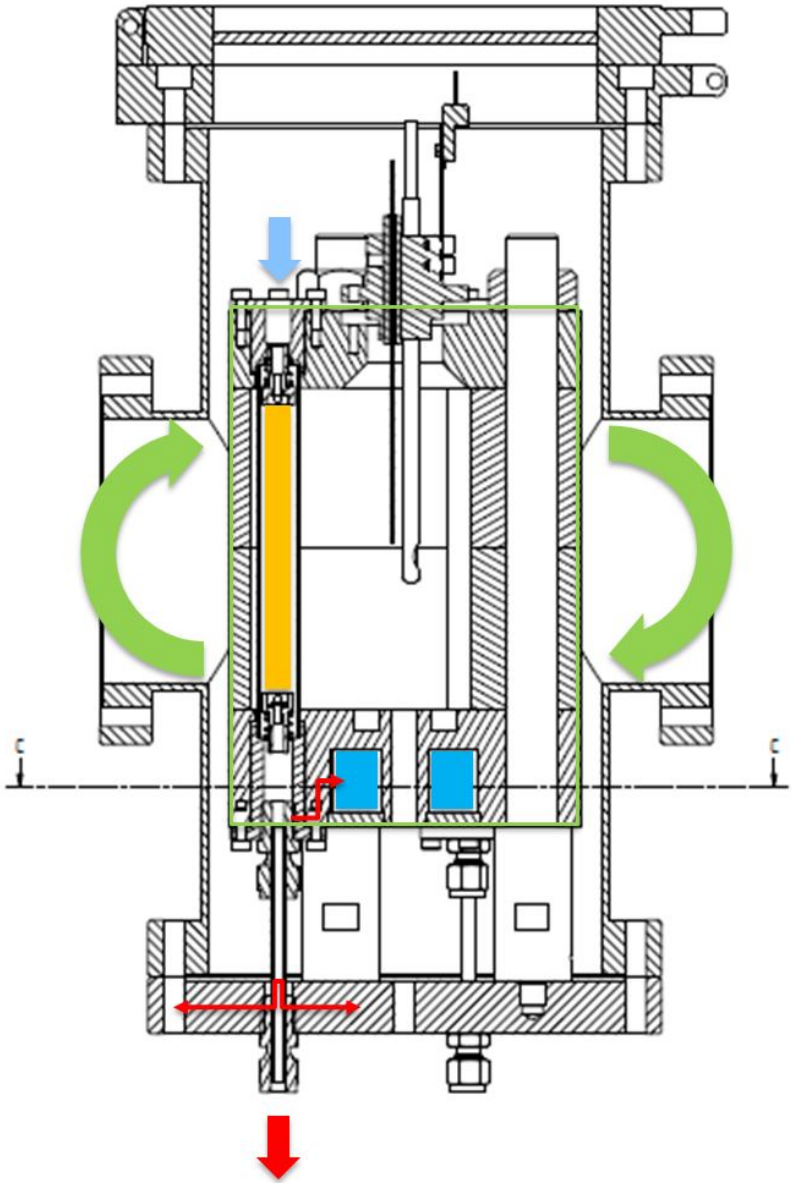

Figure 2.13: Longitudinal cut of the dilatometer showing the air stream, which is cooling the lamps (yellow) and going from the top to the bottom, while dissipating heat into the system (red arrows). The water-cooled (blue) copper plate is absorbing the heat, while at the bottom plate the heat is just heating up the bottom plate and the connected parts asymmetrically. This causes the furnace to tilt (green), which results in a deterioration of the measurement quality.

3 Basics on Vacancy Formation and Migration and thermal Expansion

3.1 Vacancy Formation

Vacancy concentration:
The absolute vacancy concentration at a given temperature in equilibrium is given as follows:

$$C_V = e^{-\frac{G_V^F}{kT}} = e^{\frac{S_V^F}{k}} e^{-\frac{H_V^F}{kT}}, \tag{3.1}$$

where T denotes the temperature, S_V^F the vacancy formation entropy and H_V^F the vacancy formation enthalpy.

Usually the formation entropy S_V^F and the formation enthalpy H_V^F are determined by means of differential dilatometry, where the length change (dilatometer) and the change of the lattice constant (XRD) are measured at the same time, or time-dependent dilatometry (see [3] and this work). By means of positron annihilation spectroscopy (see [4]) only the formation enthalpy H_V^F and the prefactor $\sigma e^{\frac{S_V^F}{k}}$ can be determined, where σ denotes the specific trapping rate and k the Boltzmann constant.

Relation between vacancy concentration and relative length change:
A change in the number of vacancies ΔN_V caused by e.g. a temperature change corresponds to a change in length $(\Delta L)^{Vac}$ of the sample due to vacant lattice sites. Since C_V is defined as the ratio between vacancies and lattice sites containing atoms, one can write down a relation between the change in vacancy concentration and the resulting length change, where one has to consider that the volume of a lattice site and the volume of a lattice vacancy are not the same due to lattice relaxation effects, which are taken into account by the relaxation parameter r: [5]

$$\frac{(\Delta L)^{Vac}}{L_{ref}} \approx \frac{1}{3}\frac{(\Delta V)^{Vac}}{V_{ref}} = \frac{1}{3}(1-r)\frac{\Delta N_V}{N} = \frac{1}{3}(1-r)\,\Delta C_V, \tag{3.2}$$

where ΔN_V is the change of the number of vacancies, N the number of atoms, r the relaxation parameter, $(\Delta V)^{Vac}$ ($(\Delta L)^{Vac}$) the change in volume (length) due to vacancies, V_{ref} (L_{ref}) the specimen volume (length) at RT and ΔC_V the change of

the vacancy concentration.

3.2 Vacancy Migration

When heating a material two effects come into play with respect to thermally induced length changes [3]:

Contribution of the lattice:
The greatest part is due to the change of the lattice constant. The reason for this change lies in the type of the atomic potential which is anharmonic and therefore is getting broader with increasing temperature, i.e. the lattice constant gets larger with increasing temperature. The expansion due to the lattice constant is described by the thermal expansion coefficient, which depends on the temperature:

$$\alpha = \frac{1}{L_{ref}} \frac{\mathrm{d}L}{\mathrm{d}T}. \tag{3.3}$$

Contribution of the vacancies:
The other part arises from the formation of thermal vacancies, which is, in contrast to the lattice expansion, delayed with the time constant given by

$$\frac{1}{\tau} = \frac{1}{\tau_0} e^{-\frac{H_V^M}{kT}}, \tag{3.4}$$

where T denotes the temperature, τ_0 the preexponential factor and H_V^M the vacancy migration enthalpy.

The pre-exponential factor is given by [4]

$$\frac{1}{\tau_0} = \xi \nu_0 \frac{Z}{N} e^{-\frac{S_V^M}{k}},$$

where S_V^M is the migration entropy, Z the coordination number, N the mean number of jumps per vacancy to a sink, ξ a geometrical factor and ν_0 the attempted frequency of the order of the Debye frequency.

The preexponential factor τ_0 and the vacancy migration enthalpy H_V^M can be determined by positron annihilation spectroscopy (see [4]) or time-dependent dilatometry

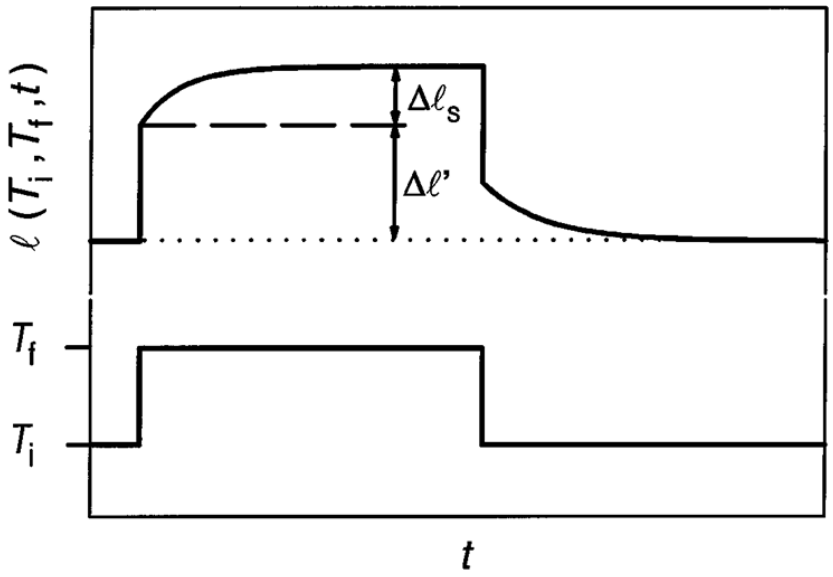

Figure 3.1: Schematic representation of a time-dependent dilatometry measurement according to [3], where the temperature instantly jumps from temperature T_i to T_f exhibiting two length change mechanisms: an instantaneous $\Delta l'$ due to the change of the lattice constant and a delayed Δl_s due to the formation and migration of thermal vacancies. Reprinted with permission from [3]. Copyright (2020) by the American Physical Society.

(see [3] and this work).

For a visualization of the two expansion mechanisms, we have a look at a schematic representation of an idealized time-dependent dilatometry measurement as performed in [3]. In such a measurement the temperature instantly jumps from temperature T_i to T_f resulting in an instantaneous length change due to the lattice and a delayed length change due to the vacancies. This is shown in fig. 3.1 with the corresponding relation as follows: [5]

$$l = l_0(T_i) + \Delta l'(T_i, T_f) + \Delta l_s(T_i, T_f)(1 - e^{-\frac{t}{\tau(T_f)}}),$$

where $\Delta l'$ denotes the instantaneous length change due to the change of the lattice constant and Δl_s the time-delayed length change due to vacancies.

It has to be noted that time-dependent dilatometry measurements are suitable if the

[5] This relation only holds as long as there is only one diffusion coefficient for the vacancies.

condition $\frac{H_V^M}{H_V^F} > 1$ is satisfied, i.e. there have to be a lot of vacancies while the diffusion of these vacancies should be rather slow. This is the case for B2 intermetallics, which is why we are studying $Fe_{62}Al_{38}$ in this work.[6] (For pure metals this ratio is usually $\frac{H_V^M}{H_V^F} \leq 1$) [3]

[6] Other suitable materials are discussed later. (tab. 5.5)

4 Modelling of Vacancy Kinetics for a modulated Temperature Profile

In this chapter a formula for the overall length change for a modulated temperature profile superimposed to time-linear heating will be derived first. Based on this formula two approaches for the evaluation of measurements with this temperature profile will be presented, from which it is possible to determine the material parameters for vacancy formation and migration. In addition, the idea of more complicated alternatives to the two elaborated approaches will be presented.

4.1 Vacancy Kinetics for a modulated Temperature Profile at constant average Temperature

4.1.1 Derivation

In the following we will derive a formula for the time-dependent vacancy concentration in case of a sinusoidal temperature profile. For this purpose, we first derive two formulae, the first of which describes the change of the vacancy concentration upon a small change in temperature and the second of which describes the relaxation behavior, i.e. the time-dependent behavior at a given temperature in case of an initial excess vacancy concentration. Then we combine these two equations and solve the resulting differential equation for a sinusoidal temperature profile.

Initial equations:

Variation of the vacancy concentration C_V:
Since our sinusoidal temperature profile only has an amplitude of a few Kelvin, we only look at small temperature changes $\Delta T = T - T_0$, where T_0 is the average temperature.
Therefore we start out with eq. (3.1) and carry out a Taylor series expansion at the point T_0 with the corresponding vacancy concentration $C_V(T_0) = C_{V,0}$. So we are looking at the change of the vacancy concentration $\Delta C_{V,0}$ with respect to the average vacancy concentration $C_{V,0}$, i.e. $\Delta C_{V,0}(T) = C_V(T) - C_V(T_0)$.
We make the assumption that there are only small variations of $\Delta C_{V,0}$ upon small

changes in temperature $\Delta T = T - T_0$ around the point T_0, so we just consider the first term, which is the derivative with respect to the temperature times the difference in temperature $\Delta T = T - T_0$:

$$\left.\frac{\mathrm{d}C_V}{\mathrm{d}T}\right|_{T=T_0} = C_{V,0}\frac{H_V^F}{kT_0^2}. \tag{4.1}$$

This leads to

$$\Delta C_{V,0}(T) = C_V(T) - C_V(T_0) = C_{V,0}\frac{H_V^F}{kT_0}\frac{\Delta T}{T_0}, \tag{4.2}$$

where $C_{V,0}$ is the vacancy concentration at the average temperature T_0 (cf. eq. (3.1)) and $\Delta C_{V,0}$ denotes the change of the vacancy concentration upon a small change in temperature.

Until now we just treated the vacancy concentration without any time-dependencies, which means that $\Delta C_{V,0}$ corresponds to the vacancy concentration in equilibrium.

Relaxation:

Now the time-dependency comes into play. As a first step we assume a specimen with an initial excess vacancy concentration ΔC_V^{ini} with respect to the equilibrium concentration. Without any further influence of the temperature, i.e. constant temperature, the evolution of the excess vacancy concentration $\Delta C_V(T)$ is given by the relaxation equation (homogeneous equation):

$$\frac{\mathrm{d}\Delta C_V(t)}{\mathrm{d}t} + \frac{\Delta C_V(t)}{\tau} = 0,$$

where vacancies annihilate with a time constant τ, which is given by eq. (3.4).

Solving this equation gives (see fig. 4.1):

$$\ln\frac{\Delta C_V(t)}{\Delta C_V^{ini}} = -\left.\frac{t'}{\tau}\right|_0^t = -\frac{t}{\tau},$$

which leads to

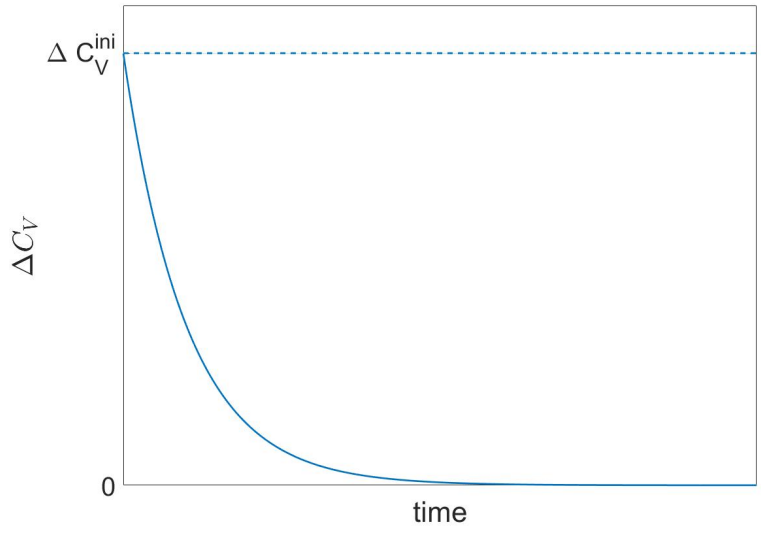

Figure 4.1: Sketch of the solution of the homogeneous equation (eq. (4.3)), which describes the relaxation process with the time constant τ upon an initial excess vacancy concentration ΔC_V^{ini}, where ΔC_V denotes the difference between the current vacancy concentration and the equilibrium concentration.

$$\Delta C_V(t) = \Delta C_V^{ini} e^{-\frac{t}{\tau}}. \tag{4.3}$$

Now the state of the sample is changed continuously, e.g. by changing its temperature with respect to a reference temperature T_0, which results in the inhomogeneous differential equation ($\Delta C_{V,0} \neq const.$)

$$\frac{\mathrm{d}\Delta C_V(t)}{\mathrm{d}t} + \frac{\Delta C_V(t)}{\tau} = \frac{1}{\tau}\Delta C_{V,0}(t) \tag{4.4}$$

with $\Delta C_{V,0}(t)$ being the deviation in equilibrium concentration between $T(t)$ and T_0, i.e. $\Delta C_{V,0}(t) = C_V(T(t)) - C_V(T_0)$.

To get a more intuitive understanding of this equation, it shall be mentioned here that in equations of this type the right side, i.e. $\Delta C_{V,0}(t)$, is sometimes considered as some type of driving force, while the left side of such equations describes the time-dependent behavior. So we could think of it as $\Delta C_{V,0}(t)$ being the equilibrium concentration for the current temperature $T(t)$, while the left side, i.e. $\Delta C_V(t)$, is trying to catch up with this equilibrium state, which it only will do in case of constant temperature as seen in fig. 4.1 and fig. 4.2.

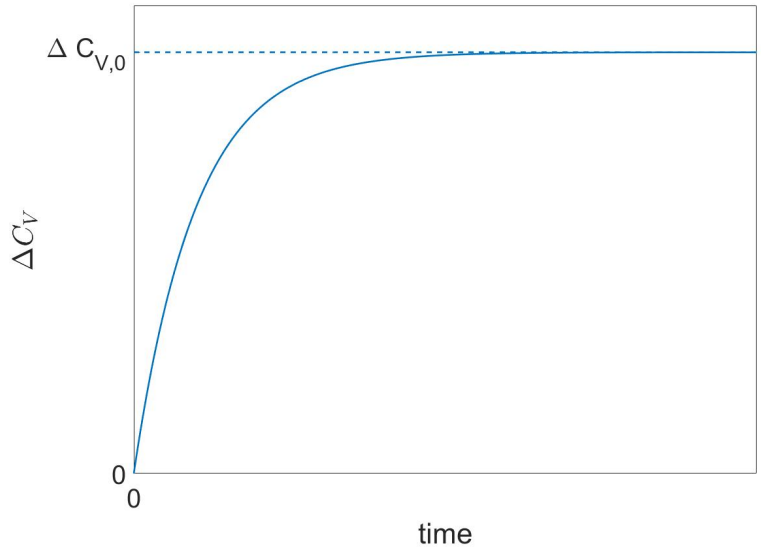

Figure 4.2: Sketch of the solution of the inhomogeneous equation (eq. (4.4)), which describes the relaxation process with the time constant τ upon a deviation of the equilibrium concentration $\Delta C_{V,0} = const.$, where ΔC_V denotes the difference between the current vacancy concentration and the equilibrium concentration.

In case of $\Delta C_{V,0} = const.$ for the inhomogeneous equation, the solution is $\Delta C_V = \Delta C_{V,0}(1 - e^{-\frac{t}{\tau}})$, i.e. the exponential function just goes upwards and converges at $\Delta C_{V,0}$ as shown in fig. 4.2.

Limiting cases:

For $\tau \to 0$ the vacancy concentration changes instantly with temperature, which means that it is always in equilibrium. Therefore, the current change in vacancy concentration ΔC_V is equal to the change in equilibrium concentration $\Delta C_{V,0}$:

$$\tau \to 0 : \Delta C_V = \Delta C_{V,0}(t). \tag{4.5}$$

For $\tau \to \infty$ the vacancy concentration doesn't change at all since the process requires infinite time:

$$\tau \to \infty : \frac{\mathrm{d}\Delta C_V}{\mathrm{d}t} = 0. \tag{4.6}$$

Insert $\Delta C_{V,0}$ from eq. (4.2) into inhomogeneous equation (4.4):

Now we consider only a sinusoidal temperature profile with a small amplitude, for which deviations in the average vacancy concentration may be approximated by eq. (4.2) with $\Delta T(t) = T(t) - T_0 = \Delta\widehat{T}\sin\omega t$, which becomes

$$\begin{aligned}\frac{\mathrm{d}\Delta C_V}{\mathrm{d}t} + \frac{\Delta C_V}{\tau} &= \frac{1}{\tau}\Delta C_{V,0}(t) = \\ &= \frac{1}{\tau} C_{V,0}\frac{H_V^F}{kT_0}\frac{\Delta\widehat{T}}{T_0}\sin\omega t.\end{aligned} \tag{4.7}$$

We already solved the homogeneous differential equation (see eq. (4.3)).

The ansatz for the inhomogeneous differential equation is as follows:

$$\Delta C_V = b\,\sin\omega t + c\,\cos\omega t. \tag{4.8}$$

Inserting eq. (4.8) into eq. (4.7) gives

$$b\,\omega\,\cos\omega t - c\,\omega\,\sin\omega t + \frac{b}{\tau}\,\sin\omega t + \frac{c}{\tau}\,\cos\omega t = \frac{C_{V,0}\frac{H_V^F}{kT_0}\frac{\Delta\widehat{T}}{T_0}}{\tau}\,\sin\omega t,$$

which leads to

$$\cos\omega t\,\left(b\,\omega + \frac{c}{\tau}\right) + \sin\omega t\,\left(-c\,\omega + \frac{b}{\tau} - \frac{C_{V,0}\frac{H_V^F}{kT_0}\frac{\Delta\widehat{T}}{T_0}}{\tau}\right) = 0.$$

Since each expression in brackets must be zero, one gets two equations for two variables, from which the prefactors b and c can be determined, namely

$$b = \frac{C_{V,0}\frac{H_V^F}{kT_0}\frac{\Delta\widehat{T}}{T_0}\frac{1}{\tau}}{\omega^2 + \frac{1}{\tau^2}}\frac{1}{\tau} \quad \text{and} \quad c = -\frac{C_{V,0}\frac{H_V^F}{kT_0}\frac{\Delta\widehat{T}}{T_0}\omega}{\omega^2 + \frac{1}{\tau^2}}\frac{1}{\tau}.$$

Inserting this result into the Ansatz for the inhomogeneous equation (eq. (4.8)) gives

$$\Delta C_V(t) = C_{V,0}\frac{H_V^F}{kT_0}\frac{\Delta\widehat{T}}{T_0}\frac{1}{\tau}\frac{1}{\omega^2 + \frac{1}{\tau^2}}\left(\frac{1}{\tau}\sin\omega t - \omega\cos\omega t\right). \tag{4.9}$$

Limiting cases:

For the same reasons as in eq. (4.5) and (4.6) (always equilibrated for $\tau \to 0$ and remains in the initial state for $\tau \to \infty$) we get

$$\tau \to 0 : \Delta C_V = C_{V,0} \frac{H_V^F}{kT_0} \frac{\Delta \widehat{T}}{T_0} \sin \omega t$$

and

$$\tau \to \infty : \Delta C_V = 0.$$

Phase shift:

From the general relation between the phase shift and the sum of a sine- and cosine-function

$$A \sin(\omega t + \varphi) = a \sin \omega t + b \cos \omega t$$

one gets the new amplitude with the corresponding phase shift:

$$A = \sqrt{a^2 + b^2} = \sqrt{\frac{1}{\tau^2} + \omega^2} \quad \text{and} \quad \tan \varphi = \frac{b}{a} = -\omega\tau. \tag{4.10}$$

Putting everything together (eq. (4.9) and (4.10)) gives the final formula:

$$\begin{aligned} \Delta C_V(t) &= C_{V,0} \frac{H_V^F}{kT_0} \frac{\Delta \widehat{T}}{T_0} \frac{1}{\tau} \frac{1}{\sqrt{\omega^2 + \frac{1}{\tau^2}}} \sin(\omega t + \varphi) \\ &= C_{V,0} \frac{H_V^F}{kT_0} \frac{\Delta \widehat{T}}{T_0} \frac{1}{\sqrt{\omega^2 \tau^2 + 1}} \sin(\omega t + \varphi). \end{aligned}$$

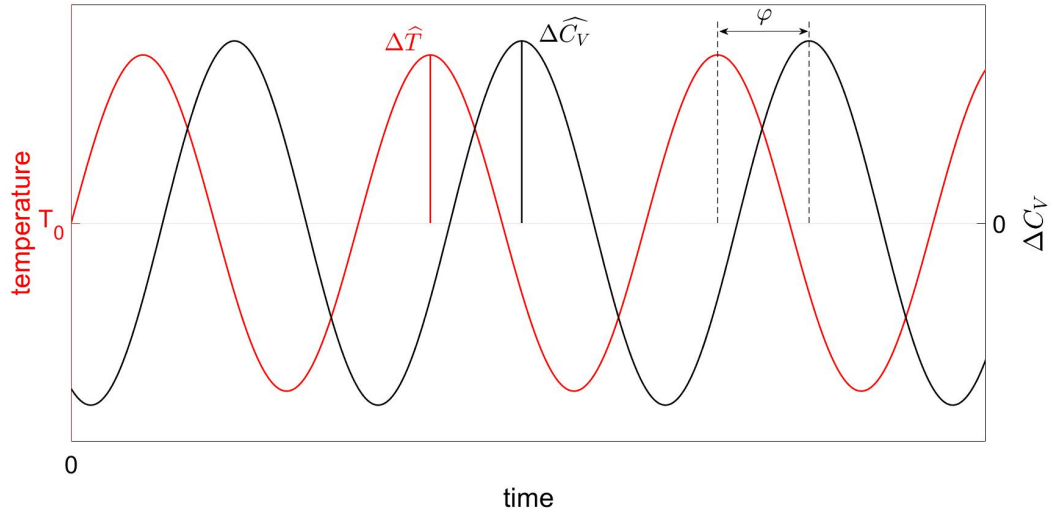

Figure 4.3: Sketch of the time-dependent vacancy concentration ΔC_V (black) (eq. (4.11)) in case of a sinusoidal temperature profile at constant average temperature T_0 (red).

4.1.2 Result

The major result for ΔC_V is summarized in eq. (4.11) once more:

$$\Delta C_V(t) = C_{V,0}\frac{H_V^F}{kT_0}\frac{\Delta\widehat{T}}{T_0}\frac{1}{\sqrt{\omega^2\tau^2+1}}\sin(\omega t+\varphi)$$
$$\text{with} \quad \varphi = \arctan(-\omega\tau), \tag{4.11}$$

where $C_{V,0}$ is the vacancy concentration at the average temperature T_0 (eq. (3.1)) and τ denotes the time constant at the average temperature T_0 (eq. (3.4)).

Eq. (4.11) describes the time-dependent vacancy concentration in case of a sinusoidal temperature profile with respect to the average vacancy concentration $C_V(T_0) = C_{V,0}$, i.e. $\Delta C_V(t) = C_V(T(t)) - C_V(T_0)$. The solution is schematically plotted in fig. 4.3.

ΔC_V is lagging behind the sine wave of the temperature, while the amplitude and the phase shift depend on the temperature T_0 and the modulation frequency ω (see below).

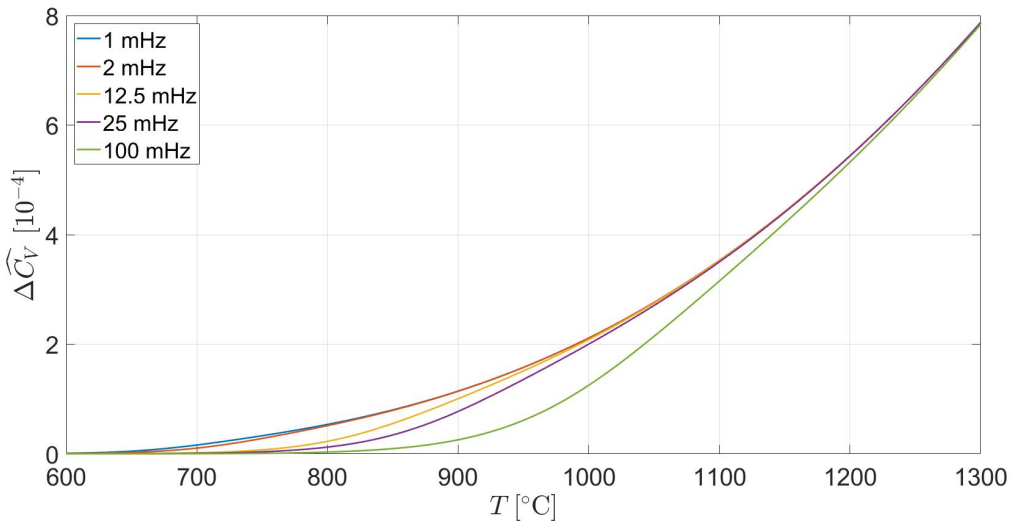

Figure 4.4: Amplitude $\Delta\widehat{C_V}$ (eq. (4.12)) of the time-dependent vacancy concentration in case of a sinusoidal temperature profile for various modulation frequencies with a temperature amplitude of $\Delta\widehat{T} = 2\,K$ ($Fe_{55}Al_{45}$: $H_V^M = 1.5\,\mathrm{eV}$, $\tau_0^{-1} = 4 \times 10^5\,\mathrm{s}^{-1}$, $H_V^F = 1\,\mathrm{eV}$, $\frac{S_V^F}{k} = 4.9$; cf. tab. 5.1 and 5.4: [3], index 1).

In general ΔC_V depends on the material properties, which are given by τ_0, H_V^M, S_V^F and H_V^F, the temperature modulation, given by T_0, $\Delta\widehat{T}$ and ω, and the time.

The amplitude $\Delta\widehat{C_V}$ of eq. (4.11) is given by

$$\Delta\widehat{C_V} = C_{V,0}\frac{H_V^F}{kT_0}\frac{\Delta\widehat{T}}{T_0}\frac{1}{\sqrt{\omega^2\tau^2+1}}$$

$$\text{with} \quad C_{V,0}(T_0) = e^{\frac{S_V^F}{k}}e^{-\frac{H_V^F}{kT_0}} \quad \text{(eq. (3.1))} \qquad (4.12)$$

$$\frac{1}{\tau(T_0)} = \frac{1}{\tau_0}e^{-\frac{H_V^M}{kT_0}} \quad \text{(eq. (3.4))}.$$

The amplitude is plotted in fig. 4.4 as a function of temperature for various modulation frequencies ω. At low temperatures the time constant τ is high and therefore the amplitude goes to zero, whereas at high temperatures the time constant is so low that the specimen is equilibrated instantly, which means that $\Delta\widehat{C_V}$ converges to the vacancy concentration in equilibrium $C_{V,0}$ (eq. (3.1)). Our temperature range of

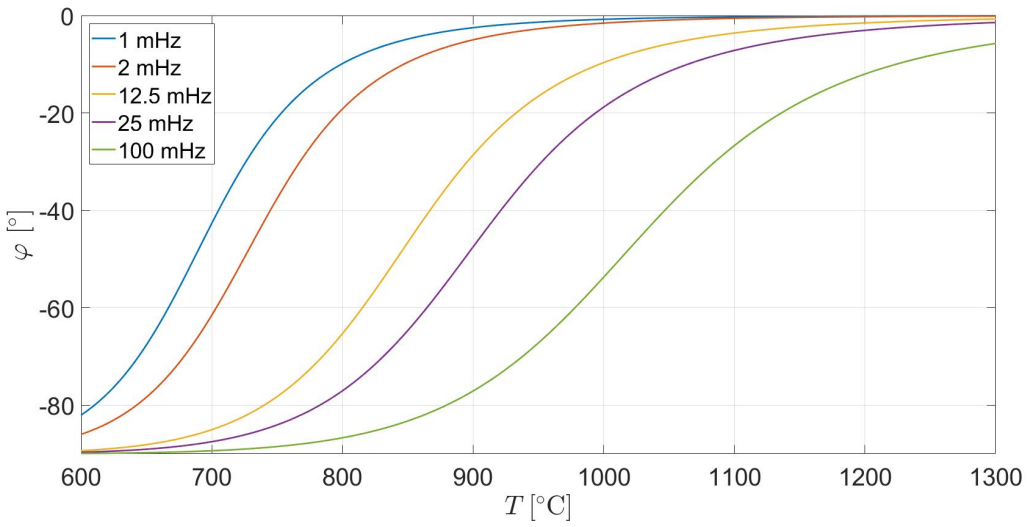

Figure 4.5: Phase shift φ (eq. (4.13)) of the time-dependent vacancy concentration in case of a sinusoidal temperature profile for various modulation frequencies ($Fe_{55}Al_{45}$: $H_V^M = 1.5\,\mathrm{eV}$, $\tau_0^{-1} = 4 \times 10^5\,\mathrm{s}^{-1}$; cf. tab. 5.1: [3], index 1).

interest lies in the area where the curves do not coincide. Otherwise we would get the same information from each measurement independent of the chosen modulation frequency. Later on the temperature range will be chosen by determining the time constants for various temperatures, which should lie somewhere in the range of the period duration of the modulation (cf. section 5.1).

The phase shift

$$\varphi = \arctan\left(-\omega\tau\right) \tag{4.13}$$

$$\text{with} \quad \frac{1}{\tau(T_0)} = \frac{1}{\tau_0} e^{-\frac{H_V^M}{kT_0}} \quad \text{(eq. (3.4))}$$

can also be plotted as a function of temperature for various modulation frequencies as shown in fig. 4.5. At low temperatures the time constant τ is high and therefore the vacancies can't catch up with the temperature, which results in a phase shift of $90°$, whereas at high temperatures the time constant is so low that the specimen is equilibrated instantly, which means that the phase shift converges to zero. Our temperature range of interest lies in the area where the slope is the highest, since only

then it is possible to assign our measured values, i.e. the phase shift, to a specific temperature accurately.

When comparing fig. 4.4 and 4.5, we can see that the temperature range, where the curves in fig. 4.4 do not coincide, corresponds to the temperature range, where the slope of the curves in fig. 4.5 is the highest, i.e. both criteria are met by one and the same temperature range. The reason for this is that within this temperature range the period duration of the modulation lies in the range of the time constant τ, which means that slightly different modulation frequencies will give us very different results, in contrast to the low and high temperature areas, where the time constant is already way too high or too low and a change of the modulation frequency would not have any effect.

4.2 Vacancy Kinetics for a modulated Temperature Profile with linear Increase of Temperature

4.2.1 Idea

The goal is to determine all material parameters (r, τ_0, H_V^M, S_V^F, H_V^F) with only a few measurements, where we also have to consider the lattice part (cf. section 3.2). Therefore, we linearly increase the average temperature (in addition to the modulation) in order to get information about the vacancy formation from the linear heating and about the vacancy formation and migration from the modulation.
For each measurement we can adjust the heating rate, the modulation frequency and the modulation amplitude.
The two most-promising approaches presented here require at least two measurements with very low heating rates in each case since we will assume the specimen to be equilibrated with respect to the average temperature T_0. Therefore, only the modulation frequency (and the amplitude if necessary) will be varied.

4.2.2 Temperature Profile

As already mentioned we apply a temperature profile, which has, in addition to the modulation, a linear increase in temperature (fig. 4.6), i.e.

$$T(t) = T_{start} + At + \Delta\widehat{T}\sin\omega t, \tag{4.14}$$

where T_{start} is the starting temperature, A the heating rate and $\Delta\widehat{T}$ the amplitude.

As discussed in section 3.2 thermal expansion arises from an increase of the lattice constant (instantaneous part) and due to vacancies, where we make the assumption that no other processes that could also change the volume (e.g. phase formations, phase transitions) are involved.

We will now look at the linear heating and the modulation separately, for which we will find a formula that describes the overall thermal expansion. Therefore, each formula consists of two summands, the first of which describes the expansion due to the change of the lattice constant and the second of which describes the expansion due to the formation of vacancies.

4.2.3 Linear Increase of Temperature At

We assume that the linear increase of the temperature (dotted line in fig. 4.6) is so slow that the specimen is equilibrated with respect to the average temperature T_0[7]. Therefore, we can use the formula for the vacancy concentration in equilibrium (eq. (3.1)) and together with eq. (3.2), which describes the relative length change upon a change in vacancy concentration, we get the overall expansion with respect to the linear increase in temperature:

$$\left(\frac{\Delta L}{L_{ref}}\right)^{HR} = \overbrace{\alpha At}^{\text{lattice}} + \overbrace{\frac{1}{3}(1-r)\left(C_{V,0}(T_{start}+At) - C_{V,0}(T_{start})\right)}^{\text{vacancies}}, \tag{4.15}$$

where A is the heating rate, α the thermal expansion coefficient, $C_{V,0}$ the vacancy concentration in equilibrium (eq. (3.1)) and HR denotes the contribution from the time-linear heating.

[7] The exact condition for the heating rate A is stated in section 4.3.4.

4.2.4 Temperature Modulation $\Delta\widehat{\mathrm{T}}\sin\omega\mathrm{t}$

Now we look only at the temperature modulation (fig. 4.6 without time-linear heating) and make the assumption that the specimen is in equilibrium with respect to the average temperature T_0. (Remember that the time-dependent vacancy concentration for a sinusoidal temperature profile ΔC_V is only valid for small temperature changes since we made a Taylor expansion where we just considered the first term (cf. sec. 4.1.1).)

Since we have a sinusoidal temperature profile we use eq. (4.11), which describes the time-dependent vacancy concentration for a sinusoidal temperature profile, and again eq. (3.2), which describes the relative length change upon a change in vacancy concentration, and get the overall expansion with respect to the temperature modulation:

$$\left(\frac{\Delta L}{L_{ref}}\right)^{Mod} = \left(\overbrace{\alpha\, T_0 \sin(\omega t)}^{\text{lattice}} + \overbrace{\frac{1}{3}(1-r)C_{V,0}(T_0)\frac{H_V^F}{kT_0}\frac{1}{\sqrt{\omega^2\tau^2+1}}\sin(\omega t+\varphi)}^{\text{vacancies}} \right) \frac{\Delta\widehat{T}}{T_0}, \tag{4.16}$$

where $\Delta\widehat{T}$ is the temperature amplitude, α the thermal expansion coefficient, $C_{V,0}$ the vacancy concentration in equilibrium (eq. (3.1)) and Mod denotes the contribution from the modulation.

4.2.5 Linear Heating (HR) and Modulation (Mod)

Now we put these two parts together to get the expansion for a temperature profile as stated in eq. (4.14), i.e. starting at T_{start} the average temperature T_0 is rising at a constant rate A, while there is a superimposed modulation with amplitude $\Delta\widehat{T}$ (fig. 4.6). In eq. (4.16) T_0 is replaced by $(T_{start}+At)$ since now the average temperature is changing over time. This also needs to be done for the time constant τ since it also depends on T_0. This gives

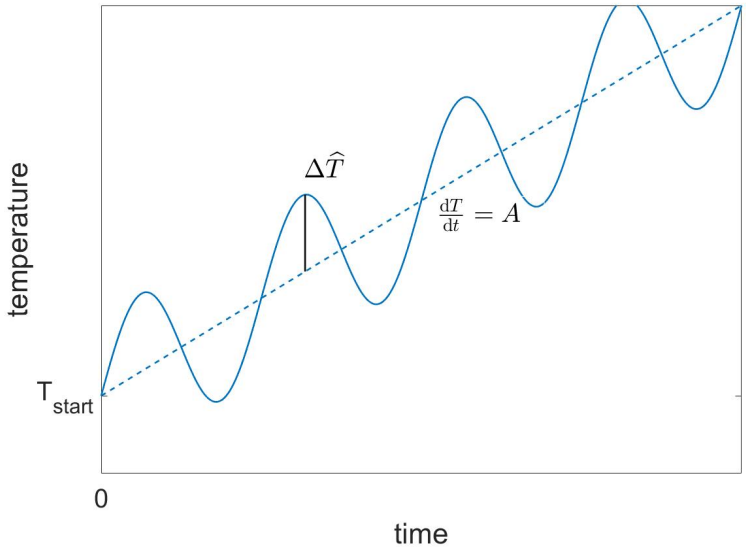

Figure 4.6: Time-linear heating with the heating rate A and with superimposed modulation (frequency $f = \frac{\omega}{2\pi}$), for which the corresponding length change is given by eq. (4.17).

$$
\begin{aligned}
\frac{\Delta L}{L_{ref}} &= \left(\frac{\Delta L}{L_{ref}}\right)^{HR,\,Lat} + \left(\frac{\Delta L}{L_{ref}}\right)^{HR,\,Vac} + \\
&+ \left(\frac{\Delta L}{L_{ref}}\right)^{Mod,\,Lat} + \left(\frac{\Delta L}{L_{ref}}\right)^{Mod,\,Vac} = \\
&= \overbrace{\alpha(T_0)At}^{\text{lattice (linear heating)}} + \\
&+ \overbrace{\frac{1}{3}(1-r)[C_{V,0}(T_0) - C_{V,0}(T_{start})]}^{\text{vacancies (linear heating)}} + \\
&+ \frac{\Delta\widehat{T}}{T_0}\left[\overbrace{\alpha(T_0)\,T_0\sin(\omega t)}^{\text{lattice (modulation)}} + \right. \\
&\left. + \overbrace{\frac{1}{3}(1-r)C_{V,0}(T_0)\frac{H_V^F}{kT_0}\frac{1}{\sqrt{\omega^2\tau^2+1}}\sin(\omega t+\varphi)}^{\text{vacancies (modulation)}}\right]
\end{aligned}
\qquad (4.17)
$$

with $T_0 = T_{start} + At$ and

$\varphi = \arctan(-\omega\tau)$,

where A is the heating rate, α the thermal expansion coefficient, $C_{V,0}$ the vacancy concentration in equilibrium (eq. (3.1)), $\Delta\widehat{T}$ the temperature amplitude, τ the time constant (eq. (3.4)), HR the contribution from the time-linear heating and Mod the contribution from the modulation.

The thermal expansion coefficient α (instantaneous length change due to the change of the lattice constant) is unknown and has to be subtracted from the measurement to get information about vacancies as we will see in the following (cf. section 4.3, 4.4 and 4.6).

4.3 First Approach: High- and Low-Frequency Measurement

4.3.1 Idea

When heating a material two effects come into play with respect to thermally induced length changes: The change of the lattice constant, which happens instantaneously, and a minor part, which arises from the formation of vacancies and is delayed by the time constant τ.
Now we take two linear heating measurements with a superimposed modulation, whereby one has a very high and the other one a low frequency. Since for high frequencies the vacancies have not enough time to migrate in or out of the material, the modulation part of the high-frequency measurement only consists of the lattice expansion, i.e. it is possible to directly determine the pure lattice expansion from the modulation of the high-frequency measurement. Since linear heating is involved, we get the expansion as a function of the temperature. With respect to length this means that we can get rid of the lattice contribution by multiplying the pure lattice expansion with the temperature profile of the low-frequency measurement and subtracting this from the low-frequency measurement leaving behind the pure vacancy signal as a response to linear heating with a superimposed modulation. Comparing it with the formula derived above (eq. (4.17)), the decisive parameters for vacancy formation and migration can be determined.

4.3.2 Procedure

For the procedure we split up each measurement into the corresponding summands given by eq. (4.17), where HR denotes the linear heating, Mod the modulation, Lat the lattice contribution, Vac the vacancy contribution, HF the high-frequency measurement and LF the low-frequency measurement, i.e.

$$\left(\frac{\Delta L}{L_{ref}}\right)_{HF} = \left(\frac{\Delta L}{L_{ref}}\right)_{HF}^{HR,\,Lat} + \left(\frac{\Delta L}{L_{ref}}\right)_{HF}^{HR,\,Vac} + \left(\frac{\Delta L}{L_{ref}}\right)_{HF}^{Mod,\,Lat} + \left(\frac{\Delta L}{L_{ref}}\right)_{HF}^{Mod,\,Vac},$$

$$\left(\frac{\Delta L}{L_{ref}}\right)_{LF} = \left(\frac{\Delta L}{L_{ref}}\right)_{LF}^{HR,\,Lat} + \left(\frac{\Delta L}{L_{ref}}\right)_{LF}^{HR,\,Vac} + \left(\frac{\Delta L}{L_{ref}}\right)_{LF}^{Mod,\,Lat} + \left(\frac{\Delta L}{L_{ref}}\right)_{LF}^{Mod,\,Vac}.$$

Subsequently, the steps of the procedure are listed.

1. $\left(\frac{\Delta L}{L_{ref}}\right)_{HF}^{Mod,\,Vac}$ is assumed to be negligible.
2. The moving average of HF is given by the sum:
$$\left(\frac{\Delta L}{L_{ref}}\right)_{HF}^{HR,\,Lat} + \left(\frac{\Delta L}{L_{ref}}\right)_{HF}^{HR,\,Vac}.$$
3. Subtract the moving average from HF and calculate the thermal expansion coefficient α by dividing the length amplitude $\Delta\widehat{L}$ by the temperature amplitude $\Delta\widehat{T}$ and the specimen length L_{ref}. [8]
Usually there is a phase shift involved originating from the vacancy part (cf. eq. (4.11)) but since the vacancy part is zero, there is no phase shift and we can directly calculate the thermal expansion coefficient without considering any phase shift (fig. 4.9): [9]
$$\left(\frac{\Delta L}{L_{ref}}\right)_{HF}^{Mod,\,Lat} = \alpha\,\Delta\widehat{T}\,\sin(\omega_{high}t) \rightarrow \alpha(T).$$

[8] Instead of calculating the moving average, we could also just directly calculate the average of each period and get the amplitude from the difference between the minimum and the maximum of each period.

[9] Checking if the phase shift is zero is also a good way to check the applicability of the high-frequency measurement.

4. Subtract the starting temperature T_{start} from the temperature profile of LF[10] and multiply it with the thermal expansion coefficient α to get the lattice contribution of LF (Note that α is a function of the temperature due to the linear heating.):

$$\alpha(T)\,T(t)_{LF} = \left(\frac{\Delta L}{L_{ref}}\right)_{LF}^{HR,\,Lat} + \left(\frac{\Delta L}{L_{ref}}\right)_{LF}^{Mod,\,Lat}.$$

5. Subtract the lattice contribution of LF from LF to get the pure vacancy signal:

$$\left(\frac{\Delta L}{L_{ref}}\right)_{LF} - \alpha(T)\;T(t)_{LF} = \left(\frac{\Delta L}{L_{ref}}\right)_{LF}^{HR,\,Vac} + \left(\frac{\Delta L}{L_{ref}}\right)_{LF}^{Mod,\,Vac}.$$

6. Repeat steps 2 and 3 but now with LF, i.e. calculate the moving average of LF and subtract it from LF to get:

$$\left(\frac{\Delta L}{L_{ref}}\right)_{LF}^{HR,\,Vac} \quad \text{and} \quad \left(\frac{\Delta L}{L_{ref}}\right)_{LF}^{Mod,\,Vac}.$$

7. Calculate the parameters from

   - the linear heating:

$$\left(\frac{\Delta L}{L_{ref}}\right)_{LF}^{HR,\,Vac} = \frac{1}{3}(1-r)(C_{V,0}(T_0) - C_{V,0}(T_{start}))$$
$$\Rightarrow r,\; S_V^F, H_V^F$$

   - the phase shift of the modulation:

$$\varphi(T_0) = \arctan\left(-\omega\,\tau\right)$$
$$\Rightarrow \tau_0, H_V^M$$

   - the amplitude of the modulation:

$$\left(\frac{\Delta \widehat{L}}{L_{ref}}\right)_{LF}^{Mod,\,Vac} = \frac{1}{3}(1-r)C_{V,0}(T_0)\frac{H_V^F}{kT_0}\frac{1}{\sqrt{\omega^2\tau^2+1}}\frac{\Delta\widehat{T}}{T_0}$$
$$\Rightarrow r,\; S_V^F, H_V^F, \tau_0, H_V^M$$

[10] $T(t) = T_{start} + At + \Delta\widehat{T}\sin(\omega t)$ (eq. (4.14))

with $T_0 = T_{start} + At$,

$\varphi = \arctan(-\omega\tau)$ (eq. (4.11)),

$C_{V,0}(T_0) = e^{\frac{S_V^F}{k}} e^{-\frac{H_V^F}{kT_0}}$ (eq. (3.1)) and

$\frac{1}{\tau(T_0)} = \frac{1}{\tau_0} e^{-\frac{H_V^M}{kT_0}}$ (eq. (3.4)).

4.3.3 Requirements: Modulation Frequencies

For the conditions derived in section 4.3.3, 4.3.4 and 4.3.6 a reasonable value for the time constant τ at various temperatures, the formation enthalpy H_V^F and the formation entropy S_V^F has to be considered. These values are known for several FeAl-alloys, from which we will consider $Fe_{55}Al_{45}$ to get a reasonable estimate for the material investigated in this work, namely $Fe_{62}Al_{38}$. In addition, one could also take measurements as shown in fig. 3.1 with different temperature differences and to different temperatures to determine these values and compare it with literature values (cf. section 5.1).

There are two conditions that must be fulfilled with regard to the modulation part of the vacancies $\left(\frac{\Delta L}{L_{ref}}\right)^{Mod,Vac}$ (last summand in eq. 4.17):

- For the low-frequency measurement LF the amplitude must be higher than the measurement error of the setup $\Delta\Delta L$, i.e. $\left(\Delta\widehat{L}\right)_{LF}^{Mod,Vac} > \Delta\Delta L$.

- For the high-frequency measurement HF it must be negligible, i.e. $\left(\frac{\Delta L}{L_{ref}}\right)_{HF}^{Mod,Vac} \to 0$, which means that it should stay below the measurement error, i.e. $\left(\Delta\widehat{L}\right)_{HF}^{Mod,Vac} < \Delta\Delta L$.

For these conditions we need the relation between $\left(\frac{\Delta\widehat{L}}{L_{ref}}\right)_{LF}^{Mod,Vac}$ and $\Delta\widehat{C_V}$, which is

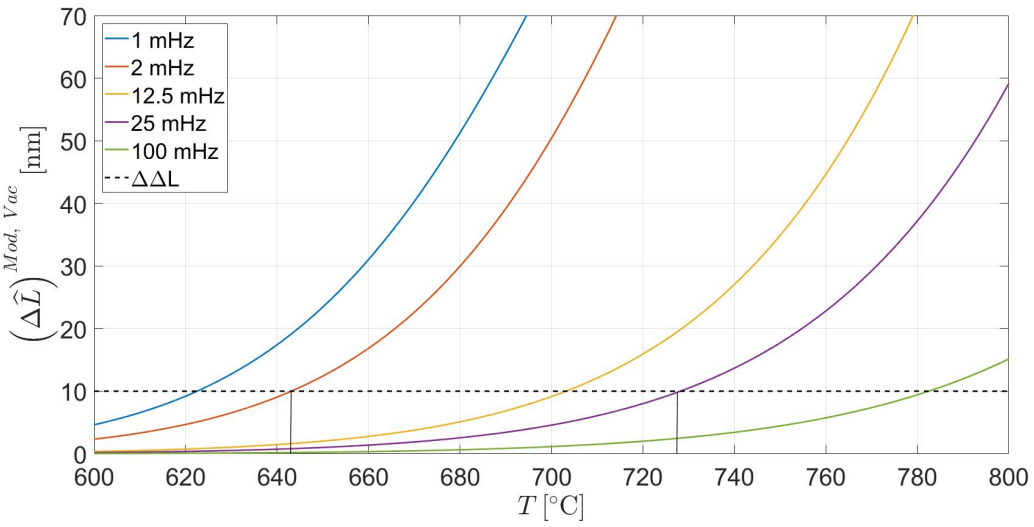

Figure 4.7: Conditions for the determination of the temperature range (eq. (4.18)) plotted for several frequencies. These two conditions require the amplitude of the sinusoidal vacancy signal of the low-frequency measurement $\left(\Delta\widehat{L}\right)^{Mod,Vac}_{LF}$ to be larger and the amplitude of the high-frequency measurement $\left(\Delta\widehat{L}\right)^{Mod,Vac}_{HF}$ to be smaller than the measurement error $\Delta\Delta L$, which was set to 10 nm (see dashed line). The solid lines indicate the temperature range in case of a 2 mHz- and a 25 mHz-measurement. **This relation is only valid for $Fe_{55}Al_{45}$,** which has the values $H_V^M = 1.5\,\mathrm{eV}$, $\tau_0^{-1} = 4 \times 10^5\,\mathrm{s}^{-1}$, $H_V^F = 1\,\mathrm{eV}$ and $\frac{S_V^F}{k} = 4.9$ (cf. tab. 5.1 and 5.4: [3], index 1).

(cf. eq. (4.12) and (4.16)):

$$\frac{1}{3}(1-r)\Delta\widehat{C_V} = \left(\frac{\Delta\widehat{L}}{L_{ref}}\right)_{LF}^{Mod,Vac}.$$

Since there are no literature values for the relaxation parameter r, we set it to zero and calculate the resulting length change due to vacancies with regard to the modulation and see if it is larger than the measurement error for the low-frequency measurement and smaller for the high-frequency measurement[11], i.e.

$$\begin{aligned}\left(\Delta\widehat{L}\right)_{LF}^{Mod,Vac} &\approx \frac{1}{3}\Delta\widehat{C_{V_{LF}}}L_{ref} > \Delta\Delta L \quad \text{and}\\ \left(\Delta\widehat{L}\right)_{HF}^{Mod,Vac} &\approx \frac{1}{3}\Delta\widehat{C_{V_{HF}}}L_{ref} < \Delta\Delta L.\end{aligned} \tag{4.18}$$

In case of $Fe_{55}Al_{45}$ this relation is shown in fig. 4.7 for a temperature amplitude of $\Delta\widehat{T} = 2\,\mathrm{K}$ and for an error of the measurement setup of $\Delta\Delta L = 10\,\mathrm{nm}$.

4.3.4 Requirements: Heating Rate

In section 4.2 we made the assumption that the specimen is equilibrated with respect to the average temperature T_0, hence we want the heating rate to be as low as possible. However, we cannot make the heating rate arbitrarily low, which is why we estimate a lower limit of the heating rate based on the measurement error of the setup, below which an improvement of the result is not possible. Therefore, we look at the longest equilibration process taking place in the measurement, i.e. τ_{max}, and calculate the equilibrated length change due to vacancies within this equilibration process in order to adjust the heating rate in a way that this change in length during this equilibration process is smaller than the measurement error of the setup. We do this as follows:

First, we calculate the length change with the heating rate $\frac{T}{t}$ per time in equilibrium,

[11] For a more sophisticated estimate regarding the second condition, please refer to section 4.3.6, where the remaining vacancy signal after subtraction of the lattice part was calculated.

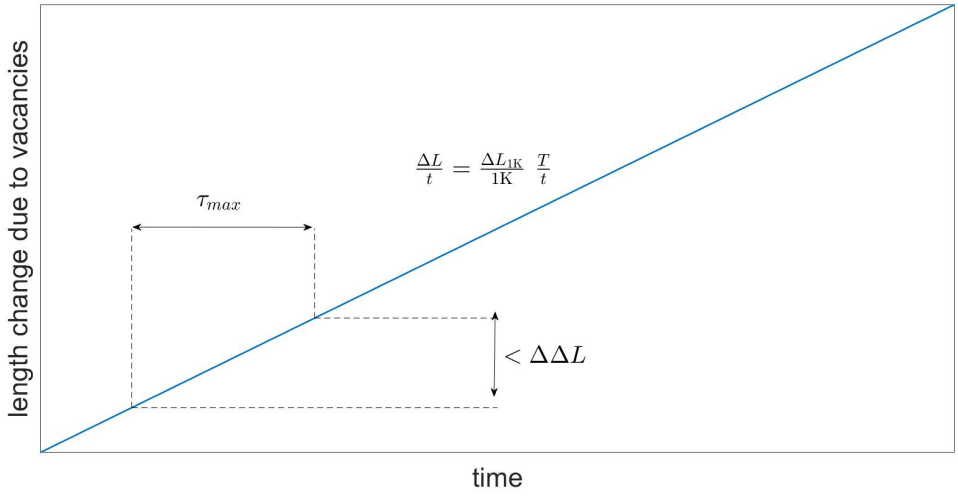

Figure 4.8: Condition for the heating rate to ensure that the specimen is equilibrated with respect to the heating rate, which can be assumed if the error $\Delta\Delta L$ of the measurement setup is smaller than the equilibrated length change due to vacancies during an equilibration process with the duration τ_{max} (eq. (4.19)).

which we do by multiplying the expansion due to vacancies per Kelvin $\frac{\Delta L_{1K}}{1K}$, i.e.

$$\frac{\Delta L}{t} = \frac{\Delta L_{1K}}{1K} \frac{T}{t}.$$

Since we now know the equilibrated length change due to vacancies per time, we multiply the highest time constant of the measurement τ_{max} to see by how much the length is changing during the longest equilibration process of the measurement and set the condition that the resulting length change is smaller than or equal to the measurement error of the setup (fig. 4.8), i.e.

$$\frac{\Delta L_{1K}}{1K} \frac{T}{t} \tau_{max} \overset{!}{\leq} \Delta\Delta L. \tag{4.19}$$

During the measurement the temperature increases, hence the time constant decreases. This means that the required time for an equilibration process decreases resulting in a smaller equilibrated length change due to vacancies during this time. Since we calculated the condition with regard to the longest equilibration process of the measurement, i.e. τ_{max}, the condition corresponds to the lower limit of the heating rate, below which an improvement of the result is not possible. Therefore, we set

the resulting length change during an equilibration process to be roughly the same as the measurement error and get the condition for the heating rate:

$$A_{min} \approx \frac{\Delta\Delta L}{\tau_{max}} \frac{1}{\frac{\Delta L_{1\mathrm{K}}}{1\mathrm{K}}}. \tag{4.20}$$

Since there are literature values available for the materials in question[12], we can determine the factor $\tau_{max}\frac{\Delta L_{1\mathrm{K}}}{1\mathrm{K}}$ together with the heating rate in case of the measurement error being $\Delta\Delta L$ = 10 nm. We will evaluate this factor at a temperature, where the time constant is about 1000 s since measurements with higher time constants won't give reasonable results because they are already higher than the period duration of the lowest modulation frequency, hence for materials, for which the ratio $\frac{H_V^M}{H_V^F}$ is just slightly above 1, the amplitude is too low to be measurable. This is the case for $Fe_{55}Al_{45}$, for which $\frac{H_V^M}{H_V^F} = 1.5$[13] (fig. 4.7 at 600 °C corresponds to τ = 1000 s [14]). If the highest time constant τ_{max} is lower than 1000 s, a higher heating rate can be chosen because the vacancies are migrating faster then resulting in a smaller length change due to vacancies within an equilibration process. To get an estimate for the expansion per Kelvin due to vacancies, we use the second term of eq. (4.17) ("vacancies (linear heating)"):

$$\frac{\Delta L_{1\mathrm{K}}}{1\mathrm{K}} = L_{ref}\,\frac{1}{3}(1-r)[C_{V,0}(T+1\,\mathrm{K}) - C_{V,0}(T)]. \tag{4.21}$$

Since there are no literature values for the vacancy relaxation of the material in question, we set the relaxation parameter r to zero and calculate these values for the materials in question (tab. 4.1).

Only for the high-frequency measurement we might choose a much higher heating rate since only the modulation part is of interest. (Remember that we only have the heating rate to get α as a function of temperature (see section 4.3.1).) Therefore, we can choose virtually any heating rate as long as the period duration T_p is much smaller than the lowest time constant τ_{min} of the measurement since only then the average vacancy concentration within one period can be regarded as constant, i.e.

[12] The parameters of these materials are listed in tab. 5.5.
[13] According to [3] (index 1) in tab. 5.1 and 5.4.
[14] According to τ_1 from literature [1] in fig. 5.4.

Table 4.1: Estimation for maximum heating rates A acceptable by means of eq. 4.20 and 4.21 for several materials in question, for which we chose a temperature, where the time constant τ_{max} is about 1000 s, and a measurement error of $\Delta\Delta L = 10\,\text{nm}$ ($Fe_{55}Al_{45}$: cf. tab. 5.1 and 5.4: [3], index 1; other materials: cf. tab. 5.5).

material	$T\,[^\circ\text{C}]$	$A\,[\frac{\text{K}}{\text{min}}]$
$Fe_{55}Al_{45}$	600	3.2×10^{-2}
CuZn	250	5.0×10^{-2}
Al	6	5.5×10^{5}
p-doped Si	430	2.4
Fe_3Si	225	1.0×10
CuZnAl	75	2.0
PdIn	600	1.8×10^{-3}

the following condition must be fulfilled:

$$T_p << \tau_{min}.$$

4.3.5 Required Measurements

In the following two measurements are needed (fig. 4.9), for which the conditions for the required parameters are described here in short.[15] The first measurement is a high-frequency measurement (HF) with

- an arbitrary heating rate, as long as $T_p << \tau_{min}$[16].
  Otherwise the heating rate should be $A = \frac{T}{t} \approx \frac{\Delta\Delta L}{\tau_{max}} \frac{1}{\frac{\Delta L_{1\text{K}}}{1\text{K}}}$ as has just been explained.

- a modulation frequency as high as possible to ensure that only a marginal amount of vacancies is diffusing into or out of the sample during one modulation period. Therefore, one has to check if the amplitude of the sinusoidal

[15] The explanation for these conditions are made in section 4.3.3, 4.3.4 and 4.3.6.

[16] The corresponding time constant can be obtained either from literature values or from measurements as shown in fig. 3.1. (cf. section 5.1)

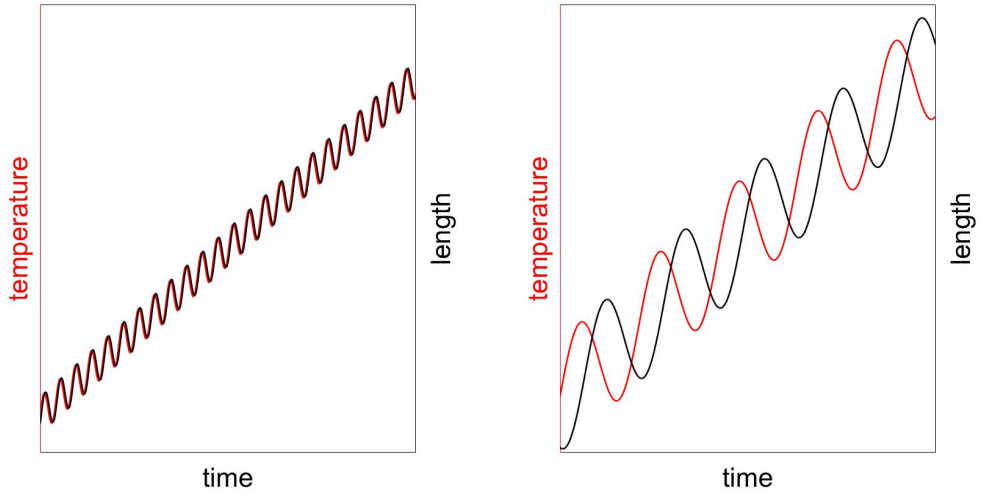

Figure 4.9: Sketch of the temperature profile (red) and the corresponding length signal (black) of the two required measurements for the approach "High- and Low-Frequency Measurement".

vacancy signal $\left(\Delta\widehat{L}\right)_{HF}^{Mod,Vac}$ to be expected is smaller than the measurement error, i.e. $\left(\Delta\widehat{L}\right)_{HF}^{Mod,Vac} \approx \frac{1}{3}\Delta\widehat{C_{V_{HF}}}L_{ref} < \Delta\Delta L$, where L_{ref} denotes the specimen length and $\Delta\widehat{C_V}$ the amplitude of the sinusoidal length signal given by eq. (4.12). This sets the upper limit of the temperature range.[17]
For $Fe_{55}Al_{45}$ this relation is shown in fig. 4.7 with L_{ref} = 14.55 mm.
A more general relation for the determination of the temperature range is shown in fig. 4.10, where the vacancy signal is considered to be negligible if the period duration T_p is higher than the time constant τ.

The second measurement is a low-frequency measurement (LF) with

- a heating rate of $A = \frac{T}{t} \approx \frac{\Delta\Delta L}{\tau_{max}} \frac{1}{\frac{\Delta L_{1K}}{1K}}$.
- a modulation frequency of 1 or 2 mHz, whereby one has to check if the am-

[17] As a more sophisticated alternative to this condition the remaining vacancy signal after subtraction of the lattice part for a combination of two measurements was calculated in section 4.3.6 with the remaining vacancy signals given by fig. 4.11, 4.12 and 4.13.

plitude of the sinusoidal vacancy signal $\left(\Delta\widehat{L}\right)_{LF}^{Mod,Vac}$ to be expected is larger than the measurement error, i.e. $\left(\Delta\widehat{L}\right)_{LF}^{Mod,Vac} \approx \frac{1}{3}\Delta\widehat{C_{V_{LF}}}L_{ref} > \Delta\Delta L$. This sets the lower limit of the temperature range.
For $Fe_{55}Al_{45}$ this relation is shown in fig. 4.7 with L_{ref} = 14.55 mm.
A more general relation for the determination of the temperature range is shown in fig. 4.10, where the vacancy signal is considered to be measurable if the period duration T_p is lower than the time constant τ. Nevertheless, one still needs to determine the amplitude of the modulated vacancy signal to be expected for the corresponding temperature range since this relation only shows the fraction of the overall amplitude, which could still be too low to be measurable for this temperature range.

4.3.6 Appendix: Remaining Vacancy Signal after Subtraction of the Lattice Part

With regard to the second condition in section 4.3.3 it was assumed that the modulation part of the high-frequency measurement is negligible, i.e. $\left(\frac{\Delta L}{L_{ref}}\right)_{HF}^{Mod,Vac} \to 0$. However, a small vacancy part remains and when we subtract this from the low-frequency measurement, we also subtract this small remaining vacancy part, hence subtract too much from the low-frequency measurement. Therefore, after subtraction the vacancy signal of the low-frequency measurement is reduced by a certain amount, which we want to determine in the following.
We look at eq. (4.11)[18] and see that in the amplitude only one factor depends on the modulation frequency:

$$\frac{1}{\sqrt{\omega^2\tau^2+1}} \quad \text{with} \quad \frac{1}{\tau(T_0)} = \frac{1}{\tau_0}e^{-\frac{H_V^M}{kT_0}} \quad \text{(eq. (3.4))}. \tag{4.22}$$

In addition, this factor also depends on the time constant τ, which itself depends on the temperature. If we plot this factor as a function of the time constant τ, we get a

[18] $\Delta C_V(t) = C_{V,0}\frac{H_V^F}{kT_0}\frac{\Delta\widehat{T}}{T_0}\frac{1}{\sqrt{\omega^2\tau^2+1}}\sin(\omega t+\varphi)$

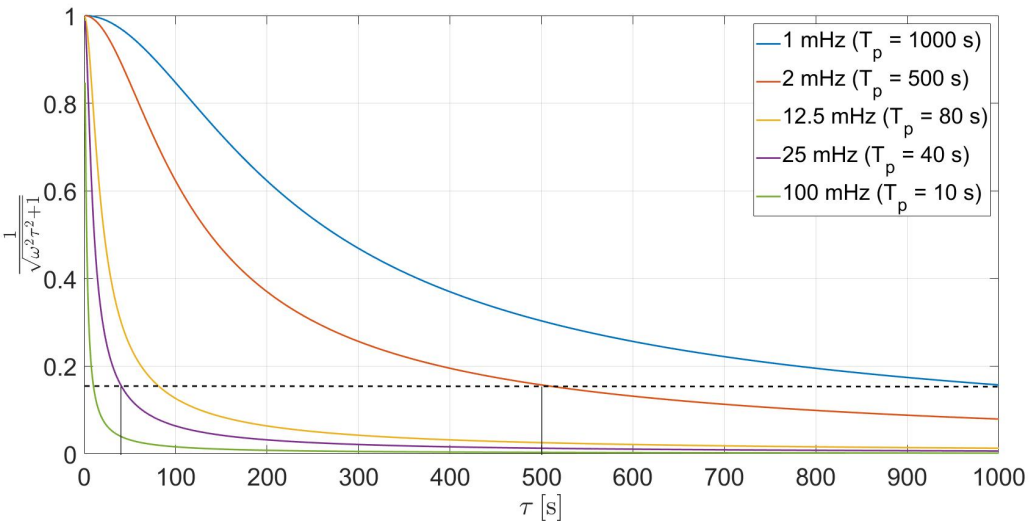

Figure 4.10: Modulation frequency-dependent factor (eq. (4.22)) plotted as a function of the time constant τ for various modulation frequencies. The dashed line indicates the limit, below which the period duration T_p is larger than the time constant τ. The solid lines show this in case of a 2 mHz- and 25 mHz-measurement.

value independent of the material (fig. 4.10). (If we plot it as a function of temperature, we have to insert the equation for τ, which contains the material parameters τ_0 and H_V^M, hence it would not be independent of the material.)
Since we are always combining two measurements here, it is reasonable to find a way to get an estimate for the remaining vacancy signal after subtraction for the combination of two measurements. Therefore, we divide the vacancy signals (of the modulation) of the two measurements to get a value that shows us by which factor the two vacancy signals are differing, i.e.

$$\frac{\left(\frac{\Delta L}{L_{ref}}\right)_{HF}^{Mod,Vac}}{\left(\frac{\Delta L}{L_{ref}}\right)_{LF}^{Mod,Vac}} = \frac{\sqrt{\omega_{LF}^2\tau^2+1}}{\sqrt{\omega_{HF}^2\tau^2+1}}$$

If we subtract this ratio from one, it corresponds to the vacancy signal that remains after we subtract the product of the thermal expansion coefficient α, which we got from the modulation part of the high-frequency measurement, and the temperature profile of the low-frequency measurement (step 4 and 5 in procedure (section 4.3.2)):

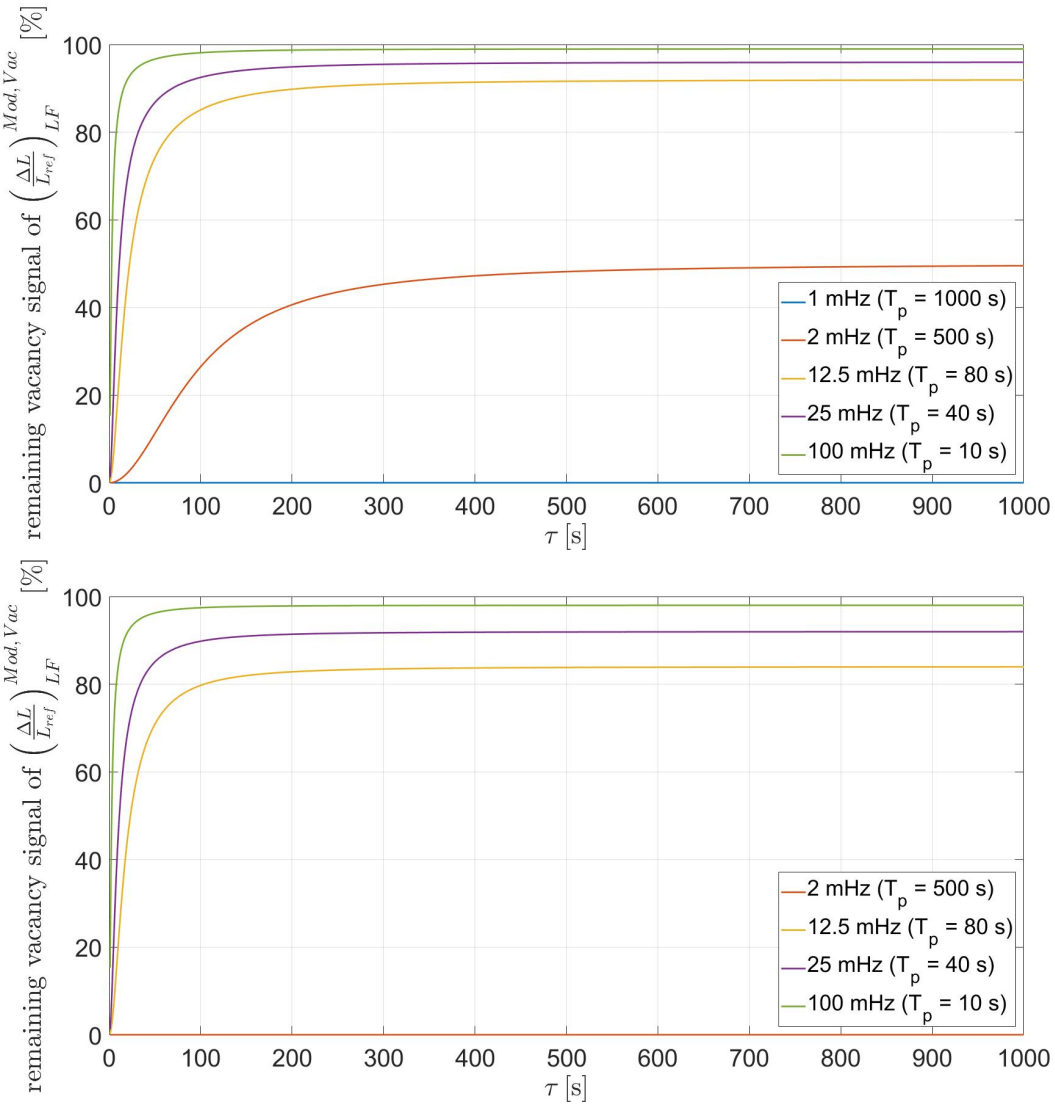

Figure 4.11: Remaining vacancy signal of the modulation $\left(\frac{\Delta L}{L_{ref}}\right)_{LF}^{Mod,Vac}$ after subtraction (eq. (4.23)) for the approach "High- and Low-Frequency Measurement" as a function of the time constant τ in case of a 1 mHz- (**top**) and a 2 mHz-measurement (**bottom**) being the low-frequency measurement and various modulation frequencies for the high-frequency measurement, where T_p denotes the corresponding period duration. **This relation is independent of the material.**

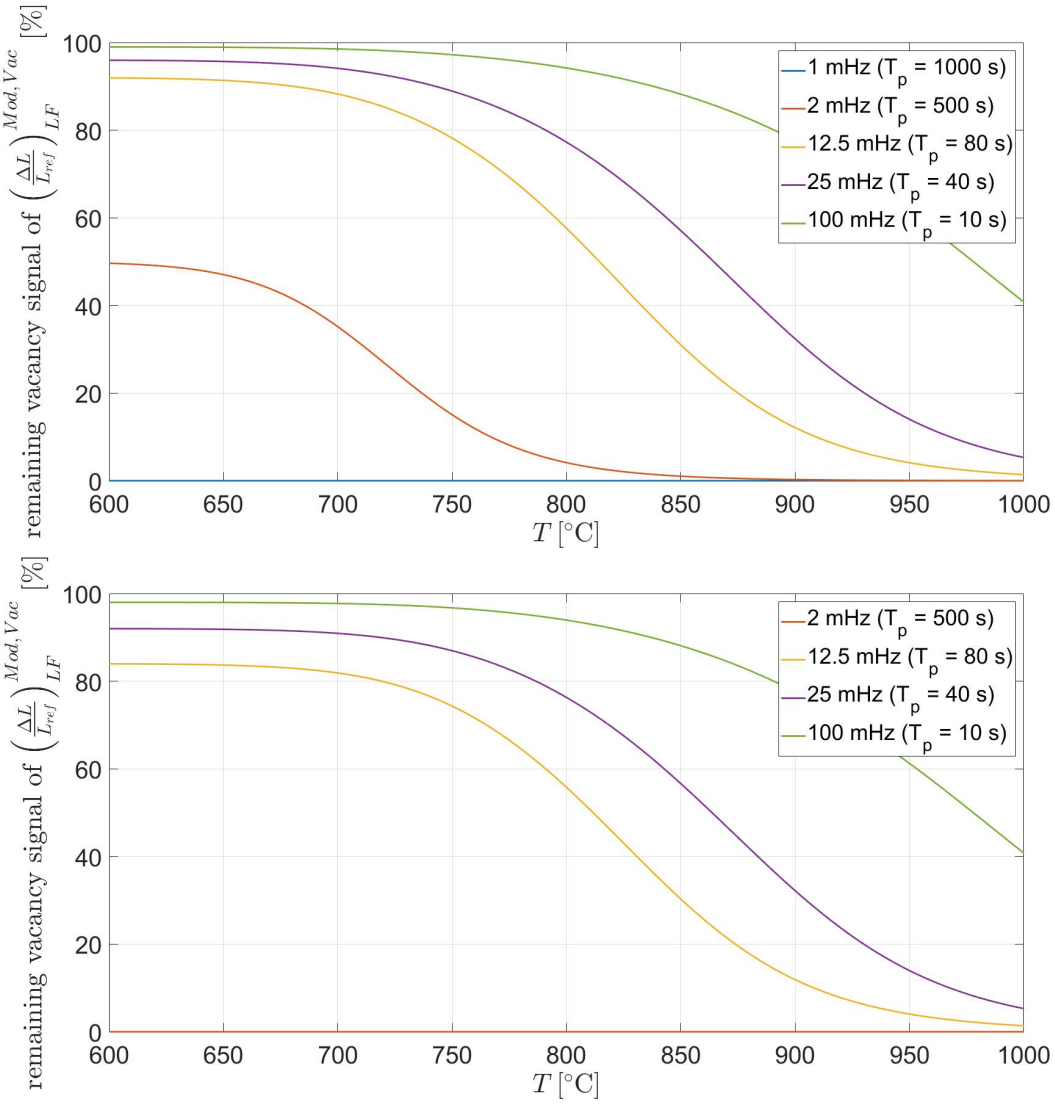

Figure 4.12: Remaining vacancy signal of the modulation $\left(\frac{\Delta L}{L_{ref}}\right)_{LF}^{Mod,Vac}$ after subtraction (eq. (4.23)) for the approach "High- and Low-Frequency Measurement" as a function of temperature T in case of a 1 mHz- (**top**) and a 2 mHz-measurement (**bottom**) being the low-frequency measurement and various modulation frequencies for the high-frequency measurement, where T_p denotes the corresponding period duration. **This relation is only valid for $Fe_{55}Al_{45}$,** which has the values $H_V^M = 1.5\,\mathrm{eV}$ and $\tau_0^{-1} = 4 \times 10^5\,\mathrm{s}^{-1}$ (cf. tab. 5.1: [3], index 1).

$$1 - \frac{\sqrt{\omega_{LF}^2\tau^2+1}}{\sqrt{\omega_{HF}^2\tau^2+1}} = \frac{\left(\frac{\Delta L}{L_{ref}}\right)_{LF}^{Mod,Vac} - \left(\frac{\Delta L}{L_{ref}}\right)_{HF}^{Mod,Vac}}{\left(\frac{\Delta L}{L_{ref}}\right)_{LF}^{Mod,Vac}} \widehat{=}$$
$$\widehat{=} \text{ remaining vacancy signal of } \left(\frac{\Delta L}{L_{ref}}\right)_{LF}^{Mod,Vac}, \tag{4.23}$$

which we get for the corresponding time constant and therefore for the corresponding temperature range.[19]
It is plotted for a 1 mHz- and a 2 mHz-measurement being the low-frequency measurement in fig. 4.11 as a function of the time constant τ, i.e. independent of the material, and in fig. 4.12 as a function of the temperature for $Fe_{55}Al_{45}$. From these plots one can see how much of the vacancy signal of the low-frequency measurement is left after subtraction to set a lower limit for the measurement, e.g. if we have a 2 mHz- and 12.5 mHz-measurement and want to get a vacancy signal of at least 80 %, we look at fig. 4.11 (bottom, yellow line) and see that the time constant has to be larger than 100 s or in case of $Fe_{55}Al_{45}$ the temperature has to stay below 720 $^\circ$C (fig. 4.12 (bottom, yellow line)).

Until now we only considered the remaining vacancy signal from the modulation of the low frequency-measurement $\left(\frac{\Delta L}{L_{ref}}\right)_{LF}^{Mod,Vac}$. But we also get a vacancy signal from the linear heating of the low frequency-measurement $\left(\frac{\Delta L}{L_{ref}}\right)_{LF}^{HR,Vac}$, which corresponds to the vacancy concentration in equilibrium. Therefore, we also calculate the remaining vacancy signal of the linear heating of the low frequency-measurement $\left(\frac{\Delta L}{L_{ref}}\right)_{LF}^{HR,Vac}$ by setting ω_{LF} to zero (equilibrium, hence no modulation) and get:

$$1 - \frac{1}{\sqrt{\omega_{HF}^2\tau^2+1}} \widehat{=} \text{ remaining vacancy signal of } \left(\frac{\Delta L}{L_{ref}}\right)_{LF}^{HR,Vac}. \tag{4.24}$$

This relation is shown in fig. 4.13. If we compare fig. 4.13 with fig. 4.11 and 4.12, we see that the remaining vacancy signal of the equilibrium part is larger than from the modulation part, e.g. in fig. 4.13 (bottom) at 750 $^\circ$C the 12.5 mHz-curve is at 80 %, whereas in fig. 4.12 at the same temperature both 12.5 mHz-curves are already below 80 %.

[19] For the determination of the temperature range please also refer to chapter 5.1, where for $Fe_{62}Al_{38}$ the time constants from various sources were compared and plotted as a function of temperature.

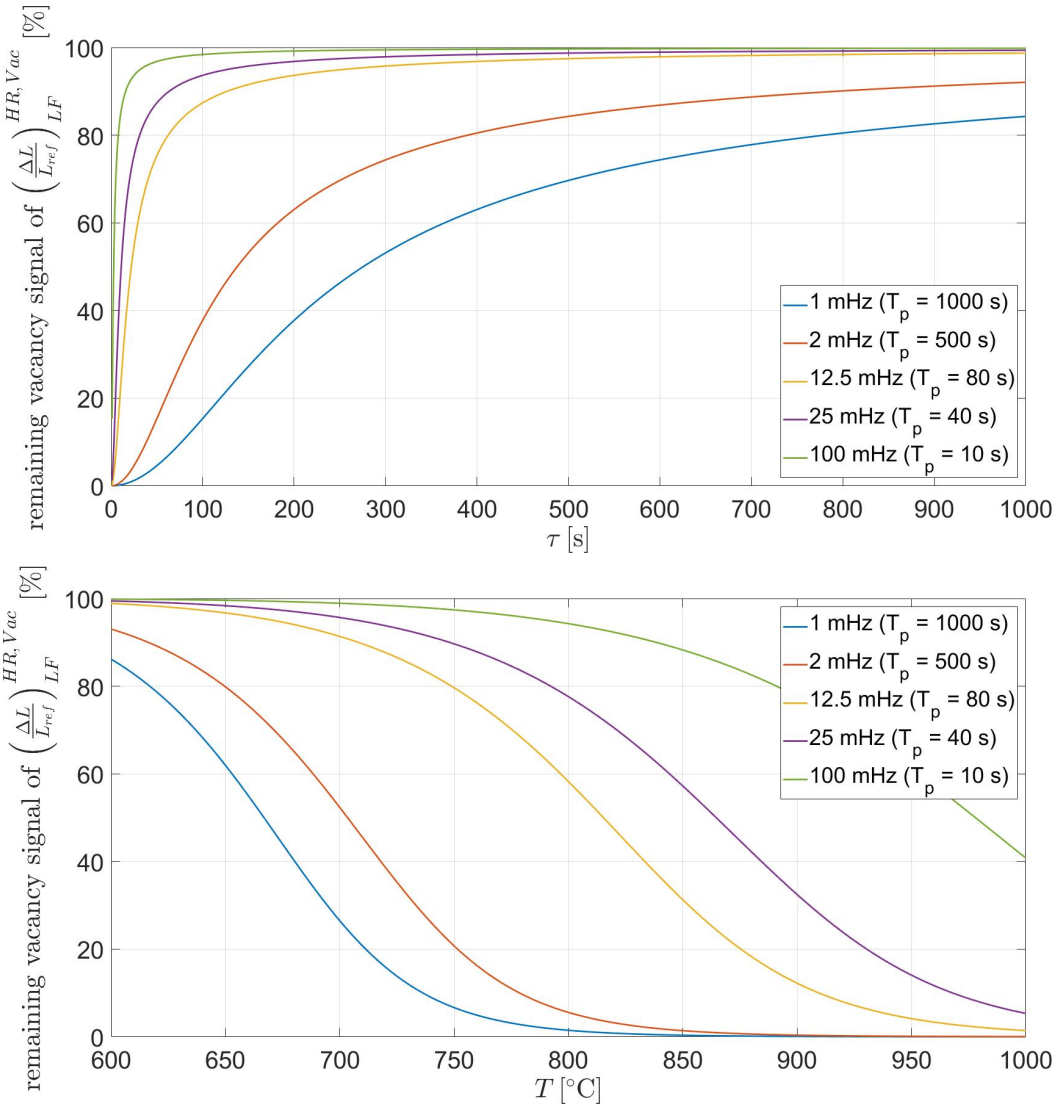

Figure 4.13: Remaining vacancy signal of the linear heating $\left(\frac{\Delta L}{L_{ref}}\right)_{LF}^{HR,Vac}$ after subtraction (eq. (4.24)) as a function of the time constant τ (**top**) and temperature T (**bottom**) for the approach "High- and Low-Frequency Measurement". ($Fe_{55}Al_{45}$: $H_V^M = 1.5\,\mathrm{eV}$, $\tau_0^{-1} = 4 \times 10^5\,\mathrm{s}^{-1}$; cf. tab. 5.1: [3], index 1).

4.4 Second Approach: At least two Measurements with arbitrary Frequency

4.4.1 Idea

When heating a material two effects come into play with respect to thermally induced length changes: The change of the lattice constant, which is given by the thermal expansion coefficient α and happens instantaneously, and a minor part, which arises from the formation of vacancies and is delayed by the time constant τ.
Now we take only one measurement with arbitrary modulation frequency and a heating rate, which we assume to be so slow that the specimen is equilibrated with respect to the linear heating (cf. section 4.3.4), and calculate the thermal expansion coefficient with respect to the linear heating α_{HR} (see step 1 and 2 in section 4.4.3). This expansion coefficient consists of a contribution from the lattice and a minor contribution from the vacancies. (In the previous approach we calculated the expansion coefficient from the modulation, whose frequency was so high that the vacancy part could be considered to be zero. This is why we directly obtained the thermal expansion coefficient α without any vacancy part included.) Since our goal is to get rid of the lattice part, we multiply α_{HR} with the whole temperature profile and subtract it from the measurement. As a result the lattice part cancels out and we are left with a sum of two sine waves, which are just consisting of contributions from the vacancies.

4.4.2 Required Measurements

In the following at least two measurements are needed (fig. 4.14) with

- a heating rate of $A = \frac{T}{t} \approx \frac{\Delta\Delta L}{\tau_{max}} \frac{1}{\frac{\Delta L_{1\mathrm{K}}}{1\mathrm{K}}}$, where $\Delta\Delta L$ denotes the measurement error of the setup. $\tau_{max} \frac{\Delta L_{1\mathrm{K}}}{1\mathrm{K}}$ with τ_{max} = 1000 s is given in tab. 4.1 for several materials in question.

- an arbitrary modulation frequency.

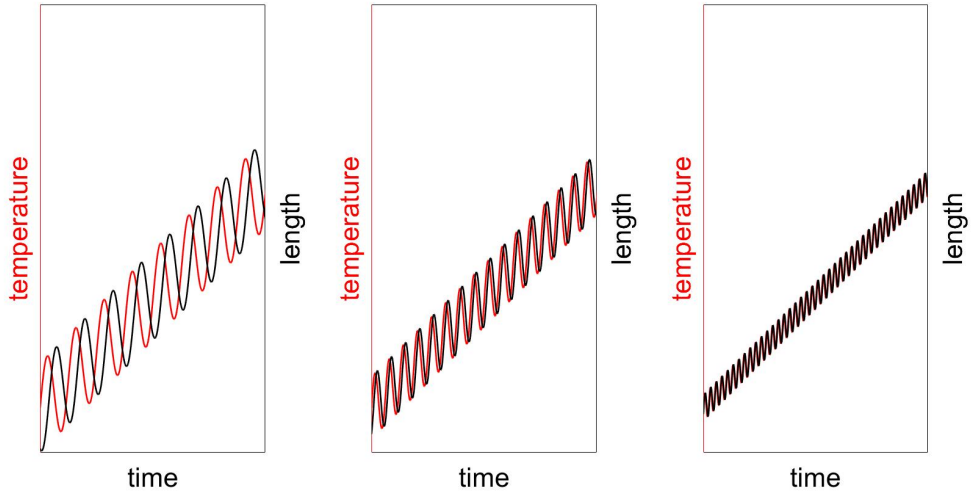

Figure 4.14: Sketch of the temperature profile (red) and the corresponding length signal (black) of the required measurements for the approach "At least two Measurements with arbitrary frequency".

4.4.3 Procedure

For the procedure we split up the measurement into the corresponding summands given by eq. (4.17), where HR denotes the linear heating, Mod the modulation, Lat the lattice contribution and Vac the vacancy contribution, i.e.

$$\left(\frac{\Delta L}{L_{ref}}\right) = \left(\frac{\Delta L}{L_{ref}}\right)^{HR,Lat} + \left(\frac{\Delta L}{L_{ref}}\right)^{HR,Vac} + \left(\frac{\Delta L}{L_{ref}}\right)^{Mod,Lat} + \left(\frac{\Delta L}{L_{ref}}\right)^{Mod,Vac}.$$

1. The moving average is given by: [20]

$$\left(\frac{\Delta L}{L_{ref}}\right)^{HR} = \left(\frac{\Delta L}{L_{ref}}\right)^{HR,Lat} + \left(\frac{\Delta L}{L_{ref}}\right)^{HR,Vac}.$$

[20] Instead of calculating the moving average, we could also just directly calculate the average of each period.

2. Calculate the expansion coefficient $\alpha_{HR}(T)$ by taking the (discrete) derivative with respect to the temperature (eq. (3.3)): [21]

$$\alpha_{HR}(T) = \frac{\Delta \left(\frac{\Delta L}{L_{ref}}\right)^{HR}}{\Delta T}.$$

3. Subtract the starting temperature T_{start} from the temperature profile of this measurement[22] to get the sum of the heating rate T_{HR} and the modulation T_{Mod} and multiply it with α_{HR}. We take into consideration that it consists of the lattice part $\alpha(T)$ and the vacancy part[23]:

$$\alpha_{HR}(T)\ T(t) = \left[\alpha(T) + \frac{\mathrm{d}\left(\frac{\Delta L}{L_{ref}}\right)^{HR,Vac}}{\mathrm{d}T}\right] \left[\overbrace{T_{HR}(t)}^{At} + \overbrace{T_{Mod}(t)}^{\Delta\widehat{T}\sin(\omega t)}\right] =$$

$$= \alpha(T)\ T_{HR}(t) + \frac{\mathrm{d}\left(\frac{\Delta L}{L_{ref}}\right)^{HR,Vac}}{\mathrm{d}T}\ T_{HR}(t) +$$
$$+ \alpha(T)\ T_{Mod}(t) + \frac{\mathrm{d}\left(\frac{\Delta L}{L_{ref}}\right)^{HR,Vac}}{\mathrm{d}T}\ T_{Mod}(t) =$$

$$= \left(\frac{\Delta L}{L_{ref}}\right)^{HR,Lat} + \left(\frac{\Delta L}{L_{ref}}\right)^{HR,Vac} +$$
$$+ \left(\frac{\Delta L}{L_{ref}}\right)^{Mod,Lat} + \frac{\mathrm{d}\left(\frac{\Delta L}{L_{ref}}\right)^{HR,Vac}}{\mathrm{d}T}\ T_{Mod}(t).$$

4. Subtract $\alpha_{HR}(T)\ T(t)$ from the measurement and get a sum of two sine

[21] To improve the result, we could also take the average of the α_{HR} of all measurements.
[22] $T(t) = T_{start} + At + \Delta\widehat{T}\sin(\omega t)$ (eq. (4.14))
[23] We will calculate the vacancy part in section 4.4.5.

waves:

$$\left[\left(\frac{\Delta L}{L_{ref}}\right)^{HR,\,Lat} + \left(\frac{\Delta L}{L_{ref}}\right)^{HR,\,Vac} + \left(\frac{\Delta L}{L_{ref}}\right)^{Mod,\,Lat} + \left(\frac{\Delta L}{L_{ref}}\right)^{Mod,\,Vac}\right] -$$
$$- \left[\left(\frac{\Delta L}{L_{ref}}\right)^{HR,\,Lat} + \left(\frac{\Delta L}{L_{ref}}\right)^{HR,\,Vac} + \left(\frac{\Delta L}{L_{ref}}\right)^{Mod,\,Lat} + \frac{\mathrm{d}\left(\frac{\Delta L}{L_{ref}}\right)^{HR,\,Vac}}{\mathrm{d}T}\, T_{Mod}(t)\right] =$$
$$= \left(\frac{\Delta L}{L_{ref}}\right)^{Mod,\,Vac} - \frac{\mathrm{d}\left(\frac{\Delta L}{L_{ref}}\right)^{HR,\,Vac}}{\mathrm{d}T}\, T_{Mod}(t).$$

5. Calculate the amplitude and the phase shift of this sum of sine waves (see section 4.4.5), which gives:

$$\left(\frac{\Delta L}{L_{ref}}\right)^{Mod,\,Sum} = \frac{\Delta\widehat{T}}{T_0}\,\frac{1}{3}\,(1-r)\,C_{V,0}(T_0)\frac{H_V^F}{kT_0}\sqrt{1-\frac{1}{\omega^2\tau^2+1}}\,\sin\left(\omega t+\Phi\right) \tag{4.25}$$

with $\Phi = \arctan\left(\frac{1}{\omega\tau}\right)$,
$T_0 = T_{start} + At$,
$C_{V,0}(T_0) = e^{\frac{S_V^F}{k}} e^{-\frac{H_V^F}{kT_0}}$ (eq. (3.1)) and
$\frac{1}{\tau(T_0)} = \frac{1}{\tau_0} e^{-\frac{H_V^M}{kT_0}}$ (eq. (3.4)).

The equation for the maximum with T_{max} being the position of the maximum is:

$$T_{max} = \sqrt{\frac{H_V^F}{k} + \frac{1}{\omega^2\tau^2+1}\frac{H_V^M}{k}},$$

where τ also contains the temperature, which is why this equation is an implicit function.

6. Now we can simultaneously fit the measurement results of multiple measurements to the new amplitude (fig. 4.15) and the new phase shift (fig. 4.16) with r, S_V^F, H_V^F, τ_0 and H_V^M as fitting parameters.

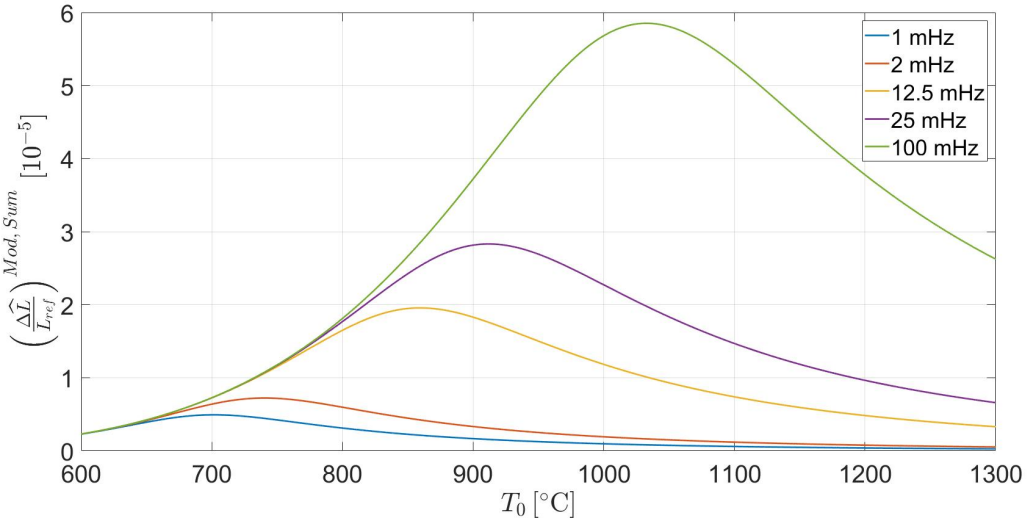

Figure 4.15: Amplitude $\left(\frac{\Delta\widehat{L}}{L_{ref}}\right)^{Mod,Sum}$ (eq. (4.25)) of the sum of the two sine waves for various modulation frequencies with a temperature amplitude of $\Delta\widehat{T} = 2\,K$. The vacancy relaxation r (cf. eq. (3.2)) is set to zero since no literature values are available. ($H_V^M = 1.5\,\mathrm{eV}$, $\tau_0^{-1} = 4 \times 10^5\,\mathrm{s}^{-1}$, $H_V^F = 1\,\mathrm{eV}$, $\frac{S_V^F}{k} = 4.9$; cf. tab. 5.1 and 5.4: [3], index 1).

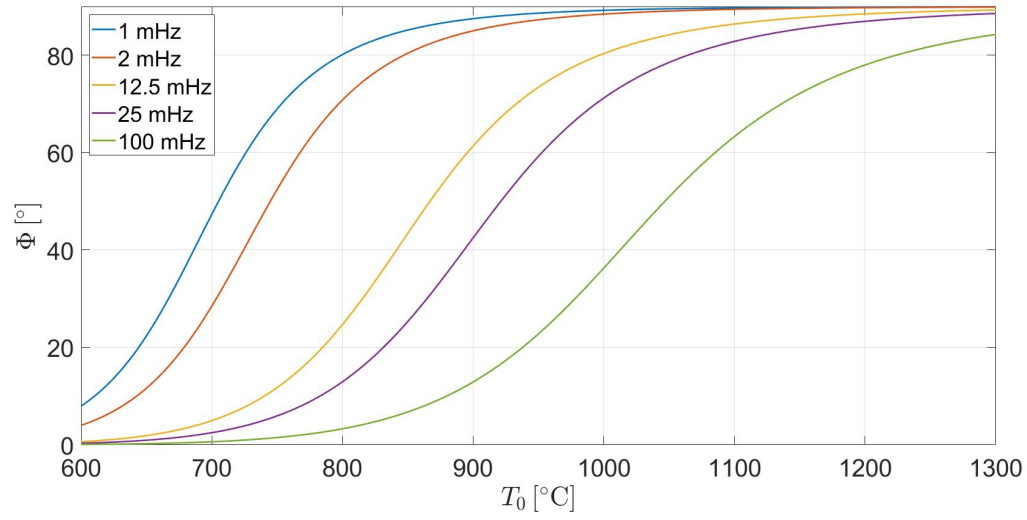

Figure 4.16: Phase shift Φ (eq. (4.25)) of the sum of the two sine waves for various modulation frequencies ($Fe_{55}Al_{45}$: $H_V^M = 1.5\,\mathrm{eV}$, $\tau_0^{-1} = 4 \times 10^5\,\mathrm{s}^{-1}$; cf. tab. 5.1: [3], index 1).

4.4.4 Discussion of the Result

Amplitude:

As seen in fig. 4.15 the amplitude has a maximum and goes to zero with increasing and decreasing temperature. For low temperatures eq. (4.25) is dominated by $C_{V,0}(T_0)$, which goes to zero with decreasing temperature. The high temperature range is dominated by the square root-term, where τ goes to zero with increasing temperature, which results in the square root-term going to zero.
The origin of the maximum lies in the fact that we take the difference between the vacancy concentration in equilibrium and the sinusoidal vacancy signal, the latter of which converges to the vacancy concentration in equilibrium with increasing temperature. Therefore, the whole amplitude in fig. 4.15 goes to zero at high temperatures. In the middle a temperature range exists, where both summands are large enough and differ from each other due to the time-dependency. This behavior becomes obvious in fig. 4.4, where we could think of the 1 mHz-curve being the vacancy concentration in equilibrium and the other curves being the sinusoidal vacancy signal.

Phase shift:

According to eq. (4.25) the phase shift converges at 0° (fig. 4.16) for low temperatures because the time constant τ goes to infinity and therefore the arctangent-function goes to zero. In case of high temperatures τ goes to zero and therefore the term in the arctangent-function goes to infinity, in which case the arctangent-function converges at 90°.
For low temperatures the phase shift is 0° because there is no modulation part. For higher temperatures the amplitude of the modulation part increases and at the same time the phase shift of the modulation part goes from 90° to 0°. However, since we are subtracting two sine functions, which are at high temperatures only differing by a slight phase shift, the extrema of this difference lie at the point, where these sine functions cross the x-axis. This is the reason why the phase shift is 90° at high temperatures.

4.4.5 Derivation

In step 4 in section 4.3.2 we got a sum of two sine waves:

$$\left(\frac{\Delta L}{L_{ref}}\right)^{Mod,\,Sum} = \left(\frac{\Delta L}{L_{ref}}\right)^{Mod,\,Vac} - \frac{\mathrm{d}\left(\frac{\Delta L}{L_{ref}}\right)^{HR,\,Vac}}{\mathrm{d}T}\, T_{Mod}(t). \tag{4.26}$$

We already know from chapter 4.2 (cf. eq. (4.17)) that

$$\left(\frac{\Delta L}{L_{ref}}\right)^{Mod,\,Vac} = \frac{\Delta\widehat{T}}{T_0}\,\frac{1}{3}\,(1-r)\,C_{V,0}(T_0)\frac{H_V^F}{kT_0}\frac{1}{\sqrt{\omega^2\tau^2+1}}\sin(\omega t+\varphi)$$
$$\text{with} \quad T_0 = T_{start} + At.$$

Since we also know that $T_{Mod}(t) = \Delta\widehat{T}\sin\omega t$ we only need to find $\frac{\mathrm{d}\left(\frac{\Delta L}{L_{ref}}\right)^{HR,\,Vac}}{\mathrm{d}T}$, which we do by starting out with eq. (4.15):

$$\left(\frac{\Delta L}{L_{ref}}\right)^{HR} = \left(\frac{\Delta L}{L_{ref}}\right)^{HR,\,Lat} + \left(\frac{\Delta L}{L_{ref}}\right)^{HR,\,Vac}$$
$$= \alpha A t \quad + \quad \frac{1}{3}(1-r)\left(C_{V,0}(\overbrace{T_{start}+At}^{T_0}) - C_{V,0}(T_{start})\right)$$
$$\text{with} \quad C_{V,0}(T_0) = e^{\frac{S_V^F}{k}}e^{-\frac{H_V^F}{kT_0}} \text{ (eq. (3.1))}.$$

In step 2 we calculated α_{HR} by taking the derivative with respect to T, which we now do with this formula:

$$\alpha_{HR}(T) = \frac{\mathrm{d}\left(\frac{\Delta L}{L_{ref}}\right)^{HR,\,Lat}}{\mathrm{d}T_0} + \frac{\mathrm{d}\left(\frac{\Delta L}{L_{ref}}\right)^{HR,\,Vac}}{\mathrm{d}T_0}$$
$$= \alpha + \frac{1}{3}(1-r)\,C_{V,0}(T_0)\frac{H_V^F}{kT_0^2}.$$

Putting $\frac{\mathrm{d}\left(\frac{\Delta L}{L_{ref}}\right)^{HR,\,Vac}}{\mathrm{d}T_0}$ into eq. (4.26) we get:

$$\begin{aligned}
&\left(\frac{\Delta L}{L_{ref}}\right)^{Mod,Vac} - \frac{\mathrm{d}\left(\frac{\Delta L}{L_{ref}}\right)^{HR,Vac}}{\mathrm{d}T_0}\, T_{Mod}(t) = \\
=&\frac{\Delta\widehat{T}}{T_0}\,\frac{1}{3}\,(1-r)\,C_{V,0}(T_0)\frac{H_V^F}{kT_0}\frac{1}{\sqrt{\omega^2\tau^2+1}}\sin(\omega t+\varphi) - \\
-&\frac{1}{3}(1-r)\,C_{V,0}(T_0)\frac{H_V^F}{kT_0^2}\,\Delta\widehat{T}\sin\omega t = \\
=&\frac{\Delta\widehat{T}}{T_0}\,\frac{1}{3}\,(1-r)\,C_{V,0}(T_0)\frac{H_V^F}{kT_0}\,\left(\frac{1}{\sqrt{\omega^2\tau^2+1}}\sin(\omega t+\varphi)-\sin(\omega t)\right).
\end{aligned} \tag{4.27}$$

For this result we only need to calculate the new amplitude and the new phase shift, for which we first derive the relations for arbitrary amplitudes. We start out with the general formula:

$$c\,\sin(\omega t+\Phi) = a\,\sin(\omega t+\varphi) + b\,\sin(\omega t).$$

Then we set $t=0$ and $\omega t=\frac{\pi}{2}$, which gives

$$\begin{aligned}
\sin\Phi &= \frac{a\sin\varphi}{c} \quad \text{and} \\
\cos\Phi &= \frac{a\cos\varphi+b}{c}.
\end{aligned} \tag{4.28}$$

By making use of the Pythagorean trigonometric identity $\cos^2\Phi+\sin^2\Phi=1$ we get the relation for the new amplitude:

$$\begin{aligned}
c^2 &= (a\cos\varphi+b)^2+(a\sin\varphi)^2 = \\
&= a^2\cos^2\varphi+2ab\cos\varphi+b^2+a^2\sin^2\varphi \\
&= a^2+b^2+2ab\cos\varphi.
\end{aligned} \tag{4.29}$$

From eq. (4.28) we can also express the new phase shift in terms of the tangent

function:

$$\tan\Phi = \frac{\sin\Phi}{\cos\Phi} = \frac{a\,\sin\varphi}{a\,\cos\varphi + b} = \frac{\sin\varphi}{\cos\varphi + \frac{b}{a}}. \tag{4.30}$$

With $a = \frac{1}{\sqrt{\omega^2\tau^2+1}}$ and $b = -1$ (cf. eq. (4.27)) we can calculate from eq. (4.29) the new amplitude (we write the prefactors in front of it and abbreviate them with "..."):

$$\begin{aligned}
\left(\frac{\Delta\widehat{L}}{L_{ref}}\right)^{Mod,\,Sum} &= \ldots\left(a^2+b^2+2ab\cos\varphi\right)^{\frac{1}{2}} = \\
&= \ldots\left(\frac{1}{\omega^2\tau^2+1} + 1 - 2\frac{1}{\sqrt{\omega^2\tau^2+1}}\cos\left(\arctan\left(-\omega\tau\right)\right)\right)^{\frac{1}{2}} = \\
&= \ldots\left(\frac{1}{\omega^2\tau^2+1} + 1 - 2\frac{1}{\sqrt{\omega^2\tau^2+1}}\frac{1}{\sqrt{\omega^2\tau^2+1}}\right)^{\frac{1}{2}} = \\
&= \frac{\Delta\widehat{T}}{T_0}\,\frac{1}{3}\,(1-r)\,C_{V,0}(T_0)\frac{H_V^F}{kT_0}\left(1-\frac{1}{\omega^2\tau^2+1}\right)^{\frac{1}{2}},
\end{aligned}$$

where we used the trigonometric relation $\cos\left(\arctan\left(x\right)\right) = \frac{1}{\sqrt{x^2+1}}$. From eq. (4.30) we get the new phaseshift:

$$\begin{aligned}
\tan\Phi &= \frac{\sin\varphi}{\cos\varphi + \frac{b}{a}} = \\
&= \frac{\sin\left(\arctan\left(-\omega\tau\right)\right)}{\cos\left(\arctan\left(-\omega\tau\right)\right) - \frac{1}{\frac{1}{\sqrt{\omega^2\tau^2+1}}}} = \\
&= \frac{\frac{-\omega\tau}{\sqrt{\omega^2\tau^2+1}}}{\frac{1}{\sqrt{\omega^2\tau^2+1}} - \sqrt{\omega^2\tau^2+1}} = \\
&= \frac{-\omega\tau}{1-\left(\omega^2\tau^2+1\right)} = \\
&= \frac{1}{\omega\tau},
\end{aligned}$$

where we used the trigonometric relations $\cos\left(\arctan\left(x\right)\right) = \frac{1}{\sqrt{x^2+1}}$ and $\sin\left(\arctan\left(x\right)\right) = \frac{x}{\sqrt{x^2+1}}$.

Combining these two results we get:

$$\left(\frac{\Delta L}{L_{ref}}\right)^{Mod,\,Sum} = \frac{\Delta\widehat{T}}{T_0}\,\frac{1}{3}\,(1-r)\,C_{V,0}(T_0)\frac{H_V^F}{kT_0}\left(1-\frac{1}{\omega^2\tau^2+1}\right)^{\frac{1}{2}}\,\sin\left(\omega t+\Phi\right)$$

$$\text{with}\quad \Phi = \arctan\left(\frac{1}{\omega\tau}\right).$$

4.5 Comparison between the two presented approaches

4.5.1 Similarities

For both approaches we need at least two measurements. All measurements must have a heating rate which is so low that the specimen can be regarded as equilibrated with respect to the linear heating. (Only the high frequency-measurement in the first approach may have a higher heating rate depending on the modulation frequency and the time constant.)

4.5.2 Differences

Regarding the modulation frequencies the advantage of the second approach over the first approach is that we can use measurements with virtually any frequency as long as they are different from each other. For the first approach we must take measurements with the highest frequency possible to keep the remaining vacancy signal high (fig. 4.11). In the second approach we get the full vacancy signal because the vacancy part is considered here, i.e. only in the first approach we made the assumption that the vacancy part of the modulation of the high frequency-measurement is negligible (see first step in section 4.3.2). Furthermore, the calculation of the thermal expansion coefficient is different: In the first approach we directly get the thermal expansion coefficient α from the modulation of the high frequency-measurement without considering any vacancy part (steps 1, 2 and 3 in section 4.3.2), whereas in the second approach we calculate the expansion coefficient α_{HR} from the linear heating

(steps 1 and 2 in section 4.4.3), for which the vacancy part is not negligible[24]. In addition, when calculating α_{HR} we have to take the derivative by means of numerical differentiation (step 2 in section 4.4.3), which exhibits a quite large error, in contrast to the first approach, where we just divide the length amplitude by the temperature amplitude (step 3 in section 4.3.2).

4.6 Other Approaches

The two just presented approaches are the simplest ones but in the course of this work some ideas for other approaches were found, which will be presented here in short.

4.6.1 Several Measurements with arbitrary Frequency

The required measurements for this approach are the same as for the previous approach, i.e. "At least two Measurements with arbitrary Frequency" (section 4.4.2). Therefore, we will only go trough the procedure.

The first few steps are the same as in the first approach, i.e. calculate the moving average and subtract it from the measurement, but this time we do not neglect the vacancy part in the modulation. This means that since the lattice part is instantaneous and the vacancy part delayed and therefore phase shifted (cf. eq. (4.17)), we cannot just take the plain sum as we did in the second approach, but instead have to take this phase shift into account. In the previous two approaches the lattice part always canceled out directly but this is not the case here because the thermal expansion coefficient α is part of a more complicated expression within a square root. This is the reason why this approach turns out to be more complicated than the previous two approaches, which gets evident, when elaborating the first few steps of the procedure.

[24] α refers to the thermal expansion coefficient without any vacancy contribution, whereas α_{HR} includes, in addition to the lattice part, the vacancy part (cf. eq. (4.17)).

1. Calculate the thermal expansion coefficient from the modulation α_{Mod} by dividing the amplitude of the length $\Delta\widehat{L}$ by the amplitude of the temperature $\Delta\widehat{T}$ and the specimen length L_{ref}:

$$\alpha_{Mod} = \frac{1}{\Delta\widehat{T}} \left(\frac{\Delta\widehat{L}}{L_{ref}} \right)^{Mod} .$$

2. As discussed above α_{Mod} consists of a lattice and a vacancy part, which cannot be described by a plain sum, i.e. $\alpha_{Mod} \neq \alpha + \frac{1}{\Delta\widehat{T}} \left(\frac{\Delta\widehat{L}}{L_{ref}} \right)^{Mod,\,Vac}$. Therefore, we have to use the formula for the amplitude of the sum of two sine waves, of which one is phase shifted (eq. (4.29)), which gives (cf. eq. (4.17)):

$$\alpha_{Mod} = \sqrt{\alpha^2 + \left(\frac{1}{\Delta\widehat{T}} \left(\frac{\Delta\widehat{L}}{L_{ref}} \right)^{Mod} \right)^2 + 2\,\alpha \left(\frac{1}{\Delta\widehat{T}} \left(\frac{\Delta\widehat{L}}{L_{ref}} \right)^{Mod} \right) \cos(\varphi)}$$

with $\frac{1}{\Delta\widehat{T}} \left(\frac{\Delta\widehat{L}}{L_{ref}} \right)^{Mod,\,Vac} = \frac{1}{3}(1-r)\, C_{V,0}(T_0) \frac{H_V^F}{kT_0^2} \frac{1}{\sqrt{\omega^2\tau^2+1}}$ and

$\varphi = \arctan(-\omega\tau)$.

3. For the same reason we calculate the phase shift of the sum of the two sine waves (eq. (4.30)) with $a = \frac{1}{\Delta\widehat{T}} \left(\frac{\Delta\widehat{L}}{L_{ref}} \right)^{Mod,\,Vac}$ and $b = \alpha$ (Only a is phase shifted by $\varphi = \arctan(-\omega\tau)$.):

$$\begin{aligned}
\tan\Phi &= \frac{\sin\varphi}{\cos\varphi + \frac{b}{a}} = \\
&= \frac{\sin(\arctan(-\omega\tau))}{\cos(\arctan(-\omega\tau)) + \frac{\alpha}{\frac{1}{\Delta\widehat{T}} \left(\frac{\Delta\widehat{L}}{L_{ref}} \right)^{Mod,\,Vac}}} = \\
&= \frac{\frac{-\omega\tau}{\sqrt{\omega^2\tau^2+1}}}{\frac{1}{\sqrt{\omega^2\tau^2+1}} + \frac{\alpha}{\frac{1}{\Delta\widehat{T}} \left(\frac{\Delta\widehat{L}}{L_{ref}} \right)^{Mod,\,Vac}}} = \\
&= \frac{-\omega\tau}{1 + \frac{\omega^2\tau^2+1}{\frac{1}{3}(1-r) C_{V,0}(T_0) \frac{H_V^F}{kT_0^2}}},
\end{aligned}$$

where we used the trigonometric relations $\cos(\arctan(x)) = \frac{1}{\sqrt{x^2+1}}$ and

$\sin(\arctan(x)) = \frac{x}{\sqrt{x^2+1}}$.

4. From here the next steps are trying to somehow cancel out the lattice contribution by subtracting $\alpha_{Mod}(T)\,T(t)$ from the measurement and considering the phase shift Φ in the measurement.

4.6.2 Subtract two Measurements from each Other

Here one just directly subtract the measurement as it is from another measurement, which results in the sum of four sine functions. The measurements for this approach must have the same heating rate (Otherwise it won't cancel out.), which should be just low enough that the vacancy concentration is not changing significantly within one period[25] and different modulation frequencies.

For the procedure we split up each measurement into the corresponding summands given by eq. (4.17), where HR denotes the linear heating, Mod the modulation, Lat the lattice contribution, Vac the vacancy contribution, 1 the first measurement and 2 the second measurement, i.e.

$$\left(\frac{\Delta L}{L_{ref}}\right)_1 = \left(\frac{\Delta L}{L_{ref}}\right)_1^{HR,\,Lat} + \left(\frac{\Delta L}{L_{ref}}\right)_1^{HR,\,Vac} + \left(\frac{\Delta L}{L_{ref}}\right)_1^{Mod,\,Lat} + \left(\frac{\Delta L}{L_{ref}}\right)_1^{Mod,\,Vac},$$

$$\left(\frac{\Delta L}{L_{ref}}\right)_2 = \left(\frac{\Delta L}{L_{ref}}\right)_2^{HR,\,Lat} + \left(\frac{\Delta L}{L_{ref}}\right)_2^{HR,\,Vac} + \left(\frac{\Delta L}{L_{ref}}\right)_2^{Mod,\,Lat} + \left(\frac{\Delta L}{L_{ref}}\right)_2^{Mod,\,Vac}.$$

1. The heating rate is the same for both measurements, which means that

$$\left(\frac{\Delta L}{L_{ref}}\right)_1^{HR,\,Lat} = \left(\frac{\Delta L}{L_{ref}}\right)_2^{HR,\,Lat} \text{ and}$$
$$\left(\frac{\Delta L}{L_{ref}}\right)_1^{HR,\,Vac} = \left(\frac{\Delta L}{L_{ref}}\right)_2^{HR,\,Vac}.$$

[25] Same condition as for the heating rate of the high-frequency measurement in section 4.3.4.

2. We now subtract the second from the first measurement and we are left with a sum of four sine waves since the contributions from the linear heating cancel out:

$$
\begin{aligned}
&\left[\left(\frac{\Delta L}{L_{ref}}\right)_1^{HR,\,Lat} + \left(\frac{\Delta L}{L_{ref}}\right)_1^{HR,\,Vac} + \left(\frac{\Delta L}{L_{ref}}\right)_1^{Mod,\,Lat} + \left(\frac{\Delta L}{L_{ref}}\right)_1^{Mod,\,Vac}\right] - \\
&- \left[\left(\frac{\Delta L}{L_{ref}}\right)_2^{HR,\,Lat} + \left(\frac{\Delta L}{L_{ref}}\right)_2^{HR,\,Vac} + \left(\frac{\Delta L}{L_{ref}}\right)_2^{Mod,\,Lat} + \left(\frac{\Delta L}{L_{ref}}\right)_2^{Mod,\,Vac}\right] = \\
&= \left[\left(\frac{\Delta L}{L_{ref}}\right)_1^{Mod,\,Lat} + \left(\frac{\Delta L}{L_{ref}}\right)_1^{Mod,\,Vac}\right] - \\
&- \left[\left(\frac{\Delta L}{L_{ref}}\right)_2^{Mod,\,Lat} + \left(\frac{\Delta L}{L_{ref}}\right)_2^{Mod,\,Vac}\right] = \\
&= \frac{\Delta\widehat{T}}{T_0}\left[\alpha(T_0)\,T_0\sin(\omega_1 t) + \frac{1}{3}(1-r)C_{V,0}(T_0)\frac{H_V^F}{kT_0}\frac{1}{\sqrt{\omega_1^2\tau^2+1}}\sin\left(\omega_1 t+\varphi_1\right)\right] - \\
&- \frac{\Delta\widehat{T}}{T_0}\left[\alpha(T_0)\,T_0\sin(\omega_2 t) + \frac{1}{3}(1-r)C_{V,0}(T_0)\frac{H_V^F}{kT_0}\frac{1}{\sqrt{\omega_2^2\tau^2+1}}\sin\left(\omega_2 t+\varphi_2\right)\right]
\end{aligned}
$$

with $T_0 = T_{start} + At$,

$\varphi = \arctan\left(-\omega\tau\right)$ (eq. (4.11)),

$C_{V,0}(T_0) = e^{\frac{S_V^F}{k}} e^{-\frac{H_V^F}{kT_0}}$ (eq. (3.1)) and

$\frac{1}{\tau(T_0)} = \frac{1}{\tau_0} e^{-\frac{H_V^M}{kT_0}}$ (eq. (3.4)).

Extracting information out of this sum of four sine functions is for sure more tedious than doing so for the second approach presented above where we just had a sum of two sine functions.

However, since we do not need to take any derivative as in the second approach or calculate any expansion coefficient as in all other approaches, we might get better results because we only need one step to obtain the result. In addition, owing to the fact that we combine two measurements every time, we get much more information from an additional measurement as we would for the second approach above

(section 4.4) since we can combine it with all already existing measurements and therefore get $\binom{n}{2} = \frac{n!}{2!\,(n-2)!}$ combinations with n measurements. This means that in the end having a large amount of measurements we could be far better off with this approach compared to the second approach.

5 Applications of Theory of Vacancy Kinetics for temperature modulated Measurements

Because of unforeseen events the improvement of the measurement setup was interrupted and could not be finished in time, which is why no measurements with the improved setup could be conducted. However, the measurements on $Fe_{62}Al_{38}$ performed with the not yet modified setup will be presented here and comprise premeasurements for the determination of the temperature range and modulated measurements, for which we apply the two elaborated approaches. In the last part some thoughts and suggestions for future measurements are discussed.

5.1 Premeasurements

Before one can conduct modulated measurements with a linear increase in temperature as described in sec. 4.2, it is necessary to find a temperature range, in which the time constant τ lies somewhere in the range of the period duration of the temperature modulation. If not, the process of the vacancy migration would take too long in case of low temperatures, i.e. the time constant τ is too high. For too high temperatures the vacancy signal would not be distinguishable from the instantaneous expansion due to the very low time constant. This behavior was already discussed in section 4.3.6 with regard to the approach "High- and Low-Frequency Measurement", where we looked in fig. 4.10 at the factor $\frac{1}{\sqrt{\omega^2\tau^2+1}}$, which is (apart from the phase shift) the only part in the equation for a sinusoidal vacancy signal (eq. (4.11)) that depends on the time constant τ. If this factor is one, the time constant is too low and cannot be distinguished from the instantaneous length change and if it is zero, the vacancy signal is zero. Therefore we want the temperature range to be not too close to zero nor to one for any modulation frequency, which is why the time constants of the chosen temperature range should lie in the range of 10 - 1000 s. In addition, the length change due to vacancies must be high enough to be measurable. This was also already discussed in section 4.3.3.

So, we first conduct measurements as shown in fig. 3.1, i.e. a quasi-instantaneous jump from one temperature to another and stay at that temperature until an exponential change in length proportional to $(1 - e^{-\frac{t}{\tau}})$ or $e^{-\frac{t}{\tau}}$ can be observed.

Table 5.1: Values from literature for migration enthalpies H_V^M and pre-exponential factors τ_0 determined by dilatometry (DIL) and positron annihilation spectroscopy (POS). The time constants are shown in fig. 5.3 and 5.4 together with the time constants obtained from measurements in this work.

Source	Material	Exp.	$T\,[^\circ\mathrm{C}]$	$H_V^{M_1}[\mathrm{eV}]$	$H_V^{M_2}[\mathrm{eV}]$	$\tau_{0,1}^{-1}[\mathrm{s}^{-1}]$	$\tau_{0,2}^{-1}[\mathrm{s}^{-1}]$
[2]	$Fe_{61}Al_{39}$	DIL	$420-500$	1.2 ± 0.3	0.7 ± 0.3	2.7×10^4	2.2
[3]	$Fe_{55}Al_{45}$	DIL	$397-500$	1.5 ± 0.2	0.6 ± 0.1	4×10^5	0.8
[4]	$Fe_{61}Al_{39}$	POS	$350-400$	1.7 ± 0.3	-	1.9×10^8	-

As discussed in section 2 the reliability of the measurements is especially at higher temperatures rather limited since the systematic variation also exhibits some exponential behavior that goes in the opposite direction, i.e. when the temperature drops the length decreases instantly but then slowly increases again (cf. fig. 2.5 at $1.7\times10^4\,\mathrm{s}$). Therefore, it is counteracting the time-delayed length change due to vacancies, though it is not always in the same time range nor in the same length range as the time constant τ and the length change amplitude Δl. Nevertheless, all measured curves could only be fitted by the sum of two exponential functions, i.e. $\Delta l_1\, e^{-\frac{t}{\tau_1}} + \Delta l_2\, e^{-\frac{t}{\tau_2}} + c$ with Δl_1 and Δl_2 as well as τ_1 and τ_2 as fit parameters (see fig. 5.1 and 5.2), which could either be caused by the systematic variation (cf. fig. 2.12 left) or by two processes taking place in the material. The latter would be corroborated by [2] and [3], where also two time constants were measured (see tab. 5.1). Surprisingly, these two time constants can only be measured at higher temperatures as shown in table 5.1, where for measurements below $400\,^\circ\mathrm{C}$ only one time constant was observed [4]. A comparison of the time constants measured in this work with those from the literature can be seen in fig. 5.3 and 5.4 with the corresponding values in table 5.1 and 5.2.

At this point it has to be mentioned that these measurements only serve as an estimate for the temperature range of the actual measurements described in section 4.2 and were never meant to be used for the determination of the migration enthalpy or the pre-exponential factor.

When comparing the higher time constants τ_2 in fig. 5.3 and 5.4 one can see a large discrepancy between the measured time constants and the literature values,

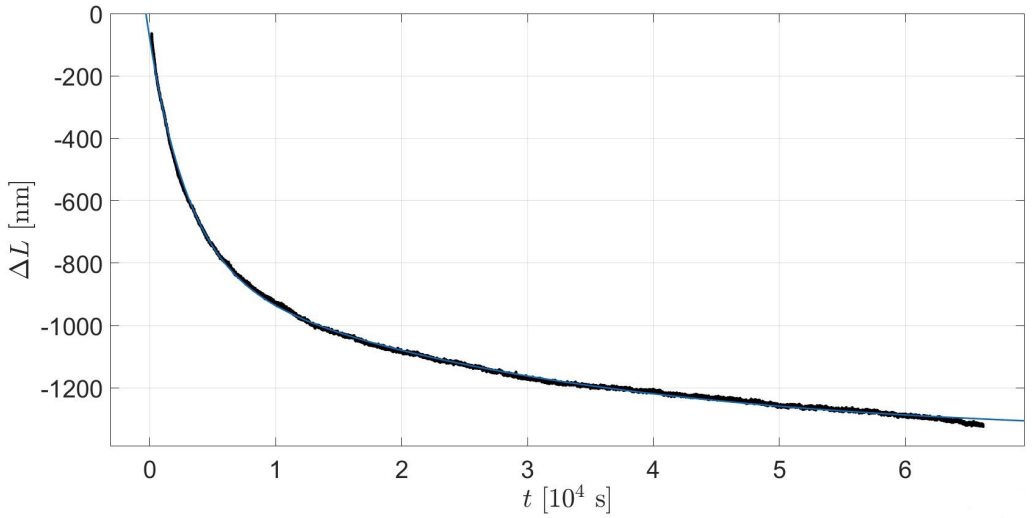

Figure 5.1: Length change ΔL after fast cooling from 600 °C to 550 °C together with the fitted function $\Delta l_1\, e^{-\frac{t}{\tau_1}} + \Delta l_2\, e^{-\frac{t}{\tau_2}} + c$ (blue line) for the determination of the time constants τ_1 and τ_2 of $Fe_{62}Al_{38}$ at 550 °C. The resulting fitting parameters of all these measurements are shown in tab. 5.2.

Table 5.2: Time constants τ_1 and τ_2 and length change amplitudes Δl_1 and Δl_2 obtained from measurements as shown in fig. 5.1 and fig. 5.2 by fitting the function $\Delta l_1\, e^{-\frac{t}{\tau_1}} + \Delta l_2\, e^{-\frac{t}{\tau_2}} + c$. The time constants are shown in fig. 5.3 and 5.4 together with the time constants from literature obtained from eq. (3.4) with the literature values given in tab. 5.1.

T [°C]	$600 \to 550$	$650 \to 600$	$700 \to 650$	$750 \to 700$	$20 \to 750$
τ_1 $[10^2\,\mathrm{s}]$	31.0	2.2	0.5	5.0	-
Δl_1 $[10^2\,\mathrm{nm}]$	7.2	3.7	97.2	5.4	-
τ_2 $[10^3\,\mathrm{s}]$	28.2	62.7	22.7	8.6	3.4
Δl_2 $[10^2\,\mathrm{nm}]$	5.5	5.0	4.5	8.6	5.3

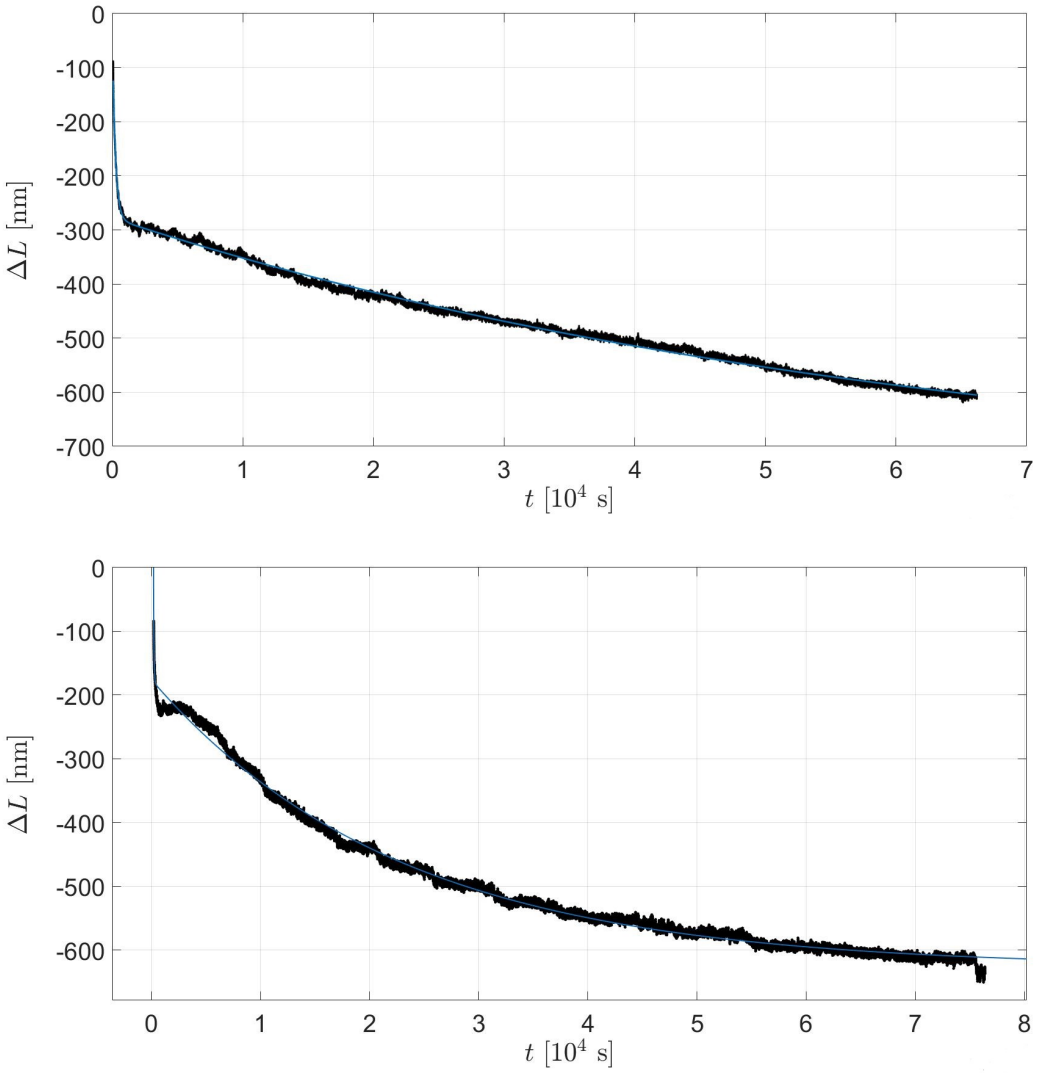

Figure 5.2: Length change ΔL after fast cooling from 650 °C to 600 °C (**top**) and from 700 °C to 650 °C (**bottom**) together with the fitted function $\Delta l_1\, e^{-\frac{t}{\tau_1}} + \Delta l_2\, e^{-\frac{t}{\tau_2}} + c$ (blue line) for the determination of the time constants τ_1 and τ_2 of $Fe_{62}Al_{38}$ at 600 °C and 650 °C. The resulting fitting parameters of all these measurements are shown in tab. 5.2.

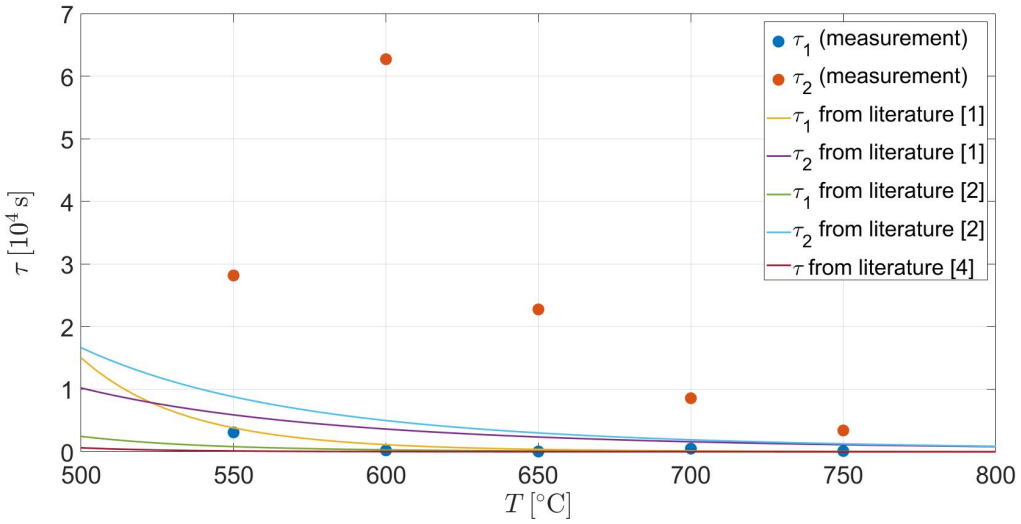

Figure 5.3: Low time constant τ_1 and high time constant τ_2 of $Fe_{62}Al_{38}$ as a function of temperature obtained from the measurements in this work (tab. 5.2) and from eq. (3.4) with the literature values given in tab. 5.1.

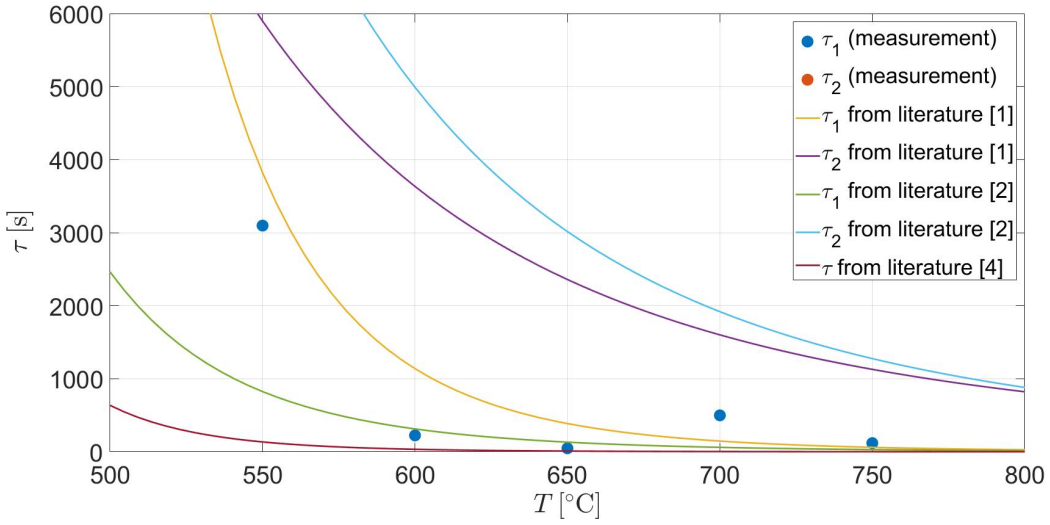

Figure 5.4: Enlarged view of the low time constant τ_1 and the high time constant τ_2 of $Fe_{62}Al_{38}$ as a function of temperature obtained from the measurements in this work (tab. 5.2) and from eq. (3.4) with the literature values given in tab. 5.1.

whereas the two literature values themselves coincide quite well with each other. The discrepancy at 600 °C and 650 °C might be due to the fitted curves, which have a very steep slope at the beginning (fig. 5.2), in contrast to the other measurements such as fig. 5.1. In tab. 5.2 we see that for the higher time constant τ_2 the length change amplitudes Δl_2 of the fitting function lie all in the same range. For the lower time constant τ_1 the length change amplitude Δl_1 at 650 °C deviate from the other factors significantly, though the lower time constant τ_1 lies in the range of the literature values. Therefore, the measurements at 550 °C and 700 °C can be considered as the most reliable ones. The reason for the higher time constant τ_2 being generally higher than the literature values might be that we are actually not measuring any higher time constant but only the systematic variation of the measurement setup (cf. fig. 2.12 left).

As discussed above the time constant should lie in the range of 10 - 1000 s for the modulated measurements. Since a suitable temperature range for the higher time constant τ_2 lies somewhere beyond 800 °C, in which range the systematic variation of the dilatometer is much larger (cf. fig. 2.12), we chose the temperature range according to the lower time constant τ_1 to be 600-700 °C.

5.2 Modulated Measurements

Five modulated measurements with a linear increase in temperature as described in section 4.2 were performed with the corresponding measurement parameters given in tab. 5.3. In fig. 5.5 the first and in fig. 5.6 the fifth measurement, i.e. the modulated temperature profile together with the corresponding length change, is shown.
In the following we will use these measurements to apply the two elaborated approaches (cf. section 4.3 and 4.4).

5.2.1 First Approach: High- and Low-Frequency Measurement

For this approach we will use the first and the fifth measurement (tab. 5.3), i.e. a 2 mHz and a 25 mHz measurement, which will be denoted as LF and HF, respectively (fig. 5.5 and 5.6). We will go through the procedure step by step as described in section 4.3.2.

Table 5.3: Measurement parameters of the performed modulated measurements with a temperature profile according to eq. (4.14), i.e. a linear heating rate with a superimposed modulation. The first and the fifth measurement is shown in fig. 5.5 and 5.6.

No.	T [°C]	$A\,[\frac{\mathrm{K}}{\mathrm{min}}]$	f [mHz]	$\Delta\widehat{T}$ [K]
1	$600-695$	0.06	2	2
2	$600-700$	0.06	2	2
3	$600-710$	0.06	12.5	2
4	$600-690$	0.06	25	2
5	$600-740$	0.06	25	2

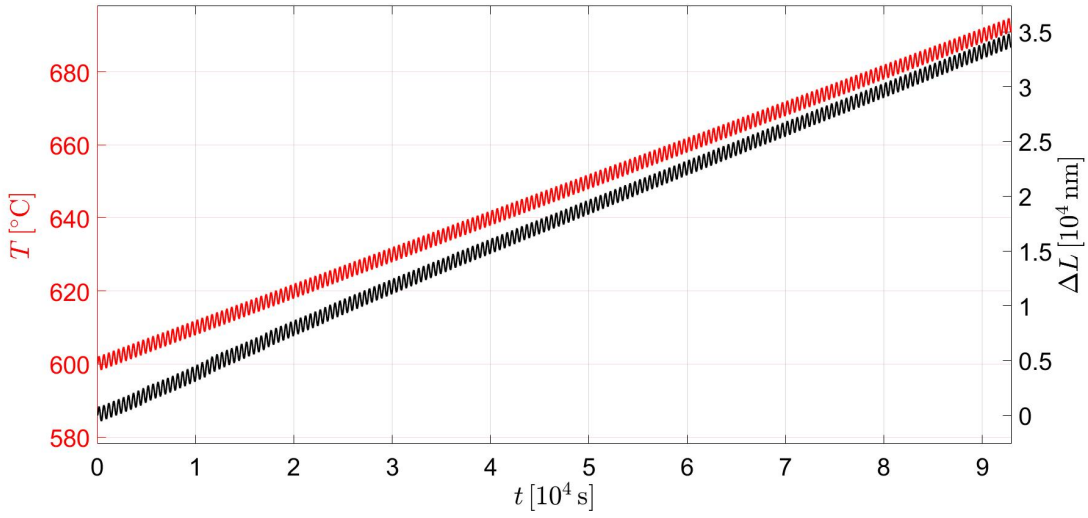

Figure 5.5: Measurement of length change ΔL upon modulated time-linear heating from 600 to 695 °C (heating rate: 0.06 K / min, modulation frequency: 2 mHz, modulation amplitude: 2 K; cf. tab. 5.3: No. 1).

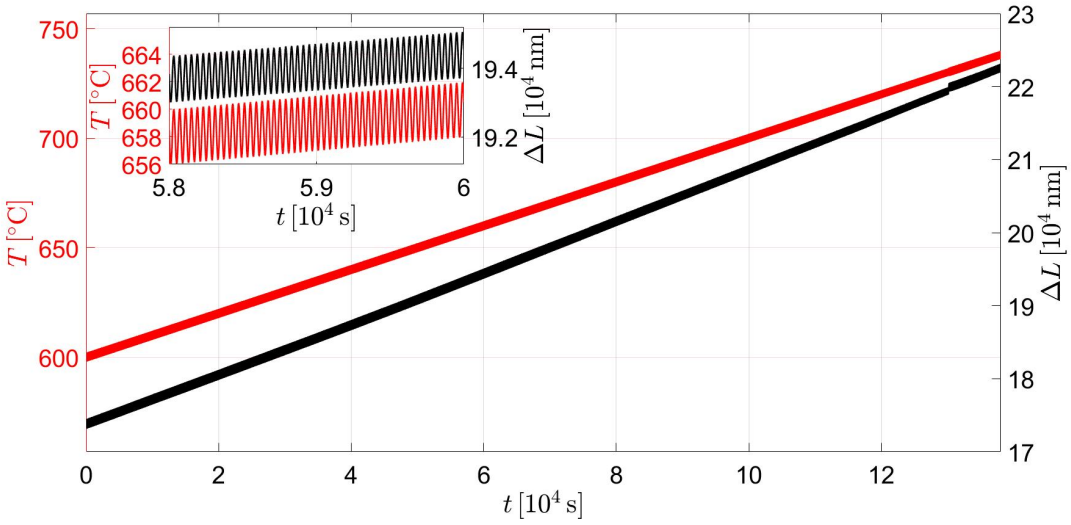

Figure 5.6: Measurement of length change ΔL upon modulated time-linear heating from 600 to 740 °C (heating rate: 0.06 K / min, modulation frequency: 25 mHz, modulation amplitude: 2 K; cf. tab. 5.3: No. 5).

1. $\left(\frac{\Delta L}{L_{ref}}\right)_{HF}^{Mod,Vac}$ is assumed to be negligible.

   According to tab. 5.2 the time constant τ_1 is higher than 50 s. By looking at fig. 4.11 (bottom) we see that for a 2 mHz- and 25 mHz-measurement and $\tau > 50$ s the remaining vacancy signal is larger than 85 %.

2. The moving average of HF is given by:

$$\left(\frac{\Delta L}{L_{ref}}\right)_{HF}^{HR,Lat} + \left(\frac{\Delta L}{L_{ref}}\right)_{HF}^{HR,Vac}. \tag{5.1}$$

   When calculating the moving average with a fixed number of values per period, it turned out that this dilatometer suddenly reduces the number of recorded values, which means that the modulation does not cancel out any more as seen in fig. 5.7 at $6 \times 10^4\,\mathrm{s}$. This makes the evaluation more tedious since we have to split up the measurement several times. Therefore,

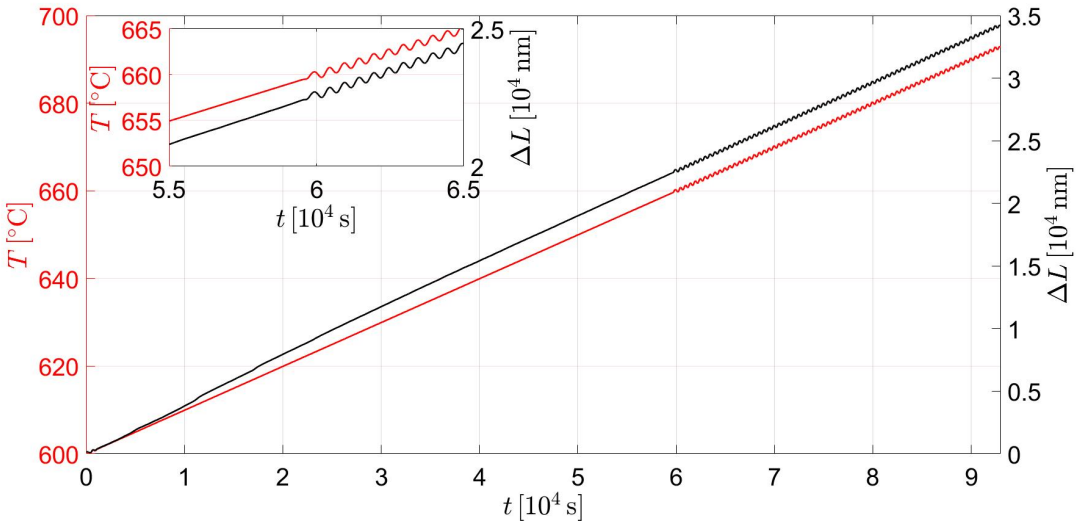

Figure 5.7: Moving average versus time of the temperature (red) and the corresponding length change (black) calculated with a fixed number of values per period from the low-frequency measurement in fig. 5.5.

instead of calculating the moving average, the average of each period was calculated. The amplitude was also directly determined by taking the difference between the minimum and the maximum of each period and divide it by two. This was done for both, the temperature T and the length ΔL.

3. Subtract the moving average from HF and calculate the thermal expansion coefficient α by dividing the length amplitude $\Delta\widehat{L}$ by the temperature amplitude $\Delta\widehat{T}$ and the specimen length L_{ref}:

$$\left(\frac{\Delta L}{L_{ref}}\right)_{HF}^{Mod,\,Lat} = \alpha\,\Delta\widehat{T}\,\sin(\omega_{high}t) \rightarrow \alpha(T). \tag{5.2}$$

Since we already have the amplitudes $\Delta\widehat{L}$ and $\Delta\widehat{T}$ of each period, we can calculate the thermal expansion coefficient α. Because we calculated the average value for each period of the temperature, we can use these val-

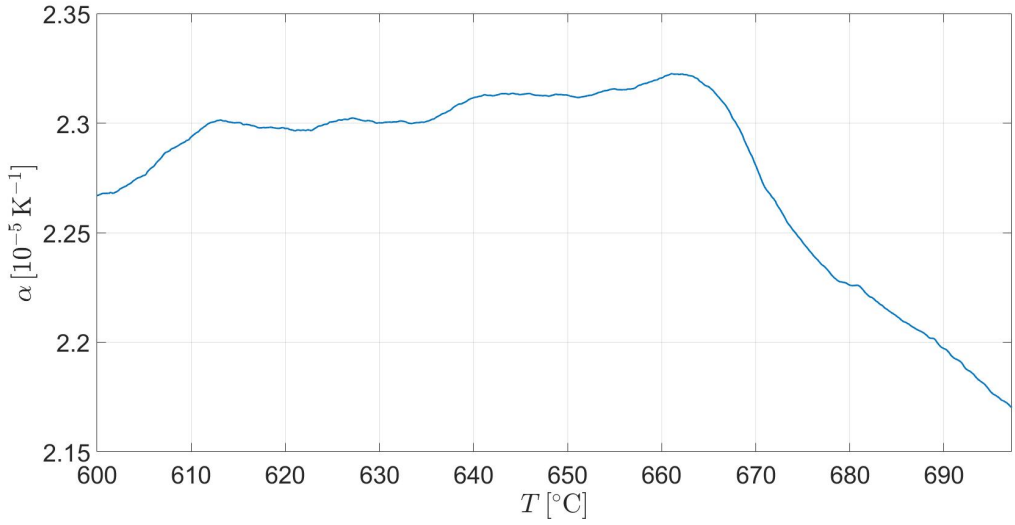

Figure 5.8: Thermal expansion coefficient α versus temperature derived from the high-frequency measurement in fig. 5.5 by means of eq. (5.1) and (5.2) (The moving average was calculated as described in step 2.). The data was smoothed in order to eliminate minor fluctuations.

ues to plot the thermal expansion coefficient α as a function of temperature (fig. 5.8).

4. Subtract the starting temperature T_{start} from the temperature profile of LF[26] and multiply it with the thermal expansion coefficient α to get the lattice contribution of LF:

$$\alpha(T)\,T(t)_{LF} = \left(\frac{\Delta L}{L_{ref}}\right)_{LF}^{HR,\,Lat} + \left(\frac{\Delta L}{L_{ref}}\right)_{LF}^{Mod,\,Lat} . \tag{5.3}$$

In order to take the temperature dependency of α into account, we have to split up our measurement into segments of different temperature and multiply the average α of this segment with the corresponding segment of the

[26] $T(t) = T_{start} + At + \Delta\widehat{T}\sin\omega t$ (eq. (4.14))

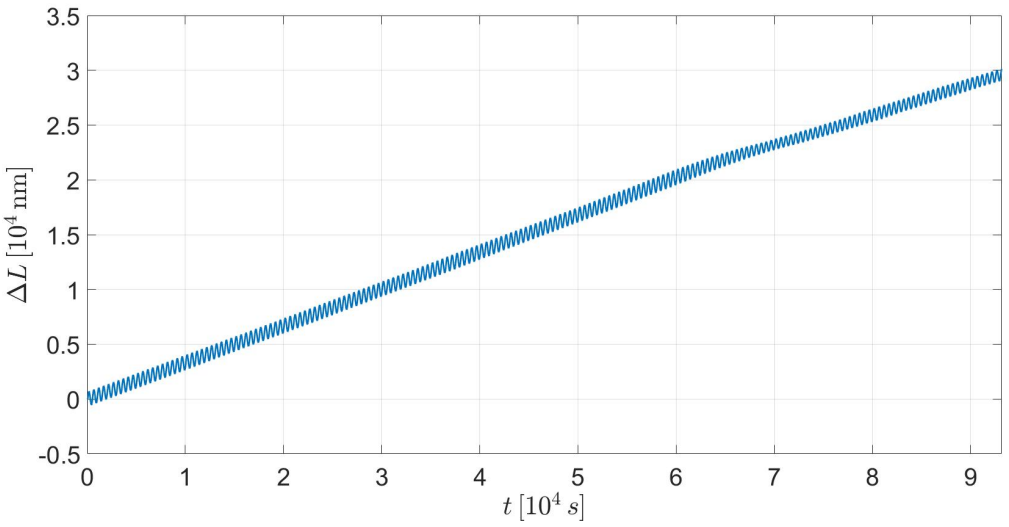

Figure 5.9: Lattice contribution of the low-frequency measurement in fig. 5.5 versus time derived from the thermal expansion coefficient α in fig. 5.8 by means of eq. (5.3).

temperature profile of the low-frequency measurement (fig. 5.9). To improve the result the data of the thermal expansion coefficient α was smoothed, i.e. the upper and lower limits of the corresponding temperature segment were slightly extended.

5. Subtract the lattice contribution of LF from LF to get the pure vacancy signal:

$$\left(\frac{\Delta L}{L_{ref}}\right)_{LF} - \alpha(T)\ T(t)_{LF} = \left(\frac{\Delta L}{L_{ref}}\right)_{LF}^{HR,Vac} + \left(\frac{\Delta L}{L_{ref}}\right)_{LF}^{Mod,Vac}. \tag{5.4}$$

In fig. 5.10 the low-frequency measurement is plotted before and after subtraction.

6. Repeat steps 2 and 3 but now with LF, i.e. calculate the moving average of LF and subtract it from LF to get:

$$\left(\frac{\Delta L}{L_{ref}}\right)_{LF}^{HR,Vac} \quad \text{and} \quad \left(\frac{\Delta L}{L_{ref}}\right)_{LF}^{Mod,Vac}. \tag{5.5}$$

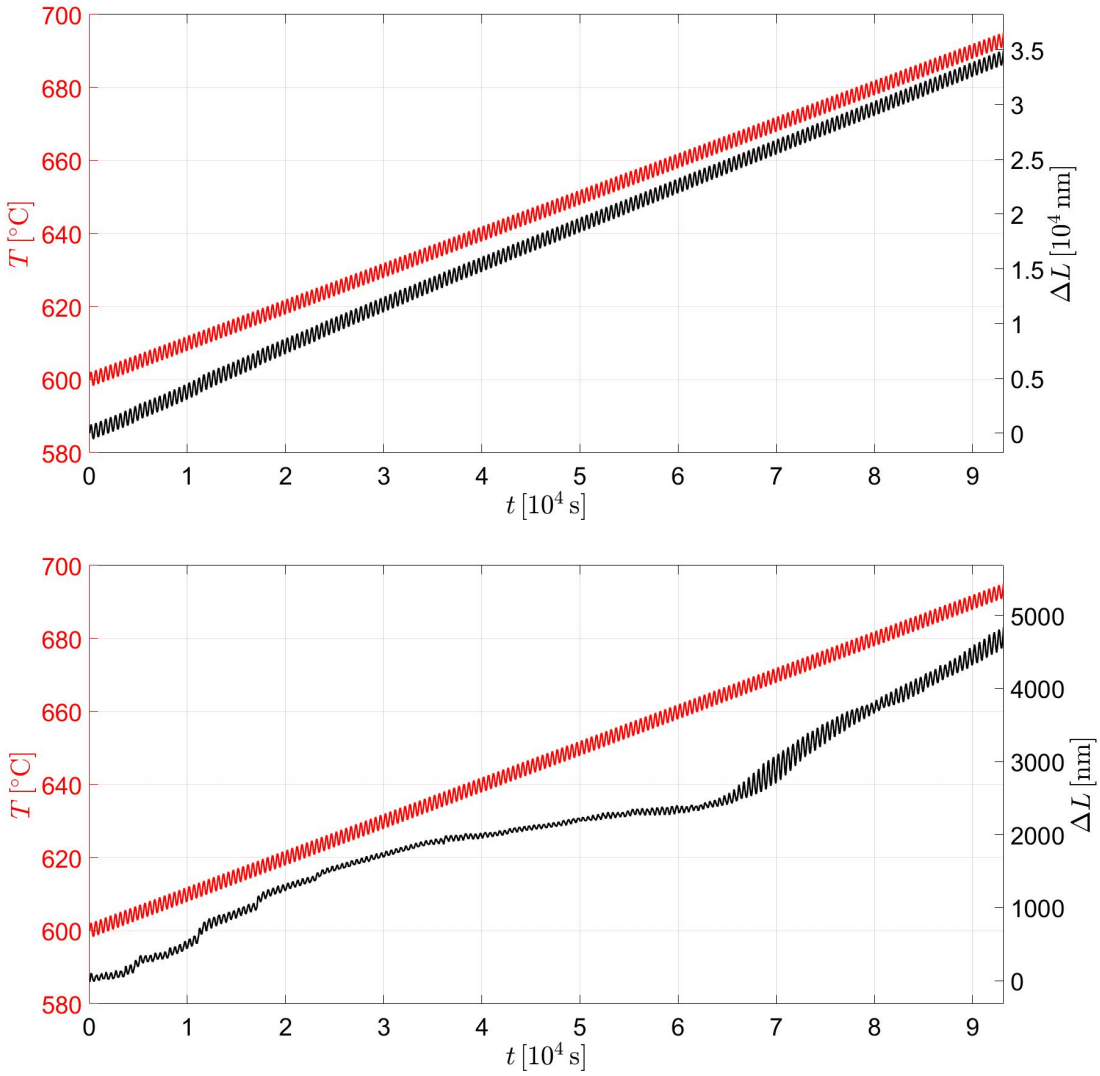

Figure 5.10: Low-frequency measurement in fig. 5.5 before (**top**) and after (**bottom**) subtraction of the lattice contribution (fig. 5.9) from the length ΔL by means of eq. (5.4).

Here again, we calculated the amplitudes and the average of each period directly, i.e. without calculating the moving average first (see step 2). In addition, we also calculated the phase shift (fig. 5.11).

7. Calculate the parameters from

   - the linear heating:

$$\left(\frac{\Delta L}{L_{ref}}\right)_{LF}^{HR,Vac} = \frac{1}{3}(1-r)(C_{V,0}(T_0) - C_{V,0}(T_{start})) \Rightarrow r,\ S_V^F, H_V^F \tag{5.6}$$

   - the amplitude of the modulation:

$$\left(\frac{\Delta \widehat{L}}{L_{ref}}\right)_{LF}^{Mod,Vac} = \frac{1}{3}(1-r)C_{V,0}(T_0)\frac{H_V^F}{kT_0}\frac{1}{\sqrt{\omega^2\tau^2+1}}\frac{\Delta\widehat{T}}{T_0} \Rightarrow r,\ S_V^F, H_V^F, \tau_0, H_V^M \tag{5.7}$$

   - the phase shift of the modulation:

$$\varphi(T_0) = \arctan(-\omega\,\tau) \Rightarrow \tau_0, H_V^M$$

with $T_0 = T_{start} + At$,
$\varphi = \arctan(-\omega\tau)$ (eq. (4.11)),
$C_{V,0}(T_0) = e^{\frac{S_V^F}{k}} e^{-\frac{H_V^F}{kT_0}}$ (eq. (3.1)) and
$\frac{1}{\tau(T_0)} = \frac{1}{\tau_0} e^{-\frac{H_V^M}{kT_0}}$ (eq. (3.4))

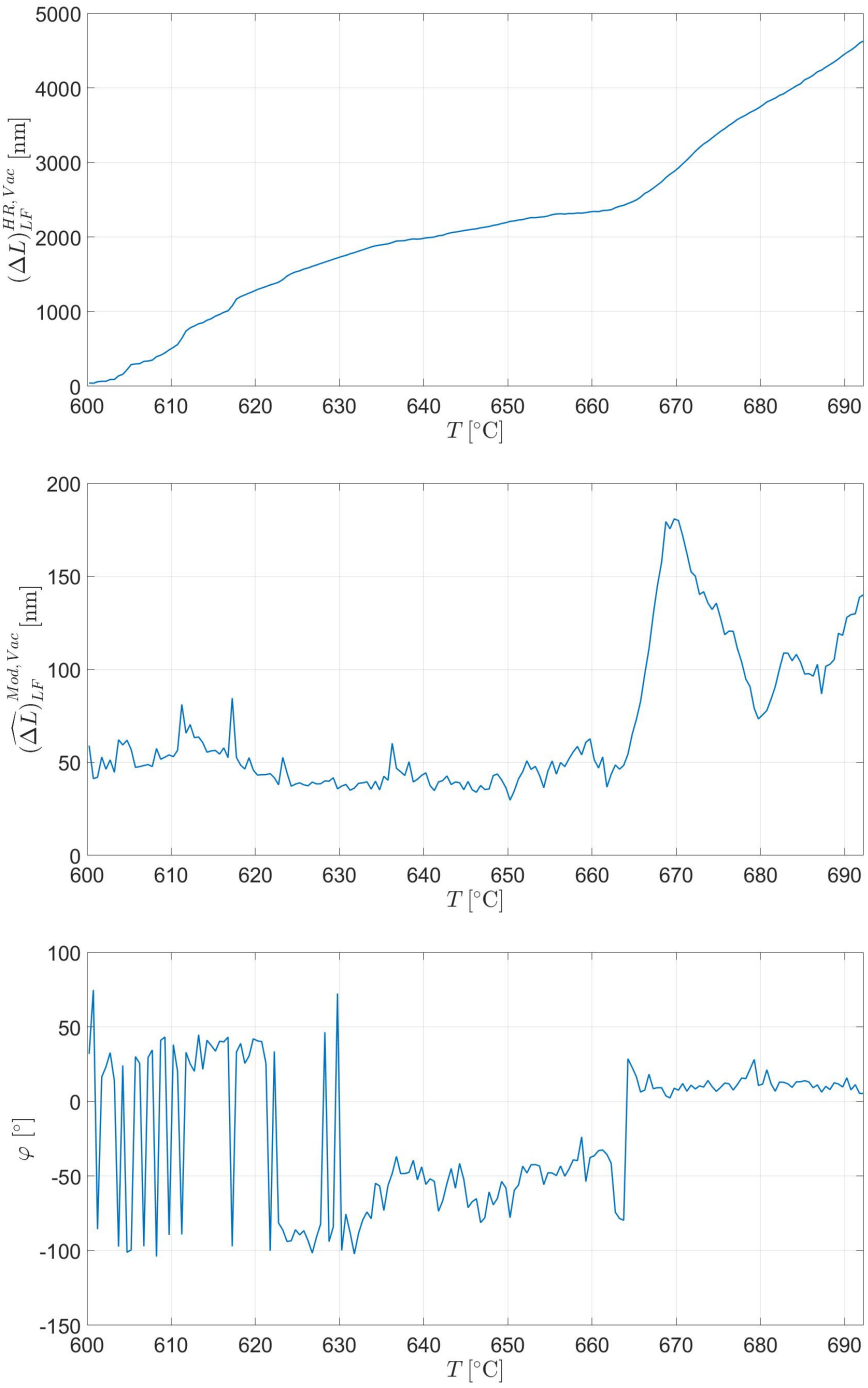

Figure 5.11: Average length $(\Delta L)_{LF}^{HR,Vac}$ (**top**), amplitude $\left(\Delta\widehat{L}\right)_{LF}^{Mod,Vac}$ (**middle**) and phase shift (**bottom**) versus temperature derived from the low-frequency measurement (fig. 5.5) after subtraction as shown in fig. 5.10 (bottom) by means of eq. (5.5) (The moving average was calculated as described in step 6.).

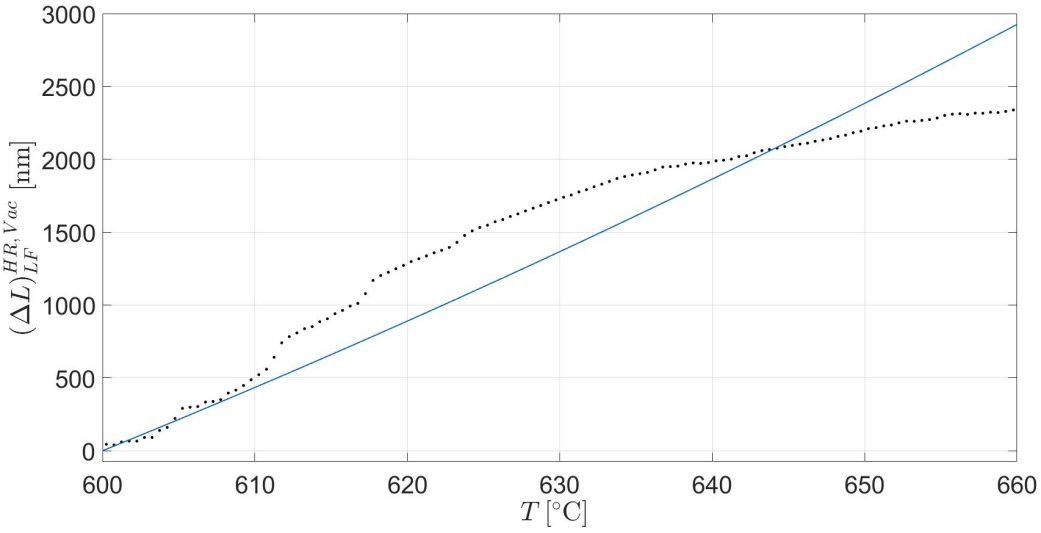

Figure 5.12: Average length $(\Delta L)_{LF}^{HR,Vac}$ versus temperature (cf. fig. 5.11 (top)) together with the corresponding fitted function given by eq. (5.6). The only significant fitting parameter is $H_V^F = (0.47 \pm 0.36)\,\mathrm{eV}$. To enhance the quality of the fit, only the data up to 660 °C was used and the relaxation parameter r was assumed to be 0.4.

Now the curves in fig. 5.11 have to be fitted with the corresponding equations above. In order to get reasonable results we reduce the number of fitting parameters by assuming the relaxation parameter $r = 0.4$ (based on results for nickel [5]). The only significant parameter from these fits was $H_V^F = (0.47 \pm 0.36)\,\mathrm{eV}$ with the corresponding fit shown in fig. 5.12, where only the data below 660 °C was used. This value does not coincide with the literature values (cf. tab. 5.4). The other resulting parameters had no significance and had to be discarded.

However, we can still have a look at the values and compare it with literature values to check if the result lies in the correct range. The overall average length change (fig. 5.11 (top)) is 5000 nm, which does coincide with literature values very well since from 600 °C to 700 °C the overall length change due to vacancies, i.e. $(\Delta L)_{LR}^{HR,Vac}(700\,^\circ\mathrm{C}) - (\Delta L)_{LR}^{HR,Vac}(600\,^\circ\mathrm{C})$[27], is 3000 nm and 2000 nm ([3] in tab. 5.4) and 9000 nm ([4] in tab. 5.4). The amplitude lies in the range of 50-150 nm, whereas the theoretical value, i.e.

[27] $(\Delta L)_{LR}^{HR,Vac}$ is given by eq. 5.6 (L_{ref} = 14.55 mm and r was set to zero because no literature values are available).

Table 5.4: Values from literature for formation enthalpies H_V^F and formation entropies S_V^F determined by dilatometry (DIL) and positron annihilation spectroscopy (POS).

Source	Material	Exp.	$T\,[^\circ\mathrm{C}]$	$H_V^{F_1}[\mathrm{eV}]$	$H_V^{F_2}[\mathrm{eV}]$	$\frac{S_V^{F_1}}{k}$	$\frac{S_V^{F_2}}{k}$
[3]	$Fe_{55}Al_{45}$	DIL	$397-500$	1.0 ± 0.1	0.9 ± 0.1	4.9	3.3
[4]	$Fe_{61}Al_{39}$	POS	$378-467$	0.98 ± 0.07	-	5.7	-

$(\Delta\widehat{L})_{LR}^{Mod,Vac}(700\,^\circ\mathrm{C}) - (\Delta\widehat{L})_{LR}^{Mod,Vac}(600\,^\circ\mathrm{C})$[28] according to [3] (index one) in tab. 5.1 and 5.4, should be 2.3-49 nm. The phase shift is in the temperature range 630-660 $^\circ\mathrm{C}$ roughly in the same range as shown in fig. 4.5. At temperatures above 660 $^\circ\mathrm{C}$ the lattice contribution might be too high due to the decreasing thermal expansion coefficient (cf. fig. 5.8), hence the phase shift suddenly goes to zero. The sudden decrease of the thermal expansion coefficient can be explained by a decreasing length amplitude at higher temperatures. However, an explanation for this decrease could not be found.

5.2.2 Second Approach: At least two Measurements with arbitrary Frequency

For this approach we evaluate all five measurements, from which we will use the fifth measurement (fig. 5.6) to show how to evaluate it according to the procedure as described in section 4.4.3 and we will go through it step by step again.

1. Calculating the moving average gives:

$$\left(\frac{\Delta L}{L_{ref}}\right)^{HR} = \left(\frac{\Delta L}{L_{ref}}\right)^{HR,Lat} + \left(\frac{\Delta L}{L_{ref}}\right)^{HR,Vac}. \tag{5.8}$$

   For the same reason as before (cf. step 2 in section 5.2.1) we calculate the average of each period (instead of calculating the moving average) for both, the temperature T and the length ΔL.

[28] $(\Delta\widehat{L})_{LR}^{Mod,Vac}$ is given by eq. 5.7 (L_{ref} = 14.55 mm and r was set to zero because no literature values are available).

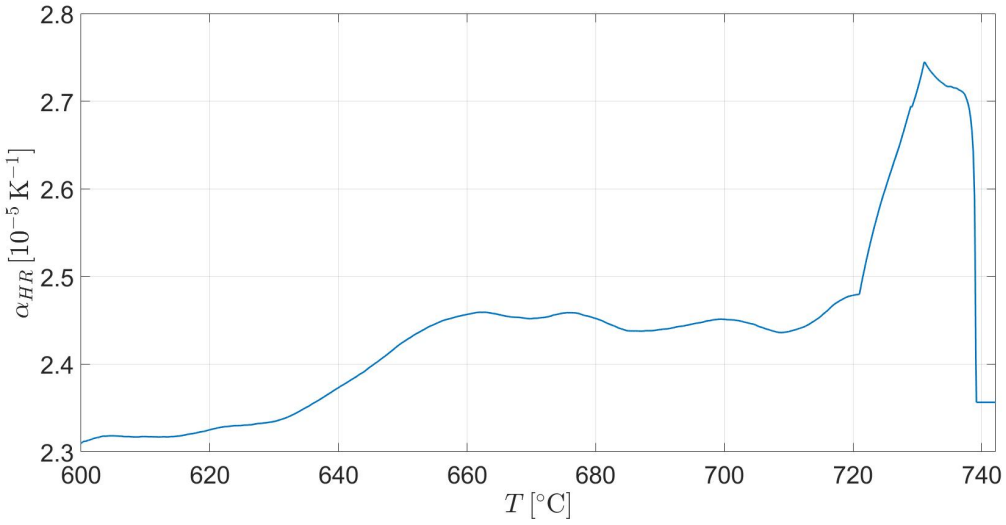

Figure 5.13: Thermal expansion coefficient α_{HR} versus temperature derived from the measurement curve in fig. 5.6 by means of eq. (5.8) and (5.9) (The moving average was calculated as described in step 1.). The data was smoothed in order to eliminate minor fluctuations.

2. Calculate the expansion coefficient $\alpha_{HR}(T)$ by taking the (discrete) derivative with respect to the temperature (eq. (3.3)):

$$\alpha_{HR}(T) = \frac{\Delta\left(\frac{\Delta L}{L_{ref}}\right)^{HR}}{\Delta T}. \tag{5.9}$$

Taking the derivative will give us large errors because the heating rate is very low, which means that we divide two values near zero. We can avoid this by taking the difference of values farther apart instead of adjacent values.
Because we calculated the average value for each period of the temperature, we can use these values to plot the thermal expansion coefficient α_{HR} as a function of temperature (fig. 5.13).

3. Subtract the starting temperature T_{start} from the temperature profile of this measurement[29] to get the sum of the heating rate T_{HR} and the modulation T_{Mod} and multiply it with α_{HR}. We take into consideration that it consists of the lattice part $\alpha(T)$ and the vacancy part:

$$\alpha_{HR}(T)\,T(t) = \left[\alpha(T) + \frac{\mathrm{d}\left(\frac{\Delta L}{L_{ref}}\right)^{HR,\,Vac}}{\mathrm{d}T}\right]\left[\overbrace{T_{HR}(t)}^{At} + \overbrace{T_{Mod}(t)}^{\Delta\widehat{T}\sin(\omega t)}\right] =$$

$$\begin{aligned}
&= \alpha(T)\,T_{HR}(t) + \frac{\mathrm{d}\left(\frac{\Delta L}{L_{ref}}\right)^{HR,\,Vac}}{\mathrm{d}T}\,T_{HR}(t) + \\
&+ \alpha(T)\,T_{Mod}(t) + \frac{\mathrm{d}\left(\frac{\Delta L}{L_{ref}}\right)^{HR,\,Vac}}{\mathrm{d}T}\,T_{Mod}(t) = \\
&= \left(\frac{\Delta L}{L_{ref}}\right)^{HR,\,Lat} + \left(\frac{\Delta L}{L_{ref}}\right)^{HR,\,Vac} + \\
&+ \left(\frac{\Delta L}{L_{ref}}\right)^{Mod,\,Lat} + \frac{\mathrm{d}\left(\frac{\Delta L}{L_{ref}}\right)^{HR,\,Vac}}{\mathrm{d}T}\,T_{Mod}(t).
\end{aligned} \tag{5.10}$$

As in the previous approach (section 5.2.1) we split up our measurement into segments of different temperature and multiply the average α_{HR} of this segment with the corresponding segment of the temperature profile of the measurement (fig. 5.14) in order to take the temperature dependency of α_{HR} into account. Also here the data of the thermal expansion coefficient α_{HR} was smoothed, i.e. the upper and lower limits of the corresponding temperature segment were slightly extended.

[29] $T(t) = T_{start} + At + \Delta\widehat{T}\sin\omega t$ (eq. (4.14))

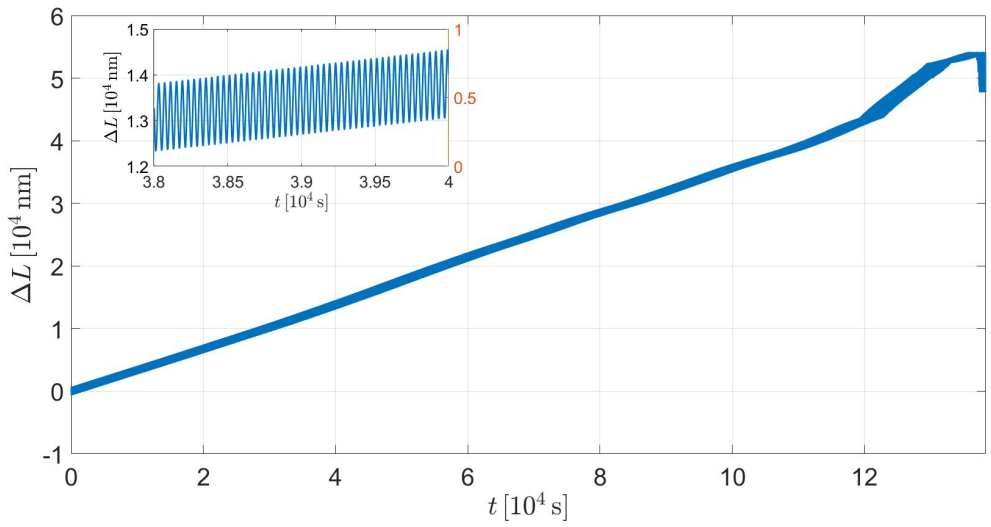

Figure 5.14: Thermal expansion coefficient α_{HR} (fig. 5.13) multiplied with the temperature profile of the measurement curve in fig. 5.6 by means of eq. (5.10).

4. Subtract $\alpha_{HR}(T)\ T(t)$ from the measurement and get a sum of two sine waves:

$$\left[\left(\frac{\Delta L}{L_{ref}}\right)^{HR,\,Lat} + \left(\frac{\Delta L}{L_{ref}}\right)^{HR,\,Vac} + \left(\frac{\Delta L}{L_{ref}}\right)^{Mod,\,Lat} + \left(\frac{\Delta L}{L_{ref}}\right)^{Mod,\,Vac}\right] -$$
$$- \left[\left(\frac{\Delta L}{L_{ref}}\right)^{HR,\,Lat} + \left(\frac{\Delta L}{L_{ref}}\right)^{HR,\,Vac} + \left(\frac{\Delta L}{L_{ref}}\right)^{Mod,\,Lat} + \frac{\mathrm{d}\left(\frac{\Delta L}{L_{ref}}\right)^{HR,\,Vac}}{\mathrm{d}T}\,T_{Mod}(t)\right] =$$
$$= \left(\frac{\Delta L}{L_{ref}}\right)^{Mod,\,Vac} - \frac{\mathrm{d}\left(\frac{\Delta L}{L_{ref}}\right)^{HR,\,Vac}}{\mathrm{d}T}\,T_{Mod}(t). \tag{5.11}$$

In fig. 5.15 the measurement is plotted before and after subtraction.

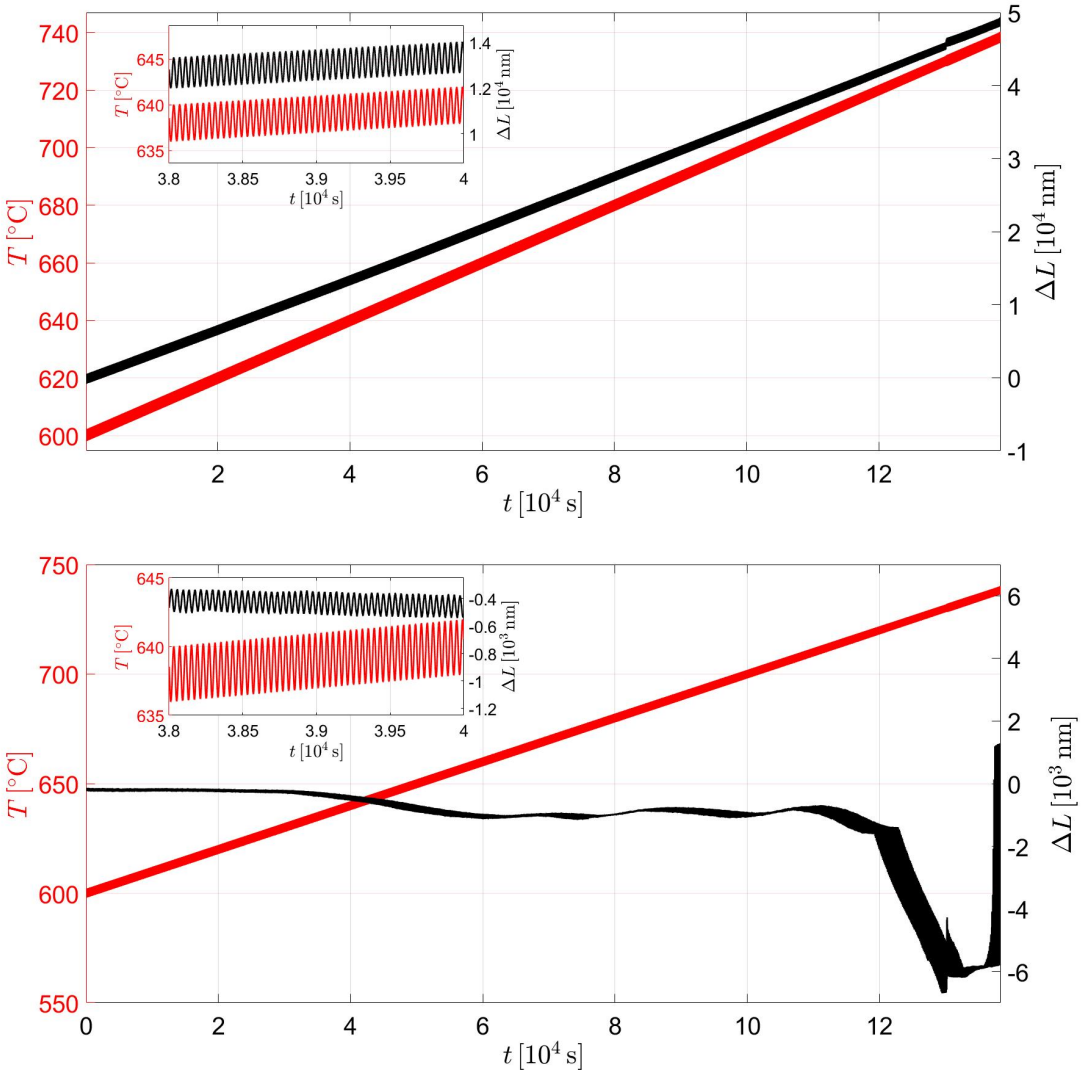

Figure 5.15: Measurement curve in fig. 5.6 before (**top**) and after (**bottom**) subtraction of the product shown in fig. 5.14 from the length ΔL by means of eq. (5.11).

5. Calculate the amplitude and the phase shift of this sum of sine waves (see section 4.4.5), which gives:

$$\left(\frac{\Delta L}{L_{ref}}\right)^{Mod,\,Sum} = \frac{\Delta\widehat{T}}{T_0}\,\frac{1}{3}\,(1-r)\,C_{V,0}(T_0)\frac{H_V^F}{kT_0}\sqrt{1-\frac{1}{\omega^2\tau^2+1}}\,\sin\left(\omega t+\Phi\right) \tag{5.12}$$

$$\begin{aligned}
\text{with}\quad & \Phi = \arctan\left(\frac{1}{\omega\tau}\right),\\
& T_0 = T_{start} + At,\\
& C_{V,0}(T_0) = e^{\frac{S_V^F}{k}}e^{-\frac{H_V^F}{kT_0}} \quad \text{(eq. (3.1)) and}\\
& \frac{1}{\tau(T_0)} = \frac{1}{\tau_0}e^{-\frac{H_V^M}{kT_0}} \quad \text{(eq. (3.4)).}
\end{aligned}$$

The equation for the maximum with T_{max} being the position of the maximum is:

$$T_{max} = \sqrt{\frac{H_V^F}{k}+\frac{1}{\omega^2\tau^2+1}\frac{H_V^M}{k}},$$

where τ also contains the temperature, which is why this equation is an implicit function.

Before calculating the amplitudes and the phase shift the subtracted measurement was multiplied by minus one since only then the maxima and minima of the temperature and length are at the same position, i.e. a 180°-phase shift turns into a 0°-phase shift.
We calculated the amplitudes directly by taking the difference between the minimum and the maximum of each period and divide it by two. In addition, we also calculated the phase shift. In fig. 5.16 the corresponding amplitudes and phase shifts of each measurement is shown.

6. Now we can simultaneously fit the measurement results of multiple measurements to the new amplitude (fig. 4.15) and the new phase shift (fig. 4.16) with r, S_V^F, H_V^F, τ_0 and H_V^M as fitting parameters.

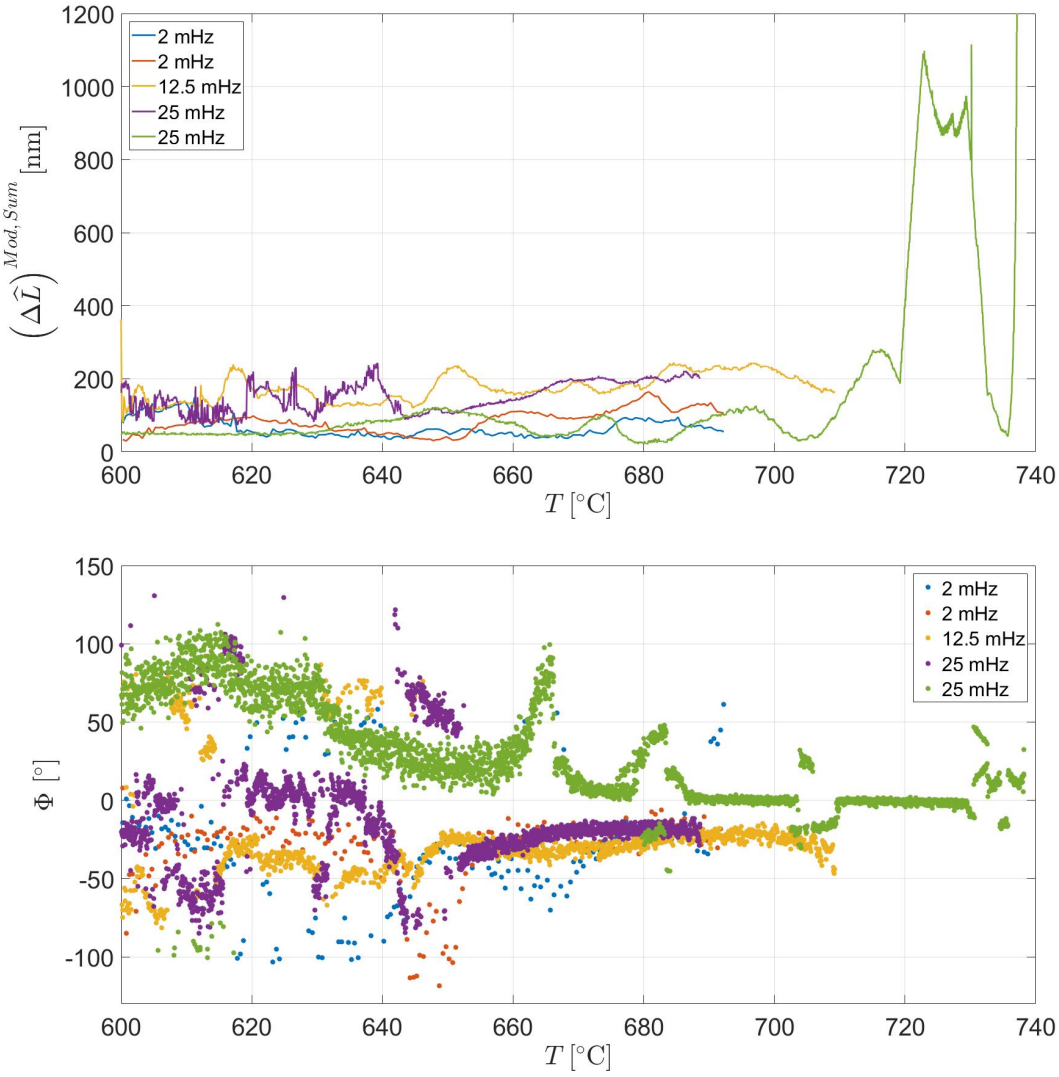

Figure 5.16: Amplitude $\left(\Delta\widehat{L}\right)^{Mod,Sum}$ (**top**) and phase shift Φ (**bottom**) versus temperature derived from the measurement curves in tab. 5.3 after subtraction (as shown in fig. 5.15 (bottom) for the measurement curve in fig. 5.6) by means of the description provided in step 5.

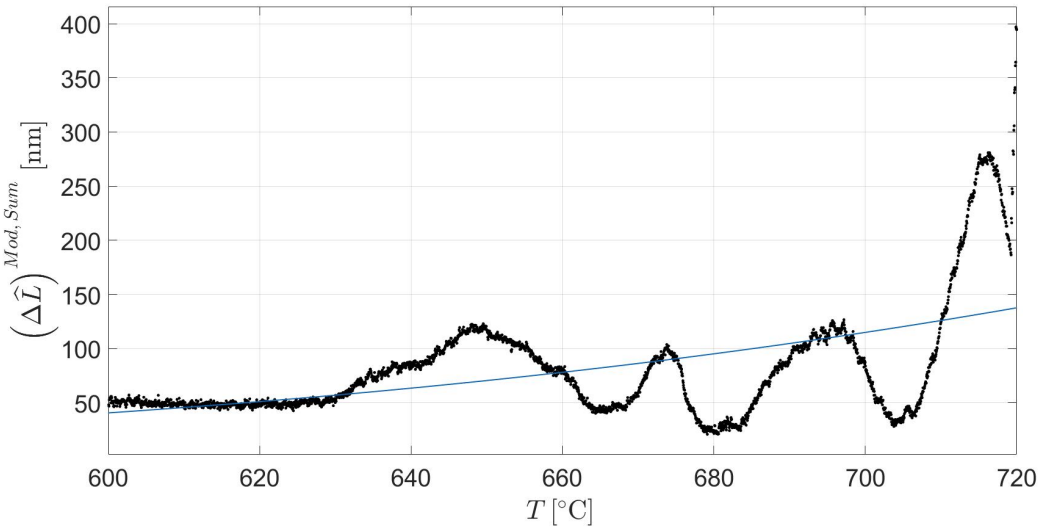

Figure 5.17: Amplitude $\left(\Delta\widehat{L}\right)^{Mod,Sum}$ versus temperature (cf. green curve in fig. 5.16 (top)) together with the corresponding fitted function given by eq. (5.12). The only significant fitting parameter is $H_V^F = (0.92 \pm 0.80)\,\mathrm{eV}$. To enhance the quality of the fit, only the data up to 720 °C was used and the relaxation parameter r was assumed to be 0.4.

As before we reduce the number of fitting parameters to improve the result by assuming $r = 0.4$. Also for this approach only one significant value was obtained from all measurements, which is $H_V^F = (0.92 \pm 0.80)\,\mathrm{eV}$ and is shown in fig. 5.17, where only the data below 720 °C was used. This value does coincide with the literature values quite well (cf. tab. 5.4) but still has a very high uncertainty.

Though also for this approach the other parameters from the fitting were not significant, we can still compare the resulting values with literature values as we did for the previous approach. The amplitude lies in the range of 30-200 nm, which is in the range of the literature values, i.e. 11-31 nm (cf. eq. 5.12 (L_{ref} = 14.55 mm and r was set to zero since no literature values are available) with values taken from [3] (index one) in tab. 5.1 and 5.4). The phase shift is converging at 0 °, which is contradicting the prediction from the theory since it should rather converge at 90 ° (cf. fig. 4.16).

5.3 Suggestions for future Measurements

As mentioned above no measurements with the improved setup could be conducted. However, some thoughts and estimates regarding future measurements have already been made, which will be presented here.

5.3.1 Feasibility of Measurements at higher Frequencies

For the first approach (cf. section 4.3) it is essential to conduct a measurement at the highest frequency possible. Therefore, we will discuss the feasibility of measurements at high frequencies together with an estimate for the highest possible frequency regarding the thermal conductance, i.e. if the entire specimen can be heated fast enough.

Time until entire specimen reaches a specific temperature:

In order to estimate an upper limit for the modulation frequency we calculate the time required for the entire specimen to reach the set temperature. Therefore, we calculate the Biot number Bi and the Fourier number Fo and then read off the required time from the corresponding Heisler chart.

The Biot number is defined as follows:

$$Bi = \frac{h}{k} r_0,$$

where h is the heat transfer coefficient, k the thermal conductivity and r_0 the radius of the specimen.

The heat transfer coefficient h is defined as

$$h = \frac{\frac{\dot{Q}}{A}}{\Delta T},$$

where $\dot{Q}$ is the heat transfer per unit time and A the surface area, where the heat transfer takes place.

We assume the outer layer of the specimen to be at the set temperature T_∞ and calculate the heat transfer coefficient h based on Fourier's law[30]:

$$h = \frac{\frac{\dot{Q}}{A}}{\Delta T} = \frac{k}{\Delta x},$$

where Δx corresponds to the thickness of the outer layer of the specimen. Since the heat transfer coefficient diverges for an infinitely small layer thickness, we calculate the lowest possible heat transfer coefficient to ensure that we get the correct result, i.e. we calculate how long the equilibration process will take at most. Therefore, the outer layer thickness is set to be the radius of the specimen r_0.

Inserting h into the definition of the Biot number gives

$$Bi = \frac{h}{k} r_0 = \frac{\frac{k}{r_0}}{k} r_0 = 1.$$

Now we calculate the Fourier number Fo, which is defined as

$$Fo = \frac{\alpha t}{r_0^2} = \frac{\overbrace{k}^{\alpha}}{\rho c_p} \frac{t}{r_0^2} = 0.605\, t,$$

where α denotes the thermal diffusivity, $k = 16.4\,\mathrm{W/m\,K}$ [6] the thermal conductivity, $\rho = 6.06\,\mathrm{g/cm^3}$ [7] the density, c_p (700 °C) $= 33\,\mathrm{J/K\,mol}$ [8] the specific heat capacity, $r_0 = 2.45\mathrm{mm}$ and t the characteristic timescale. Since c_p is given in units of J / K mol, it was converted as follows:

$$c_p\,[\mathrm{J\,/\,Kmol}] = \frac{1}{m_a N_A} c_p\,[\mathrm{J\,/\,K\,kg}] = 745\,\mathrm{J\,/\,K\,kg},$$

where $m_a = 0.6\, m_{a_{Fe}} + 0.4\, m_{a_{Al}} = 44.3\, u$ is the atomic mass and N_A the Avogadro constant.

Having obtained the Biot number and the Fourier number we can read off the required time from the corresponding Heisler chart as shown on p. W-14 in fig. 5S.4 in [9], for which we need the inverse Biot number, i.e. $Bi^{-1} = 1$. In this Heisler chart the y-axis corresponds to the temperature ratio $\frac{T_0 - T_\infty}{T_i - T_\infty}$, where T_0 denotes the temperature in the middle of the cylinder, i.e. the middle of the specimen, T_i the ini-

[30] $\frac{\dot{Q}}{A} = -k \frac{\Delta T}{\Delta x}$

tial specimen temperature and T_∞ the set temperature at the outer boundary of the specimen. The x-axis shows the Fourier number, i.e. the timescale. The red lines represent the inverse of the corresponding Biot numbers.

To reach 90 $\%$ of the lamp's temperature, i.e. 0.1 on the y-axis of the chart, it takes

$$t = \frac{Fo}{0.605} = \frac{1.6}{0.605} = 2.6\,s.$$

Therefore, the highest possible modulation frequency is about 400 mHz.

Over- and undershoot:

One problem at high frequencies (above 25 mHz) arises from some inertia of the lamps, i.e. the actual temperature produced by the lamps lack behind the set temperature resulting in a smaller amplitude (undershoot).
For one measurement at 12.5 mHz even an overshoot was observed. This might be caused by some inertia of the control system, i.e. upon reaching the maximum temperature the control system needs some time to respond, during which the temperature is still rising resulting into an overshoot.

Undershoot can be reduced by taking a lower amplitude, which on the one hand adversely affects the measurement accuracy since the received signal becomes smaller too, but on the other hand gives us a well-defined amplitude. Choosing a smaller amplitude for high-frequency measurements than for low-frequency measurements is a good way to directly compare them since then the measurements only differ by a certain factor, with which ΔL can be multiplied easily.
So, in practice we want a high and well-defined amplitude, which means that for high frequencies we could first conduct some measurements at constant average temperature to determine the highest possible amplitude for a certain frequency. Then we adapt the measurement parameters until we have a well-defined amplitude free of over- and undershoot.

Another suggestion to improve the response of the system to the set temperature

is to conduct the measurements under an Argon-atmosphere (but still below atmospheric pressure), which would lead to short-distance convection and might enhance the heat transfer.

5.3.2 Measurements with two Time Constants

As discussed in section 5.1 there are either two time constants for $Fe_{62}Al_{38}$ or the higher time constant is caused by the systematic variation of the measurement setup. We chose the temperature range according to the lower time constant τ_1 since at lower temperatures the systematic variation is lower (cf. fig. 2.12). In practice we might not be able to distinguish these two time constants and just get the average of the two time constants or just get the higher time constant depending on how close they are to each other.
In case there are two time constants indeed the two simplest explanations for the occurrence of these two time constants are as follows: Each time constant refers to a jump process within a sublattice and is therefore only influencing the vacancies of the corresponding sublattice. Another possibility is that the origin of these time constants lies in jump processes between the two sublattices, for which the vacancies of one sublattice may not exclusively refer to a specific time constant.
However, since diffusion in intermetallics is a quite complex topic, further investigation is needed in order to be able to tell, whether these two processes are somehow coupled or completely decoupled and moreover, whether these two time constants are referring to the same vacancies or not. It is important to note that we cannot find any general answers to these questions because each material has its very unique structure and properties (in case of intermetallics e.g. Laves phases, Hume-Rothery phases, Zintl phases). Even if we have the same material with the same lattice structure but slightly different stoichimetric composition, we might have to include anti-structure atoms into our considerations for one material but not for the other.

To get some insight into the type of process, we could take measurements according to the higher time constant. In this temperature range the lower time constant can be regarded as zero (cf. fig. 5.3 and 5.4), i.e. the migration of vacancies happens instantaneously, hence they are not distinguishable from the lattice contribution, which is instantaneous too. But if there are vacancies, which are not influenced by the lower time constant, we still get a vacancy signal, from which we can conclude that

these two time constants do not refer to the same vacancies.

5.3.3 Suitable Materials

As mentioned in section 3.2 materials, for which the condition $\frac{H_V^M}{H_V^F} > 1$ is satisfied, are suitable for time-dependent dilatometry measurements. Apart from the already discussed material $Fe_{62}Al_{38}$ the materials in tab. 5.5 are suitable for time-dependent dilatometry measurements and therefore for the method presented in this work. The materials are listed together with the temperature range suitable for taking measurements and the corresponding vacancy concentration within this temperature range. The temperature range was chosen according to the time constant τ (eq. (3.4)), which has to be in the range of the period duration of the modulation, i.e. 10 - 1000 s (cf. section 5.1). Regarding the vacancy concentration PdIn seems to be the best candidate for future measurements.

Table 5.5: Material parameters of suitable materials, for which the condition $\frac{H_V^M}{H_V^F} > 1$ for time-dependent dilatometry and therefore for the method presented in this work is satisfied. In addition, the temperature range suitable for taking measurements together with the order of magnitude of the vacancy concentration within this temperature range is shown.

material	$\tau_0^{-1}[\mathrm{s}^{-1}]$	$H_V^M[\mathrm{eV}]$	$\frac{S_V^F}{k}$	$H_V^F[\mathrm{eV}]$	$T[^\circ\mathrm{C}]$	$C_{V,0}$	source
p-doped Si	4×10^5	1.2	5.00	1.1	$430 - 640$	10^{-5}	[10]
CuZnAl	10^8	0.76	1.00	0.43	$75 - 150$	10^{-6}	[11]
PdIn	10^8	1.9	1.00	0.41	$600 - 790$	10^{-2}	[12]
Al	10^8	0.61	1.00	0.67	$6 - 70$	10^{-6}	[13]
CuZn	10^8	1.14	1.00	0.42	$200 - 310$	10^{-4}	[14]
Fe_3Si	4×10^5	0.85	3.70	0.8	$225 - 375$	10^{-6}	[14]

6 Summary

The first part of this work comprises a **description of the measurement setup**, which is capable of performing isothermal and non-isothermal non-contact high-precision dilatometric measurements with a modulated temperature signal.
While taking measurements we encountered **substantial systematic variations above 600** $^{\circ}\mathrm{C}$ and therefore conducted zero measurements to analyze the origin of the systematic variation. By changing various measurement parameters we found out that the **systematic variation is influenced by the choice of the specimen holder (cf. fig. 2.7) and** that the **whole setup is unintentionally tilted by its asymmetrical expansion upon heating (cf. fig. 2.12 and 2.13)**. **Countermeasures were conceived** in order to prevent the heat from being transferred asymmetrically to the setup and to reduce the total amount of heat being unintendedly introduced to parts of the setup.

The second part aims at developing a **new method for the simultaneous determination of the formation and migration enthalpy together with the corresponding prefactors** by means of a minimum number of modulated measurements with time-linear heating. For this purpose two approaches were elaborated, which aim at cancelling out the lattice part in order to get the pure vacancy signal. These approaches are

- **"High- and Low-Frequency Measurement"**, where the lattice contribution is obtained from the modulation part of the high-frequency measurement. The lattice contribution is then subtracted from the low-frequency measurement giving the pure vacancy signal. (cf. section 4.3)

- **"At least two Measurements with arbitrary Frequency"**, where the thermal expansion coefficient is calculated from the time-linear heating and (after multiplication with the temperature profile) subtracted from the same measurement resulting in a sum of two sine waves, which only consists of contributions from the vacancies. This is done for at least two measurements. (cf. section 4.4)

In addition, the idea of more complicated alternatives to these approaches is presented in section 4.6.

In the last chapter **$Fe_{62}Al_{38}$ was investigated**. In order to determine the temperature range for the modulated measurements, premeasurements were taken first, for which **two time constants were observed (cf. fig. 5.3 and 5.4)**. Using the modulated measurements, the two **approaches were applied**, for which **only the formation enthalpy could be determined**, which is shown in **fig. 5.12** for the first approach and in **fig. 5.17** for the second approach. The other resulting values are not significant. However, the overall length change, the amplitudes and (for the first approach) the phase shift lie in the correct range (cf. section 5.2.1 and 5.2.2).
In the last part some **suggestions for future measurements** are made including an estimation for the time required until the entire specimen reaches a specific temperature, how to counteract over- and undershooting for high frequencies, and a discussion about measurements with two time constants. It concludes with a list of **suitable materials for time-dependent dilatometry (tab. 5.5)**.

References

[1] M. Luckabauer et al.: A high-stability non-contact dilatometer for low-amplitude temperature-modulated measurements. Review of Scientific Instruments **87** (2016) 075116.

[2] H. Mehrer et al.: Self- and Solute Diffusion, Interdiffusion and Thermal Vacancies in the System Iron-Aluminium. Defect and Diffusion Forum **333** (2013) 1-25.

[3] K. Frenner et al.: Time-Differential Length Change Measurements for Thermal Defect Investigations: Intermetallic B2-FeAl and B2-NiAl Compounds, a Case Study. Physical Review Letters **82** (1999) 948.

[4] R. Würschum et al.: Simultaneous Study of Vacancy Formation and Migration at High Temperatures in B2-Type Fe Aluminides. Physical Review Letters **75** (1995) 97.

[5] J. Kotzurek et al.: Direct measurement of vacancy relaxation by dilatometry. Applied Physics Letters **109** (2016) 021906.

[6] B. V. Reddy et al.: Thermophysical Properties of FeAl (Fe-40 at.%Al). Intermetallics **8** (2000) 1369-1376.

[7] J. H. Schneibel: Selected Properties of Iron Aluminides. Oak Ridge National Lab., TN (United States) **CONF-940286-5** (1994).

[8] T. Zienert et al.: Heat capacity of Fe-Al intermetallics: B2-FeAl, $FeAl_2$, Fe_2 Al_5 and Fe_4 Al_{13}. Journal of Alloys and Compounds **725** (2017) 848-859.

[9] T. L. Bergman et al.: Fundamentals of Heat and Mass Transfer. John Wiley & Sons (2011).

[10] V. Ranki and K. Saarinen: Formation of Thermal Vacancies in Highly As and P Doped Si. Physical Review Letters **93** (2004) 255502.

[11] J. Macqueron et al.: Atomic Ordering and Martensitic Transition in a Cu-Zn-Al Shape Memory Alloy. Le Journal de Physique IV **1(C4)** (1991) C4-259-C4-263.

[12] C. Jiang et al.: First-principles study of constitutional and thermal point defects in B2 PdIn. Intermetallics **14** (2005) 248-254.

[13] H.-E. Schaefer: Habilitationsschrift, University of Stuttgart (1981).

[14] H.-E. Schaefer et al.: Systematics of Thermal Defect Formation, Migration and of Self-Diffusion in Intermetallic Compounds. Defect and Diffusion Forum **143** (1997) 193-208.

Acknowledgement

At this point I would like to thank everyone, who supported me in the course of this work.

Univ.-Prof Dr. Roland Würschum, Institute of Materials Physics, TU Graz

for his kind support and competent supervision throughout the course of this work.

Dipl.-Ing. Robert Enzinger, Institute of Materials Physics, TU Graz

for co-supervising, the good cooperation during the experimental work and for the numerous discussions and suggestions.

Dipl.-Ing. Ladislaus Lang-Quantzendorff, Institute of Materials Physics, TU Graz

for the good cooperation during the experimental work.

All colleagues from the Institute of Materials Physics

for providing such a friendly and motivating working environment.

Family and Friends

for their continuous support and encouragement throughout the whole time.

Nomenclature

A	heating rate
A (in section 5.3)	surface area, where the heat transfer takes place
Bi	Biot number
c_p	specific heat capacity of the specimen
$C_{V,0}$	vacancy concentration in equilibrium (eq. 3.1)
$\Delta C_{V,0}$	change of the vacancy concentration upon a small change in temperature (cf. section 4.1.1)
ΔC_V	difference between current vacancy concentration and equilibrium concentration (eq. 4.11)
$\Delta\widehat{C_V}$	amplitude of ΔC_V (eq. 4.12)
ΔC_V^{ini}	initial deviation from equilibrated vacancy concentration (cf. section 4.1.1)
f	frequency of temperature modulation
Fo	Fourier number
h	heat transfer coefficient
H_V^F	vacancy formation enthalpy
H_V^M	vacancy migration enthalpy
k	Boltzmann constant
k (in section 5.3)	thermal conductivity
L_{ref}	specimen length at RT
$(\Delta L)^{HR}$	length change from time-linear heating (eq. 4.15)
$(\Delta L)^{Lat}$	length change due to the change of the lattice parameter (cf. eq. 4.17)
$(\Delta L)^{Mod}$	length change from modulation (eq. 4.16)

$(\Delta\widehat{L})^{Mod}$	amplitude of length change from modulation (cf. eq. 4.17)
$(\Delta L)^{Mod,\,Sum}$	sum of the two sine functions from the second approach (eq. 4.25)
$(\Delta L)^{Vac}$	length change due to vacancies (cf. eq. 4.17)
$\frac{\Delta L_{1\mathrm{K}}}{1\mathrm{K}}$	length change due to vacancies per Kelvin (eq. 4.21)
$\Delta\Delta L$	measurement error of the setup
m_a	atomic mass
N (in section 3.1)	number of atoms
N (in section 3.2)	mean number of jumps per vacancy to a sink
N_A	Avogadro constant
ΔN_V	change of the number of vacancies
$\dot{Q}$	heat transfer per unit time
r	relaxation parameter (cf. eq. 3.2)
r_0	radius of the specimen at RT
S_V^F	vacancy formation entropy
t	time
T	temperature
T_0	average temperature (in reference to temperature modulation)
T_0 (in section 5.3)	temperature in the middle of the cylinder, i.e. the middle of the specimen
T_f	final temperature for measurements as shown in fig. 3.1
T_{HR}	time-linear heating part of the temperature profile according to eq. 4.14, i.e. At

T_i	initial temperature for measurements as shown in fig. 3.1
T_i (in section 5.3)	initial specimen temperature
T_{max}	temperature, where $(\Delta\widehat{L})^{Mod,\,Sum}$ has its maximum
T_{Mod}	modulation part of the temperature profile according to eq. 4.14, i.e. $\Delta\widehat{T}\sin(\omega t)$
T_p	period duration
T_{start}	starting temperature of modulated measurements with time-linear heating (cf. eq. 4.14)
T_∞	set temperature (cf. section 5.3)
$\Delta\widehat{T}$	amplitude of temperature modulation T_{Mod}
V_{ref}	specimen volume
$(\Delta V)^{Vac}$	change in volume due to vacancies
Δx	thickness of the outer layer of the specimen (cf. section 5.3)
Z	coordination number
α	linear coefficient of thermal expansion
α (in section 5.3)	thermal diffusivity
α_{HR}	linear coefficient of thermal expansion determined from the time-linear heating
α_{Mod}	linear coefficient of thermal expansion determined from the modulation
ν_0	attempted frequency of the order of the Debye frequency
φ	phase shift between temperature modulation T_{Mod} and sinusoidal vacancy signal ΔC_V (eq. 4.13)

Φ	phase shift of the sum of two sine functions in the second approach (cf. eq. 4.25)
τ	time constant of vacancy migration (eq. 3.4)
τ_0	preexponential factor of time constant τ
τ_{max}	highest time constant within a measurement
τ_{min}	lowest time constant within a measurement
ξ	geometrical factor
ρ	density of the specimen
ω	angular frequency of temperature modulation